OXIDATIVE STRESS AND BIOPROSTHETIC HEART VALVE DEGRADATION: MECHANISMS AND PREVENTION

Abigail J. Christian

A DISSERTATION

in

Pharmacology

Presented to the Faculties of the University of Pennsylvania

in

Partial Fulfillment of the Requirements for the

Degree of Doctor of Philosophy

2014

Supervisor of Dissertation

Robert J. Levy, M.D.

Professor of Pharmacology

Professor of Pediatrics

Co-Supervisor of Dissertation

Harry Ischiropoulos, Ph.D.

Professor of Pharmacology

Research Professor of Pediatrics

Graduate Group Chairperson

Julie A. Blendy, Ph.D., Professor of Pharmacology

Dissertation Committee

Vladimir R. Muzykantov, M.D., Ph.D., Professor of Pharmacology and Medicine

Andrew Tsourkas, Ph.D., Associate Professor of Bioengineering

David M. Eckmann, M.D., Ph.D., Professor of Anesthesiology and Critical Care

Robert C. Gorman, M.D., Professor of Surgery

Dedication

To my family for their love and support.

Acknowledgments

I would first like to thank my advisors Robert Levy and Harry Ischiropoulos for their support and guidance over the past few years. They both taught me a tremendous amount and enabled me to develop as a scientist. I would also like to thank all the members of the Levy lab, especially Matt Finley and Jeanne Connolly who helped me with experiments early on and gave me valuable guidance along the way. I want to acknowledge Ivan Alferiev for his chemistry expertise which was instrumental in the progression of this work. I want to thank Zoë Folchman-Wagner, Scott Forbes, Jillian Tengood-Hilllman, Katherine Clark, Rich Adamo, and Josh Slee for both scientific discussion and for creating an enjoyable lab environment. I also want to thank all the members of the Ischiropoulos lab for the interesting lab meeting discussions.

I also want to acknowledge my thesis committee: Vladimir Muzykantov, David Eckmann, Robert Gorman, Andrew Tsourkas, and Steve Thom for their expertise and guidance. They provided very valuable advice and insight which allowed my project to move forward.

This project involved numerous scientific collaborations and I would like to thank all of them for their contributions. Giovanni Ferrari, Matthew Gillespie, Robert Gorman, and Joseph Gorman for providing clinical and sheep samples; Stanley Hazen, Hongqiao Lin, and Dave Schmidt of the Cleveland Clinic for performing mass spectrometry analysis; Ines Batinic-Haberle and Artak Tovmasyan of Duke University for providing SOD mimetics; Richard Bianco, Steve Garofolo, and Laura Harvey for performing sheep surgeries; Vladimir Muzykantov, Melissa Howard, and Liz Hood for help in developing and executing the SOD mimetic liposome project.

Finally, I want to thank my family and friends for their support. I especially want to thank my fiancé Aaron Stonestrom, my mom and siblings for their support and love. I also want to thank my classmates of the Pharmacology Graduate Group: Mansi Shinde, Bridgin Lee, Sima Patel, Diana Avery, Kevin Patel, Mike Chiorazzo, Nishita Shastri, John O'Donnell, Brian Weiser, Natalie Daurio, Alan Yee, Maya Kehzam, Jackie St. Louis, and Sara Miller; you all made my time in graduate school more enjoyable by providing friendship and support. Finally, I want to thank the Pharmacology Graduate Group, especially Sarah Squire, Julie Blendy, and Vladimir Muzykantov for this experience.

ABSTRACT

OXIDATIVE STRESS AND BIOPROSTHETIC HEART VALVE DEGRADATION: MECHANISMS AND PREVENTION

Abigail J. Christian

Robert J. Levy, M.D.

Harry Ischiropoulos, Ph.D.

Bioprosthetic heart valves (BHV) are widely used in interventions for symptomatic valvular disease; however, they begin to fail clinically after 10 years, most frequently due to structural deterioration. Calcification has been considered the major mechanism of BHV degeneration although other mechanisms may be involved. In this work, we investigated the hypothesis that oxidants contribute to BHV structural degeneration. BHV have been shown to elicit an inflammatory response from the patient, thereby resulting in the production of reactive oxygen and reactive nitrogen species which may degrade BHV. To determine the role of oxidants in BHV degeneration, we analyzed clinically failed BHV explants for markers of oxidation and utilized experimental systems to identify the consequences of BHV oxidation. Clinical BHV explants were found to have elevated levels of the tyrosine oxidation product dityrosine, therefore indicating that BHV are susceptible to oxidation. Exposure of the BHV material glutaraldehyde-fixed bovine pericardium (BP) to oxidizing conditions demonstrated that oxidation of BHV results in the loss of glutaraldehyde cross-links, disruption of the collagen structure, and an increase in susceptibility to proteolytic degradation. To address this mechanism of BHV structural degeneration, we developed two antioxidant delivery strategies. Our first approach involved covalent immobilization of the oxidant scavenger 3-(4-hydroxy-3,5-di-tert-butylphenyl) propyl amine (DBP) to BHV leaflet materials whereas the second method utilized passive incorporation of a catalytic antioxidant, a superoxide dismutase (SOD) mimetic, into the material. Both strategies demonstrated efficient delivery of an antioxidant to the BHV material. DBP mitigated structural degradation of BP induced by exposure to oxidizing conditions and provided resistance to calcification in the rat subdermal implant model. The SOD mimetic approach demonstrated SOD activity following incorporation into BP as well as

after 90 day implantation in either the rat subdermal implant model or sheep circulatory patch model; thereby supporting the hypothesis that SOD mimetics may provide sustained protection from oxidants. These studies demonstrate that oxidants contribute to the structural degeneration of BHV and that an antioxidant material modification may be used to mitigate this process and to potentially improve the durability of BHV.

Table of Contents

List of Tables

List of Figures

Chapter 1: Introduction and Background

1.1 Introduction

Heart valve replacement surgery is the primary treatment option for progressive, symptomatic heart valve diseases, including aortic valve stenosis and mitral valve prolapse. Each year more than 300,000 valve replacement surgeries are performed worldwide with both mechanical and bioprosthetic heart valves (BHV)[1]. BHV are fabricated from glutaraldehyde treated heterograft tissues and, unlike the alternative mechanical prosthetic valves, have a low risk of thrombosis [2]. In addition, BHV are the only type of prosthetic valves that can be catheter-deployed, thereby providing a minimal invasive alternative to cardiac surgery [3]. Unfortunately, the use of BHV is limited by poor durability that contributes to the high device failure rate of 30% after 10 years of implantation [4]. The major cause of BHV failure is structural deterioration associated with calcification or primary leaflet degeneration [2, 5]. Therefore, there is a significant clinical need to identify the mechanisms of BHV structural deterioration in order to develop more durable BHV.

1.2 Heart valve disease

The four valves of the human heart regulate blood flow through the heart and to the peripheral tissues or lungs (Fig. 1.1) [6]. Under normal conditions, blood and pressure build behind the closed valve which forces the valve open to allow blood flow through the valve [7]. Venous blood returning to the heart from the peripheral tissues enters the right atrium where it then passes through the tricuspid valve to the right ventricle. Blood then passes through the pulmonary valve to reach the lungs via the pulmonary artery. Oxygenated blood enters the left atrium and passes through the mitral valve into the left ventricle. Blood exits the left side of the heart through the aortic valve into the aorta, which delivers blood to the peripheral tissues [7]. Under normal conditions, the atrioventricular valves (mitral and tricuspid) are open during ventricular diastole to allow for ventricular filling and are closed during ventricular systole to prevent blood flow back into the atria.

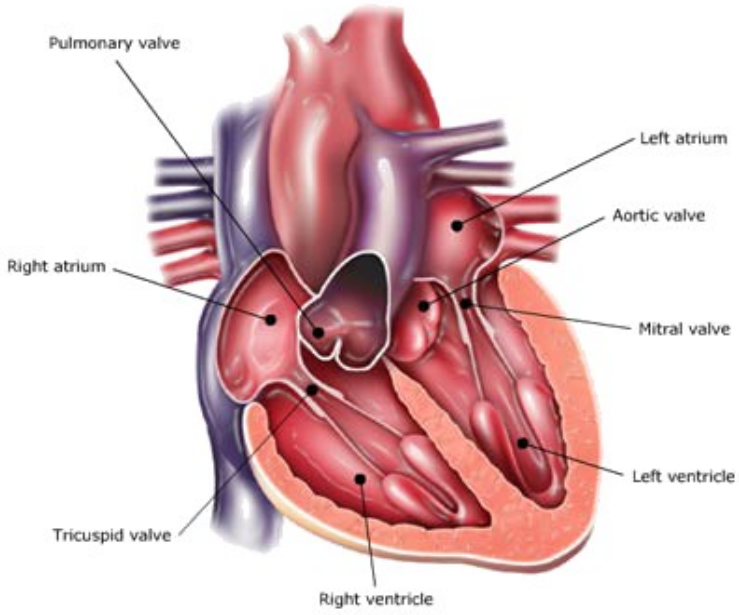

Fig. 1.1 Heart valves and chambers. The valves of the human heart are the mitral, aortic, pulmonary, and tricuspid. The mitral and tricuspid are the two atrioventricular valves which connect the atrium and ventricle on the left or right sides of the heart, respectively. The aortic and pulmonary valves, or semilunar valves, are located in the two arteries that leave the heart, the aorta and pulmonary artery. Reproduced from [6].

Heart valve disease typically results in either incomplete opening or closing of the valve which prevents normal blood flow through the valves [4]. The mitral and aortic valves are the most common sites of valve disease due to their location on the left side of the heart, which pumps blood to the entire body and therefore generates higher pressure during ventricular or atrial contraction, as opposed to the right side of the heart which pumps only to the lungs [7]. Valve stenosis, such as calcific aortic valve disease, is a narrowing of the valve opening due to leaflet thickening and impaired mechanics, which prevents the valve from fully opening, therefore allowing less blood to be pumped through the valve with each heartbeat [4, 8]. Valve regurgitation and prolapse describe conditions of incomplete valve closing, which results in backwards flow of blood [7]. Other causes of heart valve disease include infective endocarditis, congenital abnormalities such as a bicuspid aortic valve, and rheumatic disease.

Incomplete valve opening or closing requires the heart to work harder to pump enough blood through the valve with each beat. To compensate for the required workload, the myocardium

may dilate and thicken over time [7]. In progressive disease, the myocardium weakens and can no longer compensate for the valve dysfunction. Without intervention, this leads to congestive heart failure due to blood and fluid accumulation in tissues, particularly the lungs [7]. The primary treatment option for symptomatic heart valve disease is valve replacement surgery using prosthetic heart valves or surgical leaflet repair if possible; there are currently no effective pharmacologic therapies [4, 7, 9].

1.3 Prosthetic heart valves

The two major classes of prosthetic heart valves are mechanical and bioprosthetic. Mechanical valves are prepared from synthetic materials such as titanium, metal alloys, or pyrolytic carbon. The common types of mechanical valves are bileaflet or ball in cage designs (Fig. 1.2) [4]. Although the mechanical valves have good durability with lifespans ranging from 25 to 40 years [4], they are associated with a high risk of thrombosis due to high shear stress, flow separation, and red blood cell damage (hemolysis) [10]. Long-term anti-coagulant use is necessary to reduce the risk of thromboembolism. Despite the disadvantage of anti-coagulation that places the patient at risk for hemorrhage [10], mechanical valves are still used in approximately 50% of all valve replacement surgeries [5].

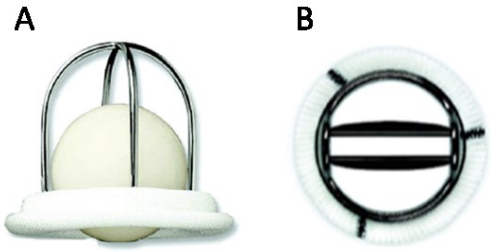

Fig. 1.2. Mechanical valves. (A) Caged ball Starr-Edwards valve (B) Bi-leaflet St. Jude Medical valve. Adapted from [4].

BHV leaflets are fabricated from glutaraldehyde treated heterograft tissues such as bovine pericardium (BP), bovine jugular venous valves (BJV), or porcine aortic valve leaflets (PAV). The glutaraldehyde fixation is necessary to reduce material immunogenicity through antigen masking

[10]. The heterograft tissues are either mounted on stent struts for catheter-deployed devices or sewn to a Dacron cushion for implantation [2, 10] (Fig. 1.3). BHV have hemodynamic properties similar to the native valve and are not associated with a high risk of thrombosis, therefore long-term anti-coagulation is not required [1, 2, 10]. However, compared to mechanical prosthetic valves, BHV have a short lifespan with a rate of failure of 30% at 10 years post-implantation and 60% by 15 years post-implantation [4]. This short life span is due to poor durability arising from leaflet structural degeneration. BHV are widely used despite the short lifespan since they provide an alternative to the thrombogenic mechanical valves. However, the use of BHV is limited in certain patient populations such as young children and adolescents, who typically have more rapid BHV calcification than older human subjects [5, 11, 12].

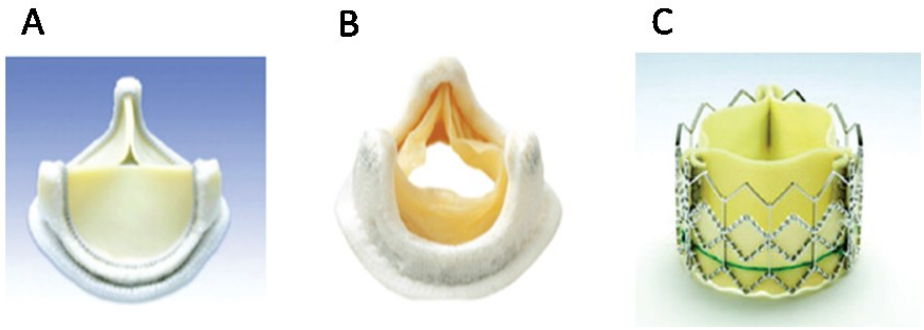

Fig. 1.3. Bioprosthetic heart valves. (A) Bovine pericardial Carpentier-Edwards bioprosthesis (B) Porcine aortic valve Medtronic bioprosthesis (C) Transcatheter Edwards Sapien bioprosthesis. Adapted from [4].

1.4 Structural degeneration of bioprosthetic heart valves

Many factors have been implicated in the structural degeneration of BHV, including calcification, mechanical stress, and inflammation [2]. Each of these processes involves collagen disruption, which is important for the structural integrity of BHV leaflets.

BHV calcification is considered the main cause of BHV structural degeneration due to its prevalence in the majority of explanted clinical BHV [5, 10]. The initiation of BHV calcification involves the interaction of circulating calcium ions with devitalized cell membranes and intracellular structures in the heterograft tissue [5]. The initial sites of calcium accumulation grow, ultimately forming calcium phosphate nodules that cause the BHV leaflets to stiffen, thereby limiting leaflet

movement [13]. There are many factors that can influence BHV calcification, including normal regulators of bone formation and calcium metabolism such as osteopontin, osteonectin, osteocalcin, and alkaline phosphatase [5]. BHV calcification is a significant issue for children and adolescents who have accelerated calcification as compared to adults [11, 12] which limits the use of BHV in this patient population.

BHV leaflets are subject to high shear and flexural stresses that have been shown to potentiate leaflet structural degeneration. These mechanical stresses can disrupt the collagen structure, which leads to leaflet weakening and in some instances leaflet tears [14]. In addition, it has been proposed that mechanical stress may also contribute to both calcification and enzymatic degradation of BHV leaflets through the loss of glycosaminoglycans as well as molecular damage to collagen [14-16]. Overall, mechanical stress leads to a breakdown of the extracellular matrix components of the BHV leaflets which leads to material weakening and failure.

The presence of a BHV elicits a host inflammatory response that could lead to BHV structural degeneration, but this mechanism of degeneration has not been fully elucidated [17-20]. BHV-associated inflammation has been identified through several histology-based studies of explanted BHV which demonstrated the presence of inflammatory cells such as macrophages and multi-nucleated foreign body giant cells (Fig. 1.4) [21, 22]. Active inflammatory cells produce reactive oxygen and nitrogen species (ROS/RNS) as well as matrix metalloproteinases (MMPs) that degrade extracellular matrix proteins such as collagen [23]; therefore BHV inflammation may lead to structural degeneration through either proteolytic degradation by MMPs or oxidative stress from ROS/RNS.

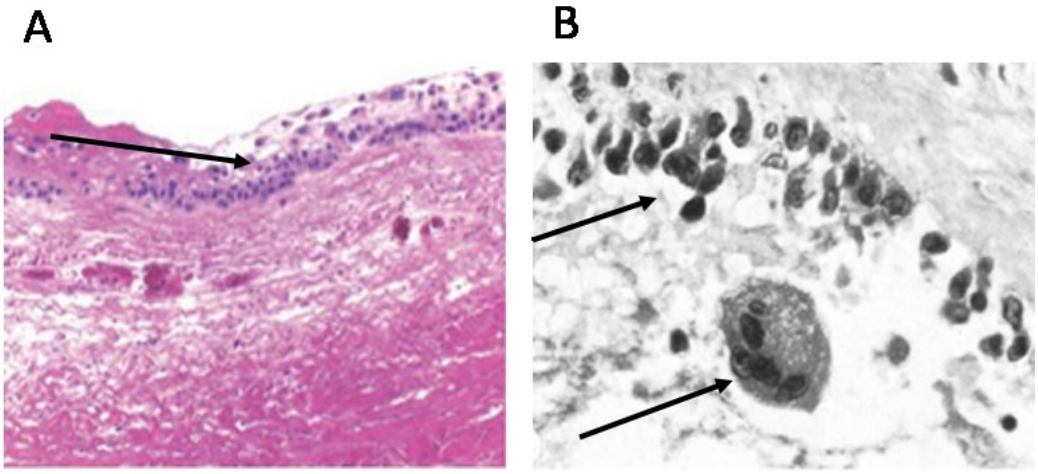

Fig. 1.4. Inflammatory cell infiltration of BHV. (A) Hematoxlyin and eosin stains of explanted BHV, arrows indicate cellular filtration (200x) [21] (B) Foreign body giant cell and cellular infiltration in explanted BHV indicated by arrows (330x) [22].

1.5 Oxidative stress and biomaterial degradation

The term foreign body reaction (FBR) has been used to describe the response to implantable biomaterials such as pacemaker leads and artificial joints that involves acute and chronic inflammation as well as fibrous tissue formation [24]. The FBR involves a localized response to the biomaterial characterized by the migration of activated inflammatory cells to the surface of the material. The production of ROS/RNS by inflammatory cells is particularly important in the degradation of synthetic biomaterials including polyurethane and metal alloys since ROS/RNS reactions with the material leads to damage including surface cracking and pitting, ultimately resulting in material failure [25-27].

The effects of ROS/RNS on tissue-based biomaterials such as BHV have not been investigated. However, studies with purified collagen, the major component of the heterograft tissues used in the fabrication of BHV, have shown that ROS/RNS reactions result in oxidation of cross-linked molecules, collagen fibril fragmentation, and increased susceptibility to proteolytic enzymes such as MMPs [28-31]. Oxidants have been shown to disrupt both the secondary and tertiary structure of collagen through cleavage of intramolecular cross-links [31]. This disruption of the collagen structure may be responsible for the increased susceptibility to proteolysis following

exposure to oxidants. In addition, collagen oxidation results in fibril fragmentation that may allow proteases to more easily access and degrade collagen [32]. Therefore, based on these effects of collagen oxidation, oxidation of a collagen-based biomaterial may contribute to BHV structural degradation.

The major focus for improving BHV durability has been the prevention of BHV calcification through the use of material pre-treatments or modifications. However, BHV degeneration remains a significant clinical issue and may be addressed by shifting the focus from calcification to alternative mechanisms of BHV structural deterioration. We hypothesize that oxidants contribute to BHV degeneration. This hypothesis is supported by evidence of BHV-related inflammation as well as the known structural and functional effects of oxidation of collagen. Furthermore, mitigation of BHV oxidative damage with compounds that scavenge oxidants could improve BHV durability.

1.6 Antioxidant modifications of biomaterials

Incorporation or modification of materials with antioxidants has been studied as an approach to prevent oxidative damage of synthetic materials used in medical applications [27, 33, 34]. Compounds such as α-tocopherol have demonstrated efficacy in preventing oxidative damage of polymers such as poly(etherurethane urea) that may be used in medical implants [35]. There are several strategies that have been employed for the modification of polymeric materials with antioxidants including incorporation prior to polymerization or surface modification [34, 36]. These proof-of-principle studies demonstrated that incorporation of an antioxidant in a biomaterial successfully prevents oxidative damage and thereby may be a useful strategy to improve the durability of clinically-used biomaterials.

Previously, antioxidant incorporation or modification to BHV has not been developed as an approach to improving BHV durability. However, attachment of a compound, such as an anti-calcification agent [37], has been done using covalent methods. These studies utilized either the residual aldehyde groups introduced with glutaraldehyde or carbodiimide-activated carboxyl groups to react and bind an amine-containing compound through the formation of either Schiff bases or amide bonds, respectively [37-39]. In addition to covalent modification, it may be possible to

passively incorporate, or without a chemically-driven reaction, a hydrophobic or ionic compound into BHV materials. Both methods will be discussed as potential strategies for modification of BHV with an antioxidant.

In order to covalently immobilize a compound to a material, the material must either contain reactive functional groups such as terminal amines or those groups must be introduced. Collagen contains lysine and asparagine residues containing terminal amines, which are utilized in glutaraldehyde fixation for BHV, as well as glutamate and aspartate with terminal carboxyl groups [40-43]. These carboxyl groups are not currently utilized in the preparation of BHV leaflet materials and therefore may be employed for antioxidant incorporation. The antioxidants previously used in studies with synthetic materials are not ideal for conjugation to carboxyl groups due to the lack of accessible functional groups necessary for reaction with the material. A commonly used conjugation reaction involving carboxyl groups is carbodiimide-driven activation of carboxyl groups and subsequent reaction with reactive amines [44]. This type of carbodiimide-driven chemistry has been studied as an alternative cross-linking strategy for BHV materials and therefore may be effective for the immobilization of a compound to the material [39, 45]. The combination of a carbodiimide-driven reaction and an antioxidant with a reactive amine may be used to modify BHV materials.

The alternative method, passive incorporation, relies on the structure of the compound that is to be incorporated. Lipophilic rather than hydrophilic compounds have more efficient uptake into tissues, such as those used in the fabrication of BHV, since these compounds are able to partition in lipid membranes and can interact with extracellular matrix proteins such as collagen through hydrogen bonding [46]. In addition, a charged compound can interact with charged regions of the tissue, which would include negatively or positively charged amino acid residues of collagen, to provide additional electrostatic interactions that could stabilize the compound within the tissue [47]. Depending on the characteristics of the compound for passive incorporation, both methods for modifying BHV could provide sustained, local delivery of an antioxidant.

1.7 Approach 1: covalent immobilization of DBP

The first proposed strategy for mitigating BHV oxidative degradation involves the immobilization of an oxidant scavenging compound to the BHV material prior to clinical use. To accomplish this, we proposed the use of an analogue of butylated hydroxytoluene (BHT) and a carbodiimide-driven modification scheme.

BHT is a phenolic compound commonly used as a food additive due to its ability to react with oxidants such as hydroxyl and peroxyl radicals to terminate potentially damaging reactions including lipid peroxidation [48, 49] (Fig. 1.5A). BHT undergoes one electron oxidation to form a phenoxyl radical which can subsequently scavenge an additional radical [48, 50]. BHT is not an ideal candidate for covalent immobilization to a BHV material since it does not contain a reactive functional group that could be utilized in a conjugation reaction. However, an analogue of BHT with the appropriate reactive group could be a candidate for immobilization to BHV.

Previously, BHT or di-*tert*-butyl phenol derivatives synthesized in the Levy lab were attached to polyurethane through bromoalkylation or bulk modification [27, 36, 51]. The same attachment scheme cannot be used BHV materials since BP does not have the appropriate surface chemistry [40, 52]. However, di-*tert*-butyl phenol with an added terminal amine could react with carbodiimide-activated carboxyl groups in BHV materials to form an amide bond. The proposed compound, 3-(4-hydroxy-3,5-di-tert-butylphenyl) propyl amine (DBP), has the BHT parent compound for antioxidant activity and an amine with an alkyl linker for reactivity with BHV materials (Fig. 1.5B).

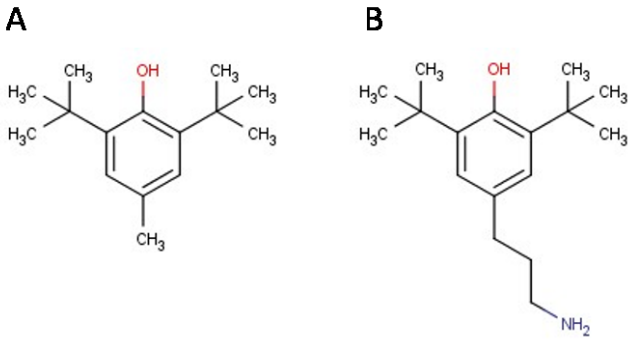

Fig. 1.5 Structures of BHT and DBP. (A) Butylated hydroxytoluene (BHT) or 2,6-di-*tert*-butyl-4-methylphenol and (B) 3-(4-hydroxy-3,5,-di-*tert*-butylphenyl)propyl amine (DBP).

Carbodiimides are frequently used in amine-carboxyl conjugation reactions [44, 53]. In the presence of N-hydroxysuccinimide (SuOH), carbodiimide activation of carboxyls results in the formation of stable N-succinimidyl ester intermediates which are then able to react with an amine to form an amide bond. The proposed reaction to attach DBP to BHV materials is shown below (Fig. 1.6).

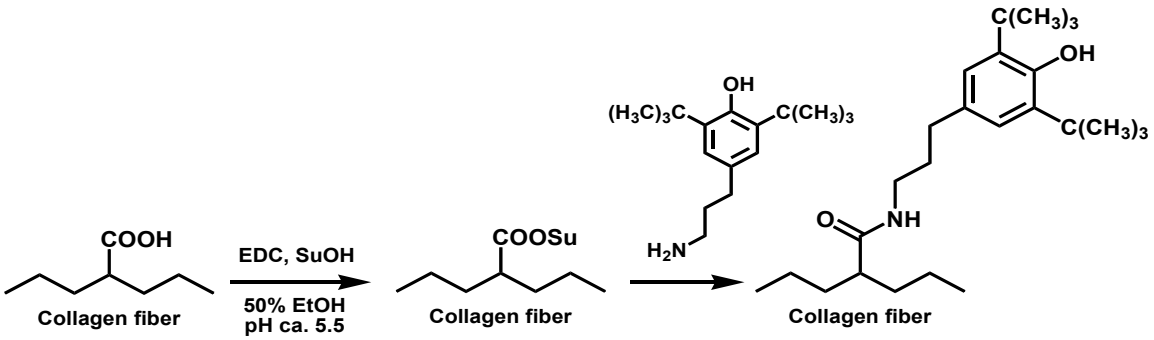

Fig. 1.6 DBP modification scheme. Carboxyl groups are activated with 1-ethyl-3-(3-dimethylaminopropyl)-carbodiimide (EDC) in the presence of SuOH to form stable N-succinimidyl ester intermediates that can then react with DBP. Scheme prepared by Ivan Alferiev.

We propose that immobilized DBP will remove oxidants that could otherwise damage the BHV material. Due to the covalent interaction between DBP and carboxyl groups of collagen in BHV heterograft materials, DBP is expected to be stably bound to the BHV material.

1.8 Approach 2: non-covalent incorporation of a superoxide dismutase (SOD) mimetic

The SOD enzymes control intracellular and extracellular superoxide levels. The three SOD enzymes are cytosolic Cu/Zn SOD (SOD1), mitochondrial MnSOD (SOD2), and extracellular Cu/Zn SOD (SOD3) [54]; the enzymes differ in terms of subcellular localization and reactive metal. These enzymes catalyze the dismutation of superoxide to hydrogen peroxide and molecular oxygen through cycling of the oxidation state of the metal center of the enzyme, which is represented by the following reactions: M^{n+1}-SOD+ $O_2^{-\bullet}$ → M^n-SOD + O_2 and M^n-SOD + $2H^+$ + $O_2^{-\bullet}$ → M^{n+1}-SOD + H_2O_2. In addition, SOD3 has been shown to prevent oxidative fragmentation of type I collagen [55]. Superoxide can cause damage to collagen [56], but compared to other oxidants, superoxide is a weak oxidant. However, superoxide is involved in the production of stronger oxidants including hydroxyl radicals and peroxynitrite through metal-catalyzed reactions with hydrogen peroxide or

nitric oxide, respectively [57, 58]. Therefore superoxide dismutation by SOD may prevent oxidative damage through both the removal of superoxide and the decreased production of hydroxyl radicals and peroxynitrite.

The pharmacological use of native SOD enzymes is limited by both the size of the enzyme, which prevents it from crossing cell membranes, as well as its short circulating half-life since it is susceptible to degradation by proteases [54]. Due to these limitations, synthetic compounds, or SOD mimetics, have been developed for potential clinical use. The conserved structural features of the currently available SOD mimetics are a redox active metal center and a protective ring structure that prevents the dissociation of the metal ion and provides electrostatic guidance for superoxide to the reactive metal center [54, 59]. The primary design concern for the development of SOD mimetics is the reduction potential of the metal center ($E_{1/2}$), which indicates the ability of the metal to accept and donate electrons in order to dismutate superoxide [60, 61]. Native SOD enzymes have an $E_{1/2}$ value of +300 mV versus the normal hydrogen electrode (NHE) and are able to equally accept and donate electrons to superoxide [61] thereby not limiting either the reduction or oxidation involved in superoxide dismutation. The SOD mimetics vary in their reduction potentials, with the most potent falling in a range of +220-350 mV [62].

Manganese pyridyl porphyrin (MnPyP) SOD mimetics have been optimized for their electrostatic properties, bioavailability, and low toxicity by the Batinic-Haberle group from Duke University. These compounds are the most potent SOD mimetics based on both the reduction potential of the manganese center as well as the k_{cat} values for SOD dismutation [62, 63]. These compounds catalyze the dismutation of superoxide through the cycling of the oxidation state of manganese, similar to the native SOD enzymes: $Mn(III)P^{+5} + O_2^{-\bullet} \rightarrow Mn(II)P^{+4} + O_2$ and $Mn(II)P^{+4} + 2H^+ + O_2^{-\bullet} \rightarrow Mn(III)P^{+5} + H_2O_2$ [64]. Three SOD mimetics were provided by the Batinic-Haberle group for use in mitigating oxidative degradation of BHV (Fig. 1.7).

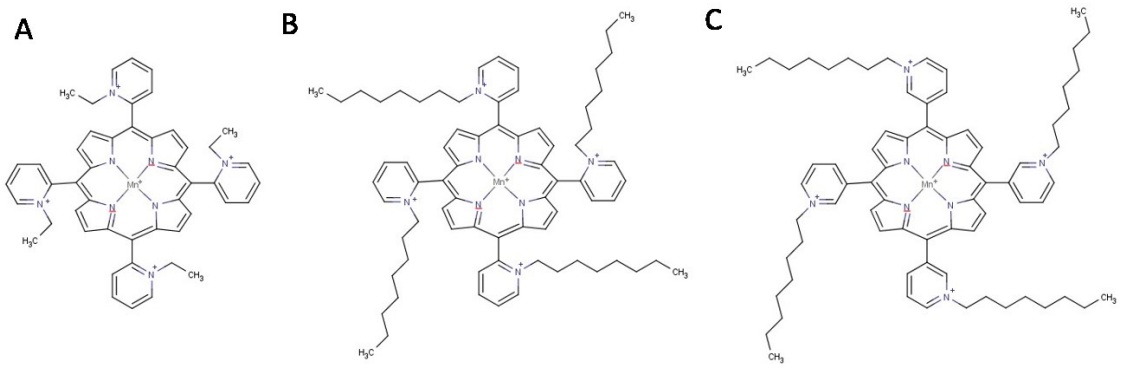

Fig. 1.7 Structures of Mn porphyrin SOD mimetics. (A) Mn(III) meso-tetrakis(N-ethylpyridinum-2-yl)porphyrin (MnTE-2-PyP), (B) Mn(III) meso-tetrakis(N-octylpyridinum-2-yl)porphyrin (MnTnOct-2-PyP), (C) Mn(III) meso-tetrakis(N-octylpyridinum-3-yl)porphyrin (MnTnOct-3-PyP).

In addition to the potent SOD activity of MnPyP, these compounds are good candidates for passive incorporation in BHV materials due to both the charge of the compounds as well as the alkyl side chains that could interact with the tissue through hydrogen bonding. Based on these properties, it may be possible to passively incorporate these compounds in BHV materials such as BP to provide stable, local antioxidant activity. Unlike DBP, an SOD mimetic catalytically removes superoxide thereby theoretically not expending its redox capacity.

1.9 Experimental systems of biomaterial oxidative damage

In order to study biomaterial oxidative stress, experimental systems that accelerate this process have been developed. Typically these systems involve exposure to hydrogen peroxide and redox-capable metal ions such as cobalt (II) or iron (II) to produce hydroxyl radicals through the Fenton reaction ($Fe^{2+} + H_2O_2 + H^+ \rightarrow Fe^{3+} + HO^{\bullet} + H_2O$) [65-67]. However, these in vitro systems are used in non-physiological levels to induce oxidative damage comparable to long-term in vivo injury [33]. Tissue-based biomaterials have not previously been tested in these accelerated systems. Therefore, it may be necessary to adjust the oxidizing conditions in order to better recapitulate the processes that occur in vivo. Although these systems do use non-physiologic conditions, they provide a means for characterization of material oxidative damage and evaluation of potential antioxidant material modifications.

1.10 Animal models

The primary animal model used to assess BHV degradation is the rat subdermal implant model. This model uses juvenile rats to achieve accelerated calcification of the BHV material implants. Compared to adult or mature rats, juvenile rats have higher serum levels of calcium, phosphorus, osteocalcin, and active alkaline phosphatase [68], which contribute to the acceleration of implant calcification. It has not been determined whether the location of the implant (subdermal rather than exposed to circulation) also contributes to accelerated calcification in this model. This model has been widely used in studies involving BHV calcification but few studies have assessed other mechanisms of BHV degradation in this system. Degeneration associated with mechanical forces, both shear and flexural, cannot be studied in this system since the implants are static. Additional characterization of this model will be necessary to determine whether oxidative stress related BHV degradation can be assessed.

The major preclinical large animal models for testing BHV are porcine or ovine valve replacement since these systems provide both exposure to circulation and shear forces in the correct anatomical location [69, 70]. However, these models have several challenges including expense, requirement for surgically trained technicians and physicians, as well as a clinical grade BHV that can be sewn in the valve position. The preparation of the clinical grade BHV is of particular concern since this typically requires a partnership with a BHV manufacturer in order to provide high quality BHV leaflets mounted to either a stent or Dacron sewing ring. An alternative ovine model has been developed in order to avoid both the valve replacement surgery and need for a clinical-grade BHV while still providing exposure to circulation and mechanical forces. This model involves the implantation of BHV leaflet patches in the aorta, pulmonary artery, and left atrium [71]. Since this is still an ovine model, there are significant costs associated with animal care as well as the surgical procedures, but it does have reduced costs as compared to the alternative of mitral valve replacement.

1.11 Aims of dissertation

The major aims of my dissertation were to determine whether oxidative stress contributes to BHV degeneration and to develop pharmacological interventions that could mitigate this process.

The first aim was to determine whether BHV are susceptible to oxidative stress and determine how this could lead to structural deterioration. Clinical BHV explants were analyzed for markers of oxidative stress to demonstrate that BHV are susceptible to oxidation. In order to determine the functional consequences of BHV oxidation, the BHV material BP was subject to the accelerated oxidative damage system as well as rat subdermal implantation. The endpoints assessed in studies with BP included both material and mechanical effects that could result in device failure. Together these approaches identified oxidative stress as a mechanism of BHV structural degeneration.

The second aim of my dissertation was to develop a pharmacological strategy to mitigate oxidation-mediated BHV structural degeneration, which was characterized in the first aim, and determine whether such an approach would effectively interfere with this process of BHV degradation. BP was modified through covalent immobilization of the oxidant scavenging compound DBP. Modified BP was subject to the accelerated oxidative damage model as well as the rat subdermal implant model in order to demonstrate that the DBP modification attenuated BHV oxidation.

In the final aim, a non-covalent modification of BP with an SOD mimetic was developed in order to improve upon the first modification strategy. SOD mimetics have the advantage over stoichiometric antioxidants such as DBP in that they can be regenerated by cellular reductants, thereby prolonging the antioxidant activity. In addition to comparing the type of compound used in the modification, the process of antioxidant incorporation could be optimized by determining whether covalent or non-covalent immobilization is more effective in sustained local delivery to BHV. The SOD mimetic loaded BP samples were tested in both the rat subdermal implant system and the sheep patch model in order to broadly assess the degeneration of BHV in terms of oxidation as well as calcification.

Chapter 2: The susceptibility of BHV leaflets to oxidation

This chapter has been published:

Christian AJ, Lin H, Connolly JM, Alferiev IS, Ferrari G, Hazen SL, Ischiropoulos H, Levy RJ. The susceptibility of bioprosthetic heart valve leaflets to oxidation. *Biomaterials*. 2014; 35:2097-102.

2.1 Abstract

Structural degeneration BHV leaflets is a significant clinical issue that results in early device failure. Here we investigated the hypothesis that BHV are susceptible to oxidative stress and that this process results in leaflet degeneration. Explants of failed clinical BHV explants were analyzed for markers of oxidative stress including several tyrosine oxidation products. Dityrosine, a crosslink that is an oxidation product of tyrosine, was elevated in the BHV explants, and was undetectable in non-implanted BHV materials glutaraldehyde treated bovine pericardium (BP) and porcine aortic valve leaflets (PAV). This elevation of dityrosine indicates that BHV are susceptible to oxidative stress. To identify a mechanism of oxidation-mediated structural degeneration, BP was exposed to experimental oxidizing conditions ($FeSO_4/H_2O_2$), which resulted in significant collagen deterioration, loss of glutaraldehyde cross-links, and increased susceptibility to collagenase degradation; thereby demonstrating that oxidation of BHV causes material degeneration. In the rat subdermal implant model of BHV calcification, BHV displayed only modest oxidation despite the presence of inflammation. However, in short-term sheep pulmonary artery catheter-deployed BHV explants, the elevation of dityrosine correlated with the clinical explants, which suggests that direct exposure to blood flow may be necessary for BHV oxidation. The formation of dityrosine in BHV explants and the effects of exposure to oxidizing conditions on the integrity of the collagen structure and glutaraldehyde cross-links support the hypothesis that oxidative stress is a mechanism of BHV structural degeneration.

2.2 Introduction

BHV are widely used in heart valve replacement surgeries for their hemodynamic properties and low risk of thromboembolism in comparison with mechanical heart valves [2]. Unfortunately, BHV have poor durability caused by leaflet structural deterioration associated with calcification, mechanical stress, or inflammation [5, 14, 18, 21]. Due to the prevalence of calcification in failed clinical BHV explants, calcification prevention and mechanisms have been the major focus of BHV research [5]. Despite advancements in these areas, particularly the development of BHV anti-calcification strategies, structural degeneration of BHV leaflets remains a significant clinical issue. Therefore, in this work we focused on the role of a non-calcific mechanism, oxidative stress, in BHV structural deterioration.

Oxidative stress is a significant mechanism of material degradation for synthetic biomaterials such as polyurethane since reactions of ROS/RNS with the material leads to surface pitting and cracking [25, 36]. The effects of ROS/RNS on a tissue-derived biomaterial such as BHV have not previously been investigated. However, previous studies have demonstrated that BHV elicit a host inflammatory response, thereby locally producing ROS/RNS [21, 22, 72]. In addition, collagen, the primary component of BHV materials, is susceptible to fragmentation and cross-link breakdown as a result of oxidation; this also leads to an increase in susceptibility to proteolytic degradation [28, 29, 56, 73, 74]. Based on this evidence, we hypothesized that oxidative stress resulting from the production of ROS/RNS by inflammatory cells is involved in BHV structural degeneration. In order to verify this hypothesis, we first analyzed clinical BHV explants for markers of oxidative stress to demonstrate that BHV oxidation occurs in patients.

There are several types of markers that have been used to identify oxidative stress in biological samples, which include lipid [75], DNA [76], and protein [77, 78] oxidation products. BHV leaflets are composed primarily of protein (collagen) rather than DNA and lipids since these components are removed by either glutaraldehyde cross-linking or ethanol pre-treatment, which is used in a subset of clinical valves [79]. Therefore, protein oxidation products may be more useful for identifying oxidative stress in BHV leaflets. Modifications of proteins by oxidants have been widely studied as potential biomarkers for various disease states associated with oxidative stress

[78, 80-83]. Phenylalanine and tyrosine are common sites of oxidant attack and result in the formation of *o,o*-dityrosine, ortho-tyrosine, meta-tyrosine, nitrotyrosine, chlorotyrosine, and bromotyrosine; the adduct formed is dependent on the type of oxidant involved [77, 78, 84]. For example, bromotyrosine and chlorotyrosine are formed through reactions involving brominating and chlorinating species such as hypobromous acid and hypochlorous acid, respectively [85]. Higher levels of product oxidation products are expected in tissues subject to oxidative stress, potentially such as BHV materials. The mentioned phenylalanine and tyrosine oxidation products were therefore assessed in clinical BHV explants.

Due to the significance of oxidative damage to synthetic biomaterials, experimental systems of accelerated oxidative damage have been developed to study these processes [65-67]. BHV materials such as BP and PAV have not previously been tested in such a system. However, these accelerated systems may be useful in the identification of functional consequences of oxidative stress which would otherwise be difficult to study in short-term animal models. Since oxidation is known to cause collagen fragmentation, cross-link breakdown, and an increase in susceptibility to proteolytic degradation, these effects were assessed in BHV materials using an accelerated oxidative degradation model.

The rat subdermal implant model is commonly used to assess BHV degradation associated with calcification since this system results in accelerated implant calcification due to the use of juvenile rats that have higher serum concentrations of pro-calcification factors such as alkaline phosphatase [43, 68]. BHV oxidation was assessed in this model to determine whether this system could be useful in studying non-calcific mechanisms of BHV structural degeneration. In addition to inflammation, which can be studied in the subdermal implant model, other factors such as direct circulatory contact and exposure to mechanical forces are likely involved in the progression of BHV oxidation and are not represented in this system [86, 87]. Therefore, it may be necessary to use alternative animal models to fully recapitulated non-calcific mechanisms such as oxidative stress.

In addition to clinical BHV explants and rat subdermal explants, catheter-deployed BHV explants from a sheep circulatory model were analyzed for BHV oxidation to determine whether circulatory exposure is necessary for BHV oxidation. The availability of these explants provided

valuable comparison between animal models used in the assessment of BHV as well as with clinical BHV explants.

Here we used several approaches to assess the susceptibility of BHV leaflets to oxidation and the functional consequences of this process. These approaches included analysis of clinical and sheep BHV explants for protein oxidation products, BHV degradation in an accelerated oxidative damage model, and rat subdermal implantation of the BHV material BP for assessment of oxidation endpoints.

2.3 Materials and Methods

Materials

Glutaraldehyde and a Von Kossa staining kit were purchased from Polysciences, Inc (Warrington, PA). Biosol and Bioscint were purchased from National Diagnostics (Atlanta, GA). ^{3}H-glutaraldehyde was purchased from American Radiolabeled Chemicals (St. Louis, MO). All chemicals unless otherwise specified were purchased from Sigma Aldrich (St. Louis, MO).

Human BHV explants

Between 2010 and 2012, 3 PAV BHV and 16 BP BHV were collected from patients according to the University of Pennsylvania IRB approved protocol #809349. Informed consent was obtained from patients requiring repeat aortic valve replacement due to a failing BHV at the Hospital of the University of Pennsylvania. Patients with bioprosthetic aortic valve failure due to pannus, thrombus, and endocarditis were excluded from the study. Explanted bioprosthetic aortic valves were fixed in 10% buffered formalin overnight, followed by dehydration in 70% ethanol solution, and stored at 4˚C. A single leaflet from each clinical BHV explant was embedded in paraffin according to standard procedures for histology and quantification of oxidized amino acids.

Calcification

For quantification of calcium content in clinical BHV, a single leaflet was hydrolyzed in 6 N HCl at 100 °C and dried under air flow. The hydrolysates were reconstituted in 0.01 N HCl. Calcium quantification was done using a Perkin Elmer 2380 atomic absorption spectrophotometer [88]. The Von Kossa staining method was used for qualitative calcification determination [89]. Paraffin sections of explanted BHV were rehydrated with ethanol and stained with silver nitrate using a Von Kossa Calcium Kit according to manufacturer directions.

Morphology

Masson's trichrome and picrosirius red stains were used to assess explant morphology. Paraffin sections (6 μM) were prepared for staining procedures. Slides were rehydrated through xylene and ethanol. For Masson's trichrome, slides were stained according to the kit protocol (Sigma). For picrosirius red, slides were stained for 1 hour with 0.1% Sirius red in saturated picric acid [90]. Stained sections were then dehydrated and mounted with permount for microscopy.

Quantification of oxidized amino acids

Oxidized amino acid quantification was performed by the lab of Stanley Hazen at the Cleveland Clinic. Oxidized amino acids were quantified by established stable isotope dilution liquid chromatography tandem mass spectrometry (LC MS/MS) methods on an AB SCIEX API 5000 triple quadrupole mass spectrometer interfaced with an Aria LX Series HPLC multiplexing system (Cohesive Technologies Inc., Franklin, MA) [85]. Briefly, paraffin embedded BHV leaflets were deparaffinized by xylene. [$^{13}C_6$]-labeled oxidized amino acid standards and universal labeled precursor amino acids ([$^{13}C9$,$^{15}N1$]tyrosine and [$^{13}C9$,$^{15}N1$]phenylalanine) were added to samples after protein delipidation and desalting with a single phase mixture of H_2O/methanol/H_2O-saturated diethyl ether (1:3:8 v/v/v). Proteins were hydrolyzed under argon gas in methane sulfonic acid, and then samples were passed through C18 solid-phase extraction column (Discovery – DSC18 minicolumn, 3 ml, Supelco, Bellefone, PA) prior to MS analysis. Individual oxidized amino acids and their precursors were monitored by characteristic parent to product ion transitions unique for

each isotopologue monitored. Results are expressed relative to the content of the precursor amino acids, tyrosine and phenylalanine.

BP preparation

Fresh BP obtained from an abattoir was treated with 0.625% glutaraldehyde or 0.625% ^{3}H-glutaraldehyde (specific activity 24 μCi/mmol) in HEPES buffer pH 7.4 for 7 days at room temperature with gentle shaking. All BP samples were stored in 0.2% glutaraldehyde [68].

Accelerated oxidative damage model

A modified model of accelerated oxidative damage previously used with polymeric biomaterials was used to assess BP oxidation [66]. BP samples were incubated in PBS or 1% H_2O_2/100 μM $FeSO_4$ for 7 days with solution changes every 2-3 days. Lyophilized samples were weighed at the start and end of treatments to determine bulk material loss. Picrosirius red staining was done on formalin-fixed, paraffin-embedded samples. BP treated with ^{3}H-glutaraldehyde was monitored for the release of ^{3}H into the reaction solutions, as well as in the solubilized tissues at the end of the treatments. ^{3}H-BP were solubilized with Biosol and analyzed by liquid scintillation counting in Bioscint following exposure to oxidizing conditions. Collagenase digestion was performed on lyophilized BP following the 7 day oxidation assay. Collagenase (600 U/mL) was added to BP samples and incubated for 24 hours at 37°C. Digestion by collagenase was measured as a loss of weight following collagenase treatment.

Rat subcutaneous BP implants

Three week old male, Sprague-Dawley rats (60-90 grams) were used for subdermal implantation studies [68]. Surgical procedures were performed according to guidelines from the Institutional Animal Use and Care Committee at the Children's Hospital of Philadelphia. Rats were anesthetized with isofluorane and shaved prior to preparing two dorsal subdermal pouches. BP samples were implanted in subdermal pouches for 2-3 samples per animal. The BP samples were explanted with (en bloc) or without surrounding tissue intact at 7, 21, or 90 days. For "pre-oxidized" studies, BP was exposed to 1% H_2O_2/100 μM $FeSO_4$ prior to implantation. In order to assess the

inflammatory response to the BP implant, the implants were removed en bloc, with the surrounding tissue intact. Formalin-fixed en bloc sections were embedded in paraffin and stained with Masson's Trichrome, hematoxylin and eosin (H&E), or myeloperoxidase (MPO) immunohistochemistry. MPO immunohistochemistry was performed by the CHOP Pathology core facility. Image analysis of H&E and Masson's Trichrome stains was used to determine the thickness of the cellular and fibrous capsules, respectively. For image analysis 5-10 images were taken of each biologic replicate (n=3-5 per group) and 5 measurements were made per image to account for heterogeneity in the inflammatory or fibrous capsules. For cellular infiltration localization studies, en bloc explants were oriented in the plane of the tissue rather than in a cross-sectional area. Three 8 μm serial sections were made at each depth with 100 μm separating each depth. Image analysis was performed with ImageJ to determine the percent of hematoxylin stained cells in each section. For each biologic replicate, 3-5 images were used with 5 measurements per image to determine percent hematoxylin staining of total area.

Hydroxyproline quantification

Hydroxyproline content of rat subdermal explants was quantified with ^{1}H-NMR, performed at 400MHz on a Bruker Avance III™ 400 wide-bore spectrometer by Suzanne Werhli of the CHOP NMR core. Explant acid hydrolysates (0.6 mL) were introduced in a 5 mm NMR tube. An external standard made of a sealed capillary containing a solution of trimethylsilylpropionic acid (TSP) in D_2O was used as chemical shift reference and quantification standard. Fully relaxed proton spectra were acquired with a 5 mm BBO probe. Standard acquisition conditions were as follows: PW 45o, TR 8s, water saturation during the relaxation delay, SW 6775 Hz, TD 64k and 64 scans. Explant acid hydrolysates, hydroxyproline, or acid hydrolysates with added hydroxyproline were first analyzed to identify spectral peaks unique to hydroxyproline. Quantification of the hydroxproline peaks was performed by normalization to the TSP standard (Fig. 2.1), provided by Suzanne Werhli.

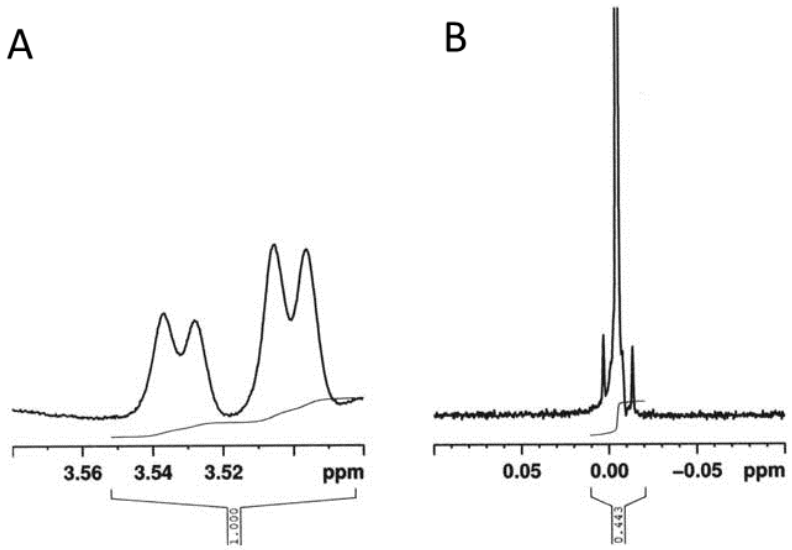

Fig. 2.1 Hydroxyproline quantification by ^{1}H-NMR. Spectral peaks corresponding to hydroxyproline in tissue acid hydrolysates (A). Normalization of peaks to the internal standard TSP (B).

Differential scanning calorimetry

Cross-linking of non-implanted glutaraldehyde fixed BP and rat subdermal BP explants was measured by differential scanning calorimetry (DSC) on a Perkin Elmer DSC 7 [91]. Samples that were hermetically sealed in aluminum pans were placed in the DSC where sample temperature was ramped from 25°C to 100° C until the endothermic peak corresponding to thermal denaturation was observed.

Sheep bovine jugular vein BHV pulmonary artery implants

Percutaneous bilateral branch pulmonary artery valve implantation of BJV BHV was performed in an ovine model of postoperative pulmonary valve insufficiency as previously described by the Gorman Cardiovascular Research Group [92]. BJV were explanted at 3 months

Statistical Methods

Results are shown as the mean ± standard error for the mean. Single ANOVA with Tukey's test, Mann-Whitney rank sum test or a two tailed t-test were used to determine significance, which was defined as a p value less than 0.05.

2.4 Results

Characterization of clinical BHV

The clinical BHV explants were characterized in terms of patient demographics, calcification, and morphology. Of the 19 clinical BHV, 16 were BP and 3 were PAV. The patient population from which the clinical BHV explants were obtained had roughly equal numbers of males and females and concomitant heart surgery was performed in 8 of the subjects (Table 2.1). The explanted BP BHV were primarily Carpentier Edwards except for one Sorin BHV. The majority of the patients had underlying medical conditions (Table 2.1). No correlations were made from patient data with BHV degeneration processes due to the small sample size.

Clinical Data	
Variable	
Age	65.3 ± 16.2 (31-84)
Gender	
Male	58% (11)
Female	42% (8)
BMI (kg/m^2)	29.2 ± 4.8
BSA (m^2)	2.0 ± 0.2
Previously Bicuspid Aortic Valve	42% (8)
Arterial Hypertension	68% (13)
Hyperlipidemia	68% (13)
Coronary Artery Disease	47% (9)
Diabetes mellitus	42% (8)
Renal Disease	21% (4)
Smoking History	21% (4)
NYHA	
Class I	0% (0)
Class II	26% (5)
Class III	37% (7)
Class IV	32% (6)
Prosthetic Valve Information	
Carpentier-Edwards	79% (15)
St. Jude	16% (3)
Sorin	5% (1)
Explanted Valve Size (mm)	
19	11% (2)
21	26% (5)
23	21% (4)
25	21% (4)
27	21% (4)
Valve Age	6.5 ± 2.3 (1.5-10.9)
Concomitant Surgery	
None	58% (11)
CABG	16% (3)
Mitral Valve Repair	11% (2)
Mitral Valve Replacement	5% (1)
Ascending Aorta Replacement	21% (4)

BMI, Body Mass Index; *BSA*, Body Surface Area; *NYHA*, New York Heart Association; *CABG*, Coronary artery bypass grafting.

Table 2.1 Clinical patient characteristics of BHV explants. NYHA, New York Heart Association; CABG, Coronary artery bypass grafting.

Calcification of the clinical BHV explants was assessed using both quantitative and qualitative methods. Variable amounts of calcification were present in both PAV (Fig. 2.2A) and BP (Fig. 2.2B) BHV explants as assessed by Von Kossa, which was scored on a scale of 0 (no calcium staining) to 3 (most severe) to demonstrate the distribution of explant calcification (Fig. 2.2C). By atomic absorption spectroscopy, the mean calcium level in explanted BHV was 106.2 μg calcium/mg tissue ± 23.9. These results demonstrate variable degrees of clinical BHV explants calcification, but with a mean corresponding to previously reported values [93].

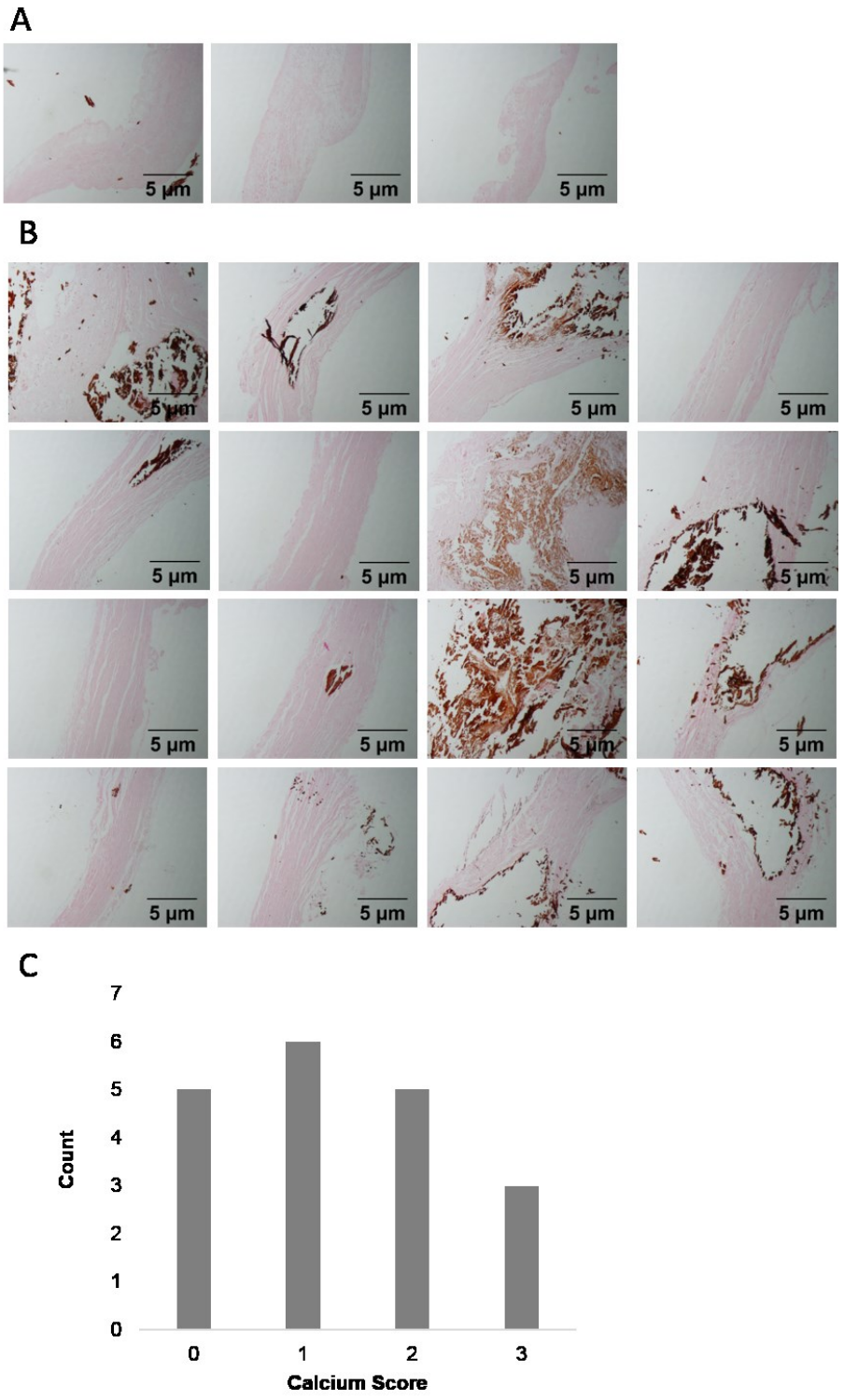

Fig. 2.2 Calcification of clinical BHV. Von Kossa staining of (A) PAV and (B) BP BHV explants, 40x. (C) Histogram showing distribution of calcium scores from Von Kossa staining.

Morphology of both the PAV and BP BHV was assessed by picrosirius red and Masson's trichrome stains to identify structural deterioration. Picrosirius red and Masson's Trichrome both stain collagen, but only Masson's Trichrome differentiates cells, smooth muscle, and collagen [94]. PAV, both non-implanted and explanted BHV, stain mostly for collagen (blue with Masson's Trichrome, red with picrosirius red) with some cellular staining (Fig. 2.3). BP is also primarily collagen but is more organized than PAV with parallel collagen fibrils (Fig 2.4). BHV explants, both PAV and BP, did not demonstrate collagen deterioration as would be expected with clinical use. These results show that despite clinical failure, the BHV explants do not have significant structural deterioration.

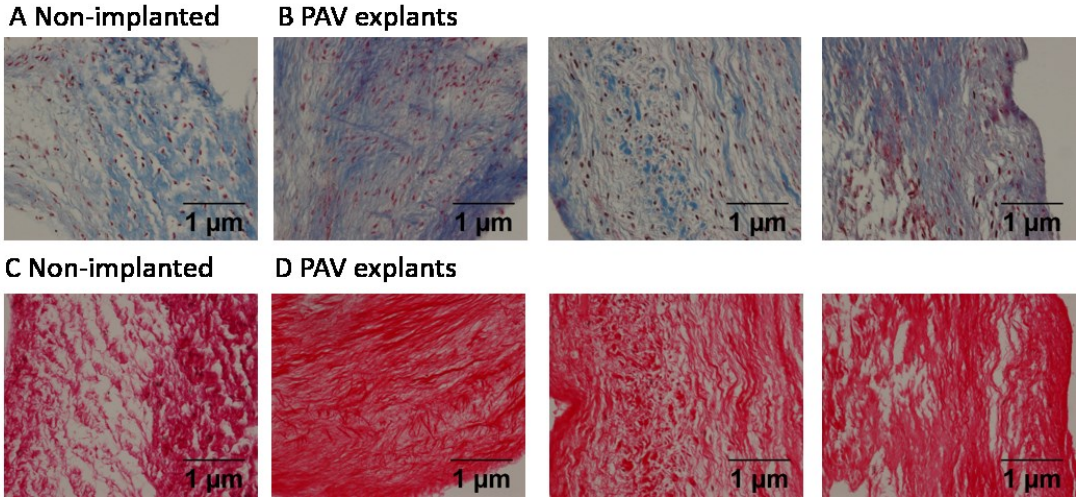

Fig. 2.3 Morphology of clinical PAV BHV. Masson's trichrome of PAV, (A) non-implanted and (B) explants Picrosirius red of PAV, (C) non-implanted and (D) explants, 200x.

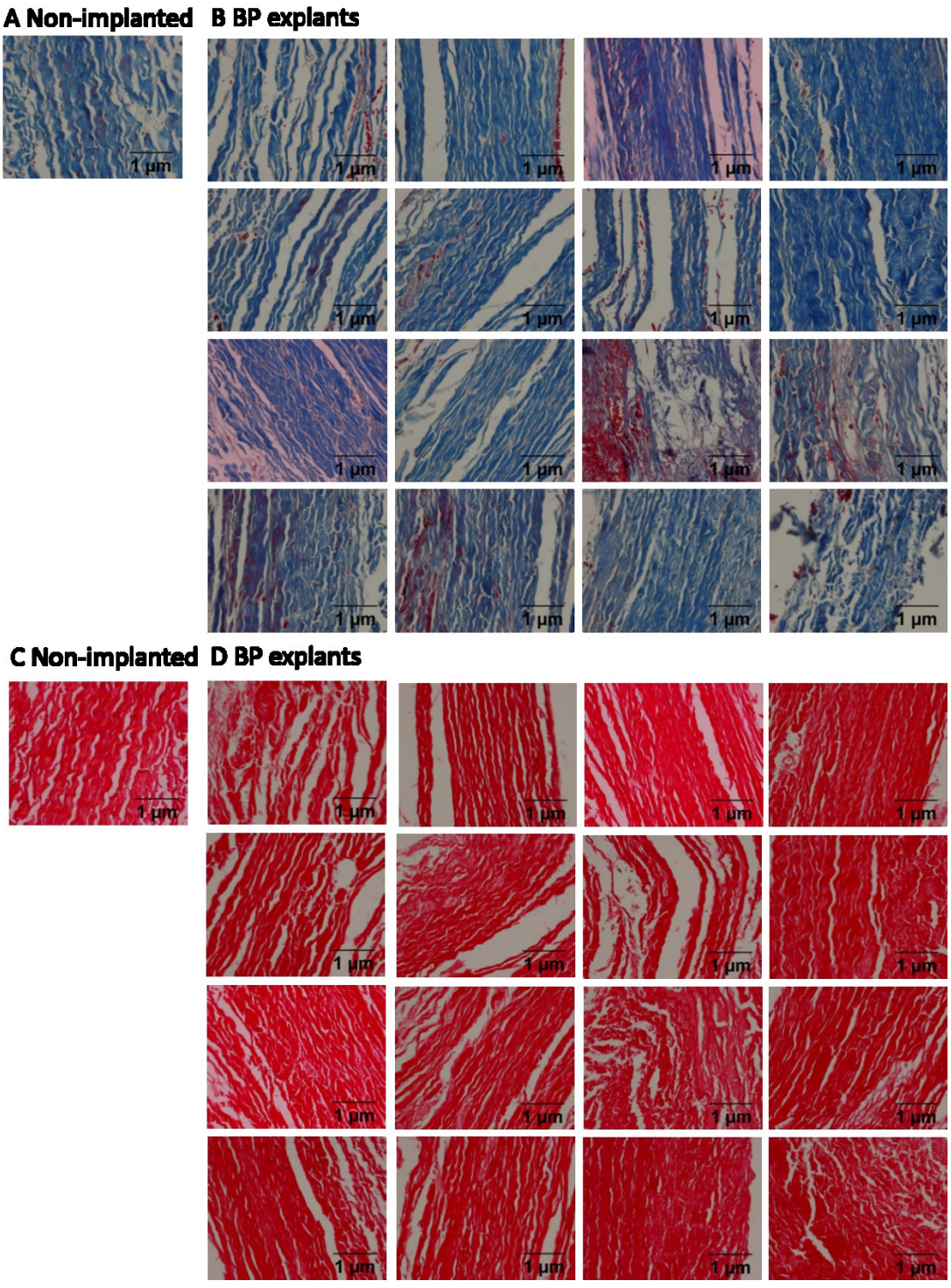

Fig. 2.4 Morphology of clinical BP BHV. Masson's trichrome (A) non-implanted and (B) explanted BP. Picrosirius red (C) non-implanted and (D) explanted BP, 200x.

Oxidized amino acids in clinical BHV

Six structurally distinct oxidized amino acids were quantified in clinical PAV and BP BHV explants to determine whether these materials are susceptible to oxidative stress and to assess whether specific oxidants or pathways are involved in BHV oxidation. PAV and BP clinical BHV were analyzed separately to determine whether oxidation was dependent on the type of heterograft material. The clinical PAV BHV explants had decreased levels of meta-tyrosine ($p<0.001$), ortho-tyrosine ($p<0.001$), and chlorotyrosine ($p=0.024$) as compared to non-implanted PAV (Fig. 2.5). Dityrosine was not present in non-implanted PAV but was measured in the PAV BHV explants ($p=0.198$). Nitrotyrosine and bromotyrosine levels were not significantly different between non-implanted PAV and PAV BHV explants. The presence of all oxidation products except dityrosine in the non-implanted control material indicates that some oxidation may occur in either the animal from which the tissue is derived or in the processing and handling of the tissues for BHV fabrication. Therefore, these markers may not represent an oxidative environment resulting from the patient's inflammatory response to the BHV. However, the accumulation of dityrosine in PAV BHV explants and absence in control material indicates that dityrosine may be a marker of oxidative stress for BHV explants.

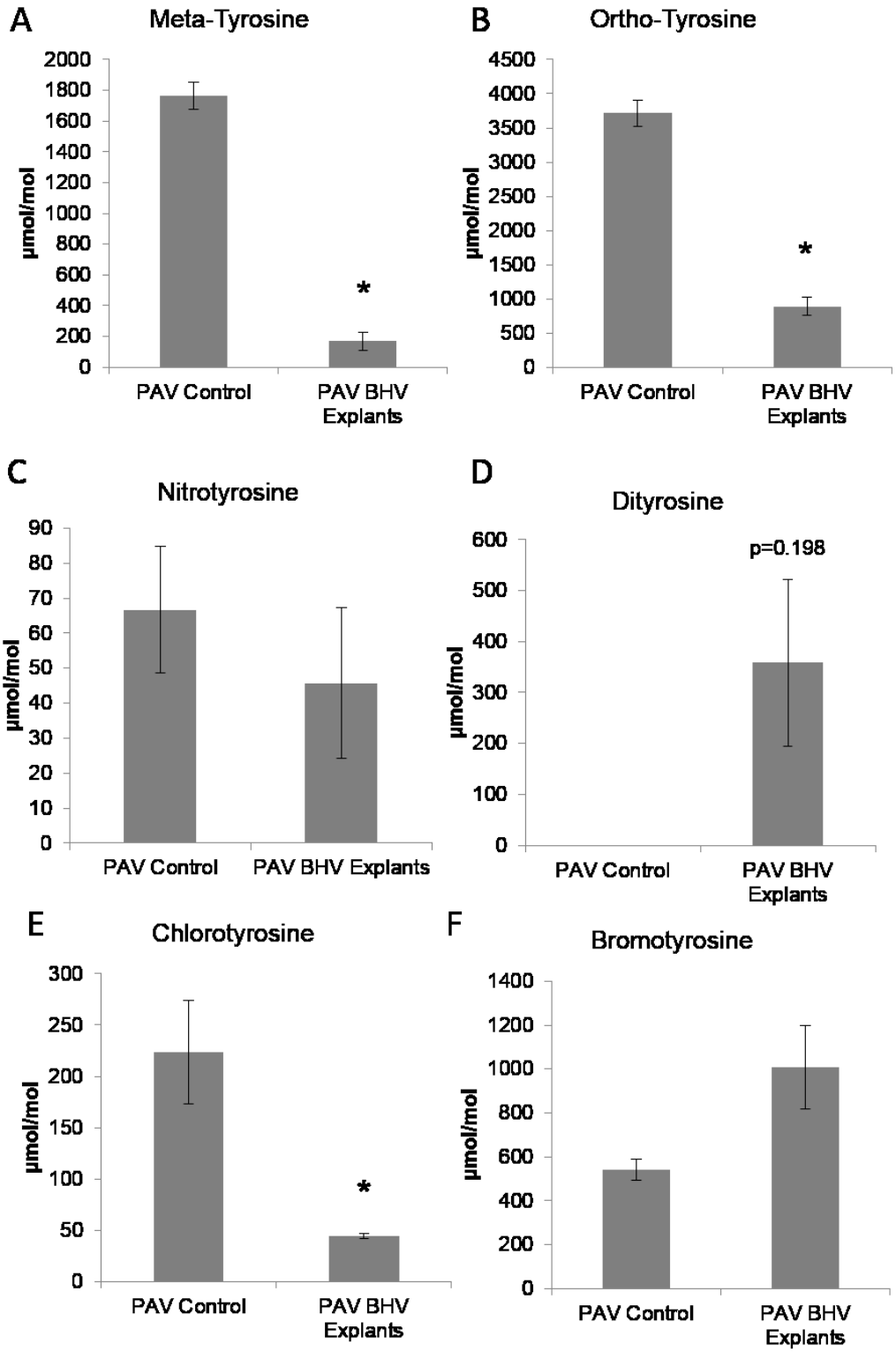

Fig. 2.5 Oxidized amino acids in clinical PAV BHV. Meta-tyrosine (A), ortho-tyrosine, (B), nitrotyrosine (C), dityrosine (D), chlorotyrosine (E), and bromotyrosine (F), n=3. * $p<0.05$ explants vs. non-implanted control.

The same structurally distinct oxidation products analyzed in PAV BHV explants were quantified in BP BHV explants. Compared to non-implanted BP, clinical BP BHV explants had elevated levels of meta-tyrosine ($p < 0.01$), ortho-tyrosine ($p < 0.01$), and dityrosine ($p < 0.01$); nitrotyrosine levels were lower in explants ($p=0.0156$) (Fig. 2.6). There were no significant differences in bromotyrosine or chlorotyrosine between non-implanted BP and BP BHV explants. These results are similar to the PAV BHV results in that all oxidation products except for dityrosine are present in non-implanted materials. Together the PAV and BP BHV results demonstrate that dityrosine may be a marker specific to BHV oxidation since it is not present in non-implanted materials and is independent of material type (PAV or BP).

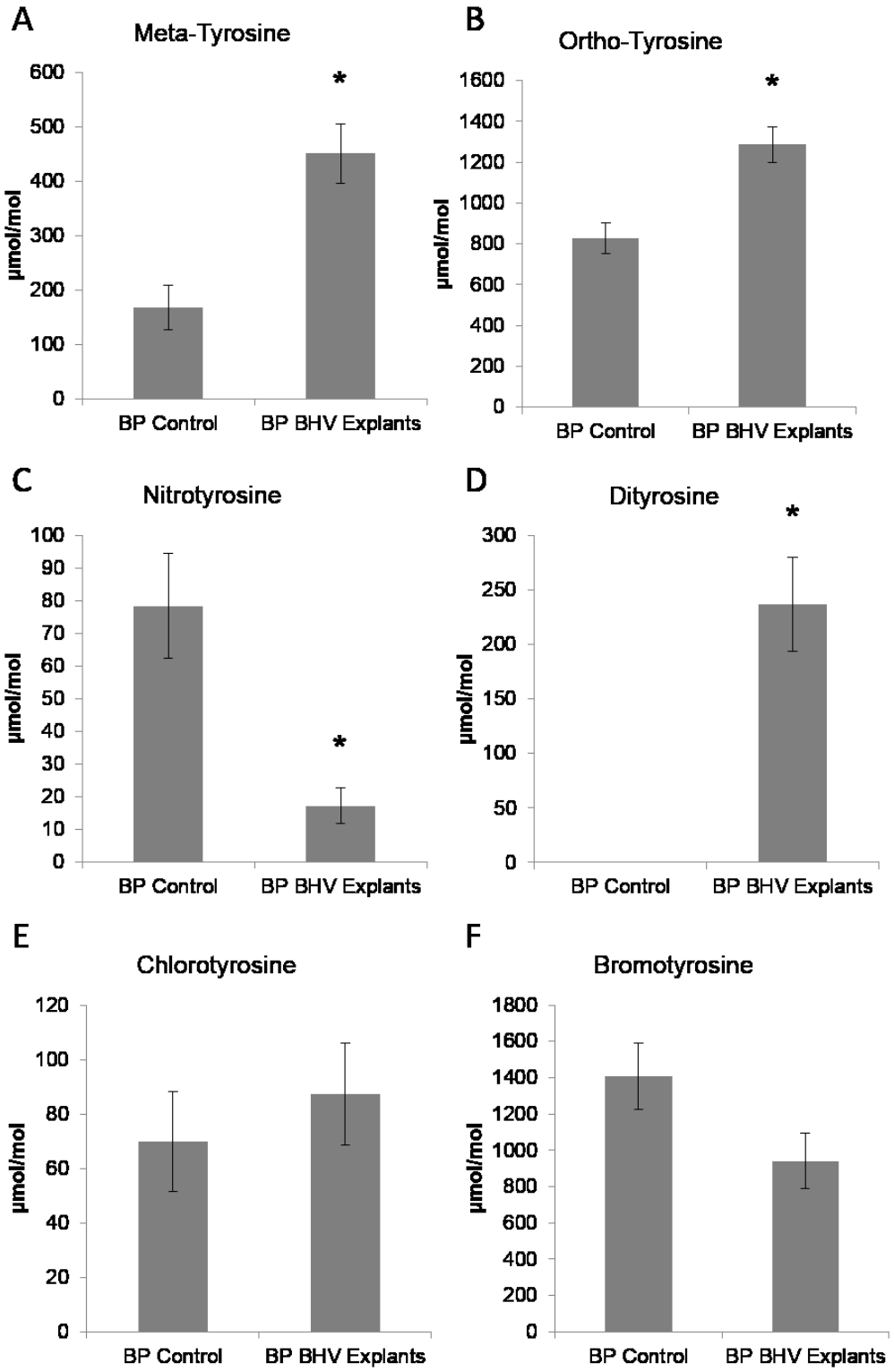

Fig. 2.6 Oxidized amino acids in clinical BP BHV. Meta-tyrosine (A), ortho-tyrosine, (B), nitrotyrosine (C), dityrosine (D), chlorotyrosine (E), and bromotyrosine (F), n=16. * $p<0.05$ explants vs. non-implanted control.

Experimental oxidation of BHV material BP

Analysis of the clinical BHV explants demonstrated BHV susceptibility to oxidation, however, no direct functional effects of oxidation were identified. Therefore, BP was subject to a model of accelerated oxidative damage (1% H_2O_2, 100 μM $FeSO_4$) to assess structural effects of BHV oxidation that may result in material failure. Oxidation of BP in this system resulted in significant destruction of the collagen structure as shown by picrosirius red staining of collagen (Fig. 2.7A-B). In addition, oxidation caused significant mass loss of BP as well as increased digestion by collagenase (Fig. 2.7C). BP that had been cross-linked with ^{3}H-glutaraldehyde was tested in this system to determine whether oxidizing conditions causes a loss of the glutaraldehyde cross-links. In PBS incubations over 7 days, the amount of ^{3}H-glutaraldehyde released was 14.1 ± 1.3% of the total ^{3}H-glutaraldehyde incorporated in the tissue, whereas with oxidation the loss was 75.7 ± 5.4% (Fig. 2.7D). These results indicate that oxidation of BP results in significant material degeneration including mass loss, collagenase digestion, and breakdown of glutaraldehyde cross-links.

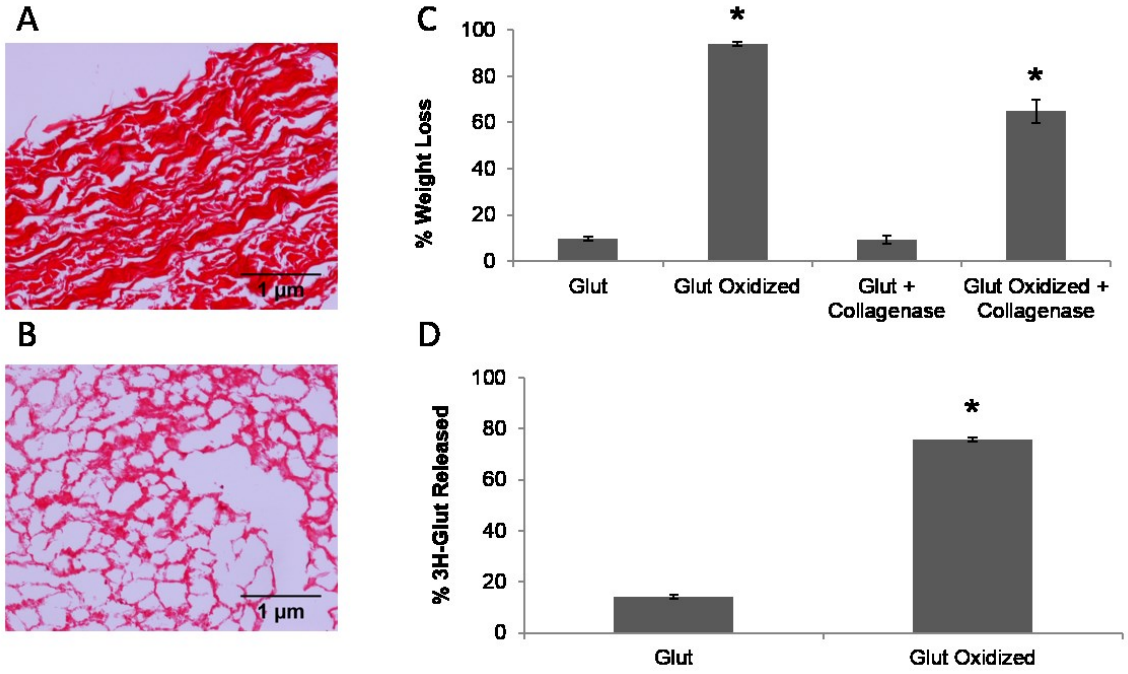

Fig. 2.7 Experimental oxidation of BP. BP exposed to 1% H_2O_2 and 100 uM $FeSO_4$ for 7 days. Picrosirius red staining, untreated BP (A) and oxidized BP (B), 200x. Material weight loss with oxidation and collagenase digestion (C). Release of ^{3}H-glutaraldehyde from BP with and without oxidation (D). $p<0.05$ oxidized BP vs untreated BP.

Oxidation of BP rat subdermal explants

To determine if oxidation of the BHV material BP occurs in the rat subdermal implant model of BHV calcification and whether this model could be useful in further studies of BHV oxidation, BP explants were assessed for endpoints that may reflect BHV oxidative damage including loss of hydroxyproline, collagenase digestion, shrink temperature, and collagen deterioration. Since BHV oxidation had not previously been assessed, several endpoints were used in order to identify parameters of oxidative damage.

Hydroxyproline is an amino acid abundantly found in collagen, the primary protein component of BHV materials such as BP [95]. A loss of hydroxyproline content would therefore correlate with a decrease in collagen content. Hydroxyproline was quantified by ^{1}H-NMR in acid hydrolysates of non-implanted BP as well as rat subdermal explants from 21 and 90 day studies. Hydroxyproline content was significantly lower in the explanted materials as compared to non-implanted BP (Fig. 2.8A). Additionally, hydroxyproline content was lowest in 90 day explants

indicating a progressive loss of hydroxyproline or collagen throughout the duration of implantation. Since the explanted materials are also highly calcified, it is possible that the accumulation of calcium is correlated with a loss of hydroxyproline since calcium deposits could add weight to the sample or disrupt collagen structure. To assess this relationship, hydroxyproline content was plotted as a function of calcium and Pearson's coefficient was used to measure correlation (Fig. 2.8B). Calcium and hydroxyproline content of rat explants have a strong negative correlation (ρ=-0.91). Therefore it is possible that calcification could be responsible for the observed loss of hydroxyproline.

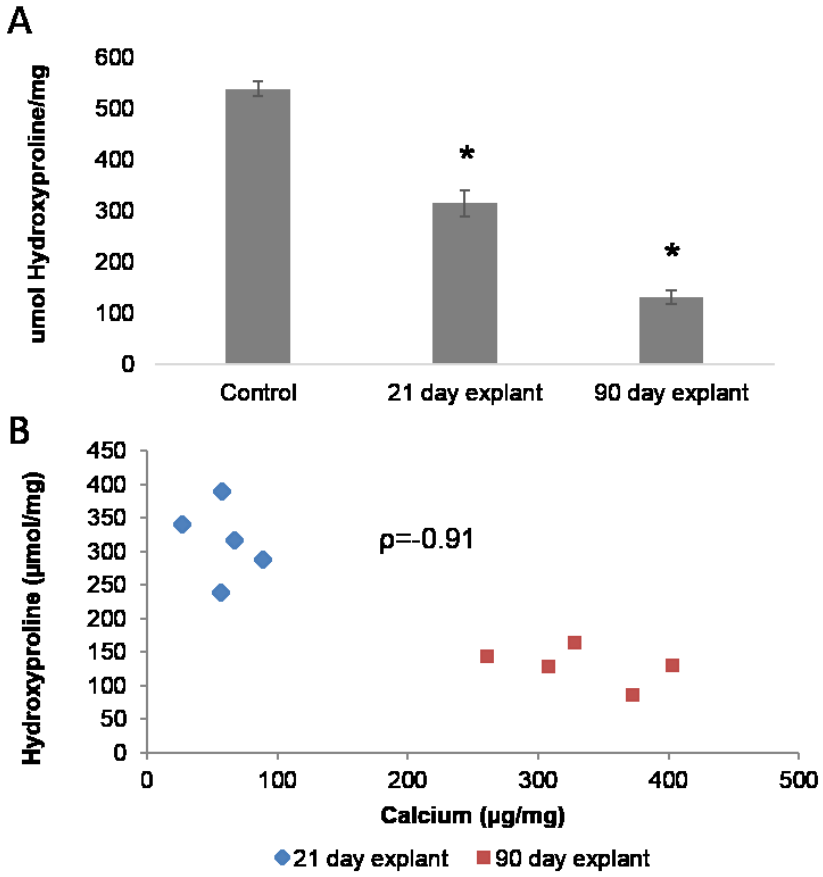

Fig. 2.8 Hydroxyproline content BP rat subdermal implants. Hydroxyproline levels in non-implanted and 21 or 90 day explants (A). Correlation between hydroxyproline content and calcium accumulation (B).

Weight loss of BHV samples due to collagenase digestion, which was elevated following oxidation in the accelerated oxidative damage model, was significantly higher in the 21 day BP rat subdermal explants, but not the 90 day samples (Fig. 2.9A). These results demonstrate that collagenase digestion may cause degradation of BP in early stages of implantation but appears to be less damaging in longer-term explants.

Differential scanning calorimetry was used to assess material cross-linking of BP to determine whether BP rat subdermal explants lose cross-linking during implantation. The shrink temperature of 90 day rat subdermal implants was significantly lower than the non-implanted BP, which indicates a loss of cross-linking (Fig. 2.9B).

Picrosirius red staining was done on non-implanted (Fig. 2.9C), 21 day (Fig 2.9D), and 90 day (Fig. 2.9E) rat subdermal explants to assess the degree of collagen damage following implantation. There were no appreciable differences in the collagen structure between the two groups. These results suggest that in this model of BHV degradation and at these time points, the BP structure is not significantly deteriorated.

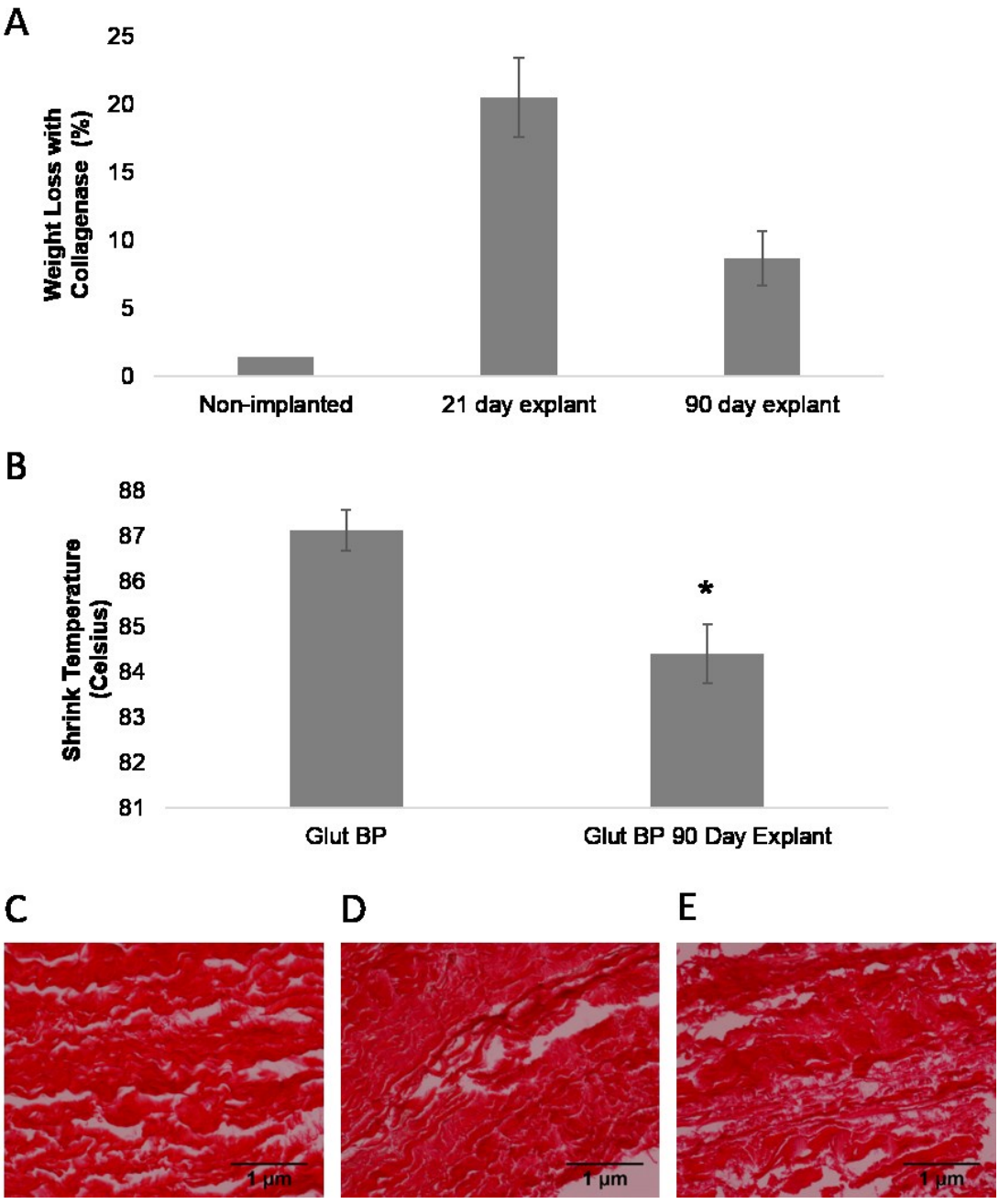

Fig. 2.9 Oxidation of BP rat subdermal implants. Weight loss after collagenase treatment (A). Shrink temperature by DSC (B). Picrosirius red staining non-implanted (C), 21 day explant (D), 90 day explant (E), 200x magnification. *p<0.05 vs non-implanted control.

Rat subdermal explants of BP from 7 and 21 day experiments were analyzed for structurally distinct oxidative modification by mass spectrometry to determine if this model correlates with levels in clinical BHV. The trends of all 6 oxidized amino acid levels correlated with the clinical BP BHV explants in terms of relatively higher or lower levels in explants as compared to non-implanted BP (Fig. 2.10). Meta-tyrosine in Glut BP explants was significantly elevated in 21 day explants but not 7 day explants (Fig. 2.10A). Ortho-tyrosine was significantly decreased in 7 day explants but was not significantly different than non-implanted tissue in 21 day explants (Fig. 2.10B). Nitrotyrosine was significantly lower in both 7 and 21 day explants as compared to non-implanted BP (Fig. 2.10C). Dityrosine was detectable only in 21 day explants (Fig. 2.10D). Chlorotyrosine and bromotyrosine levels in explants were not significantly different than non-implanted BP (Fig. 2.10E-F). All 6 adducts were analyzed although the clinical BHV explants suggested that only dityrosine was specific to BHV oxidation in order to determine whether the oxidation pathways involved were different in the rat model. Dityrosine was only present in 21 day explants and at very low levels as compared to the clinical BHV explants. Therefore, these results suggest that 21 day rat subdermal implants have modest oxidation, but longer time points or alternative animal models may more closely recapitulate the clinical BHV oxidation results.

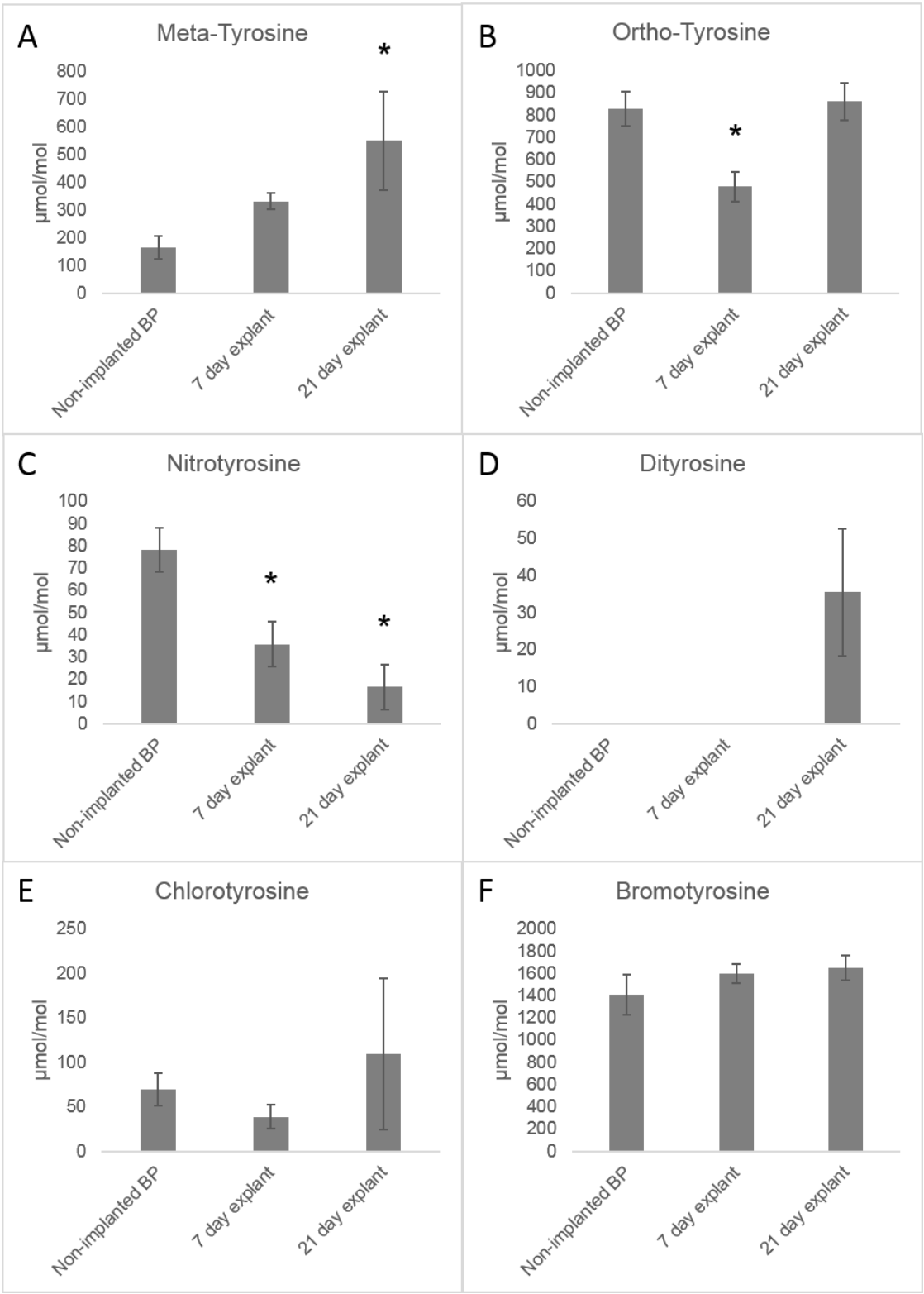

Fig. 2.10 Oxidized amino acids in BP rat subdermal explants. (A) Meta-tyrosine (B) ortho-tyrosine (C) nitrotyrosine, (D) dityrosine, (E) chlorotyrosine, and (F) bromotyrosine. * $p<0.05$ vs non-implanted control.

Calcification of pre-oxidized BP rat subdermal implants

Since calcification is a significant cause of BHV degradation, we performed a small pilot study with 5 rats where BHV materials were "pre-oxidized" with $H_2O_2/FeSO_4$ then implanted for 90 days (Fig. 2.11A). Surprisingly, these samples had nearly no calcium accumulation as compared to the control tissues that had median calcium levels around 300 μg/mg. In addition, the "pre-oxidized" samples had lower shrink temperatures prior to implantation, indicating less cross-linking (Fig. 2.11B). Therefore, this loss of cross-linking by oxidation may be associated with reduced calcification. However, since the oxidation of the BP samples was performed artificially or at non-physiologic conditions, this process may not occur in vivo.

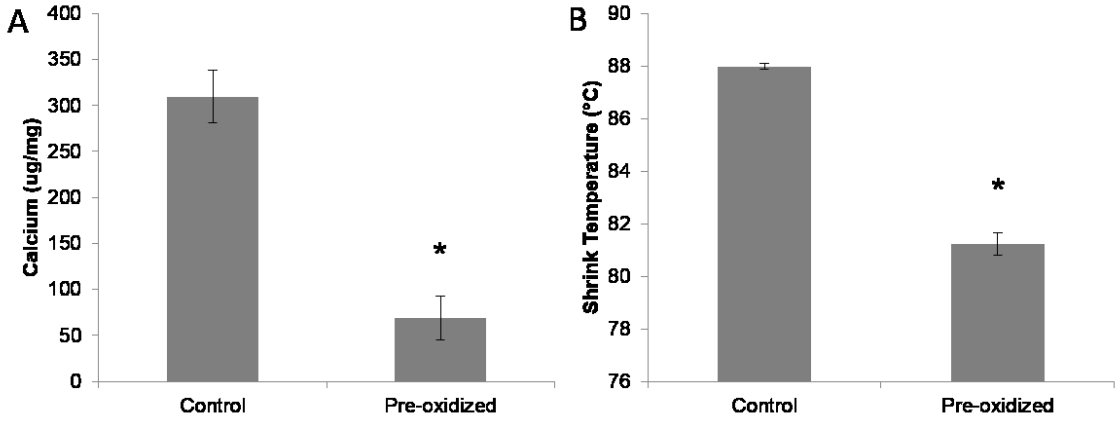

Fig. 2.11 Pre-oxidized BP rat subdermal explants. (A) Calcification of 90 day rat subdermal explants. (B) Shrink temperature of non-implanted control and pre-oxidized materials.

Inflammation in rat subdermal models

The BHV leaflet material BP had very low dityrosine accumulation in the rat subdermal implant model, which suggests that BHV oxidation may not be fully represented in this model. Due to this finding, additional studies were performed to determine whether there is an attenuated inflammatory response to the implanted materials in this system. Inflammatory cells are the primary source of ROS/RNS that would oxidize the implanted material therefore a modest inflammatory response would result in less material oxidation. In the first system, rat subdermal explants of BP (7, 21, and 90 day) were removed en bloc and stained with H&E to determine cellular recruitment to the materials (Fig. 2.12A-C). The thickness of the inflammatory capsule between the explant surface and the muscle layer was quantified with ImageJ using 40x images. The inflammatory capsule is thickest in the 21 day explants but also present in the 7 day explants (Fig 2.12D). The 90 day explants do not appear to have a cellular inflammatory capsule but rather more organized, potentially fibrous tissue (Fig. 2.12C); therefore the thickness of the capsules were quantified only in the 7 and 21 day explants. These results demonstrate a robust acute inflammatory response to the BP explants at the 7 and 21 day time points; however, by 90 days, the presence of inflammatory cells seems to be replaced by the formation of fibrous tissue. These results demonstrate a robust inflammatory response to BP in the rat subdermal implant model.

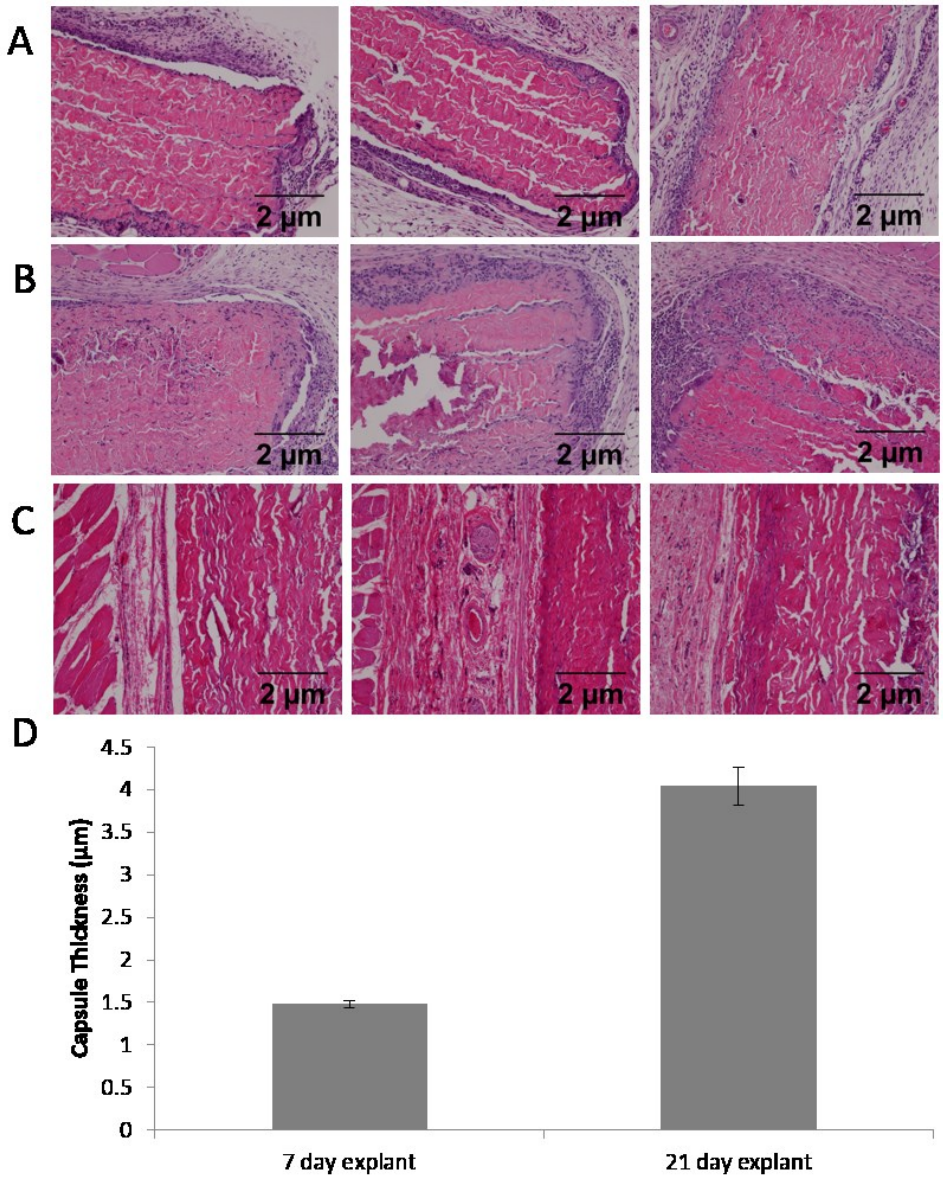

Fig. 2.12 Cellular capsule in en bloc rat subdermal explants. Hematoxylin & eosin staining of 7 day (A), 21 day (B) and 90 day (C) rat subdermal BP explants, 100x. Quantification of thickness capsule by image analysis in ImageJ of 7 day and 21 day explants (D).

Longitudinal sections of BP rat explants were analyzed to determine the localization of inflammatory cells. The highest concentration of cells was found to be at the surface of the material (Fig. 2.13A). The percent area of hematoxylin staining was much lower for all non-surface sections (Fig. 2.13B-E). This suggests that there is very little infiltration of cells into the BP explant and subsequently, that most oxidation is likely to occur on the surface of the material.

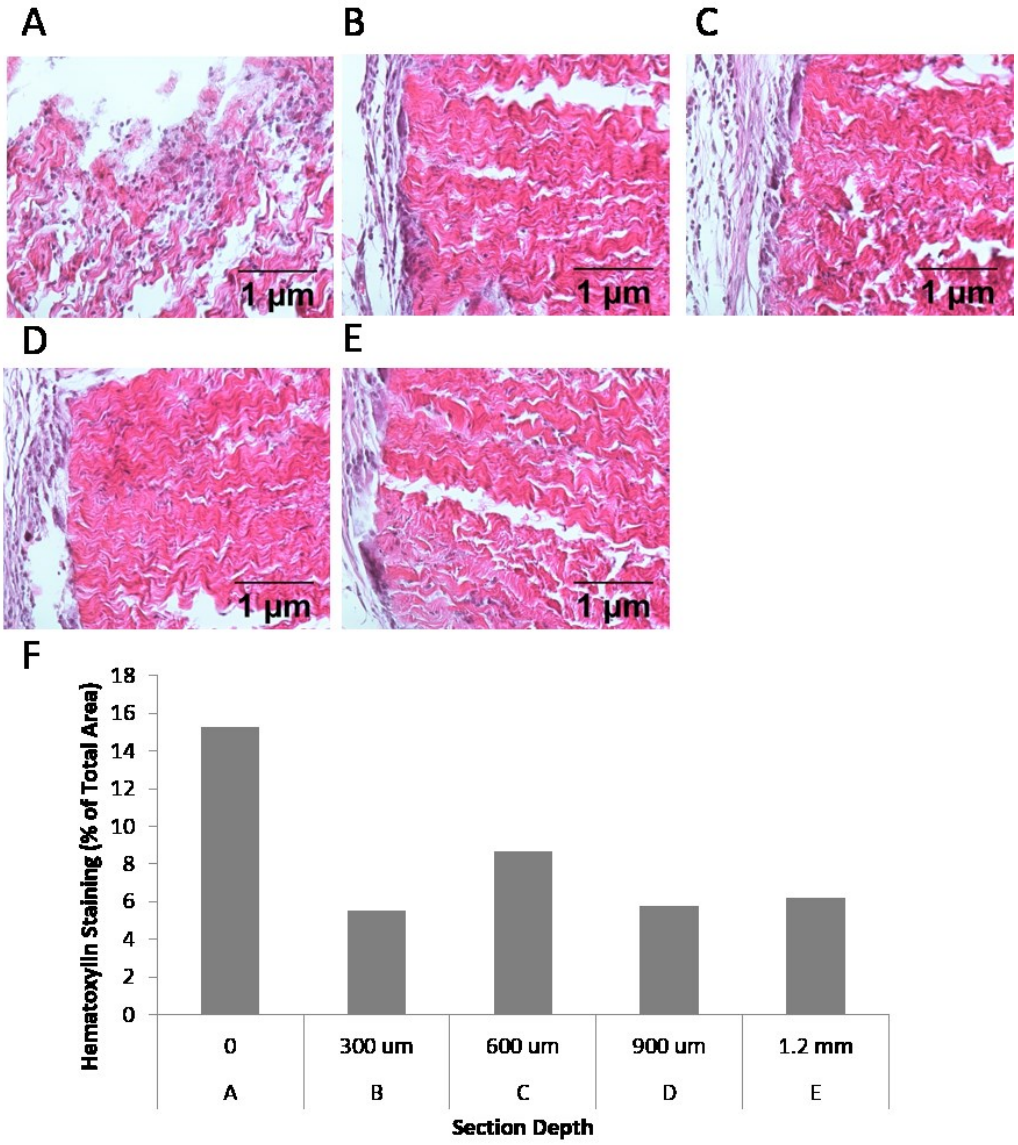

Fig. 2.13 Localization of inflammatory infiltrate in en bloc rat subdermal explants. H&E stains on serial sections of 7 day BP explants. Serial explants are separated by approximately 300 um, covering the full area of the explant where A is the top surface (0) and E is the bottom surface (1.2 mm), 200x magnification. Quantification of hematoxylin staining in each section (F).

En bloc BP rat subdermal explants were stained for myeloperoxidase (MPO) to assess the presence of an ROS/RNS producing enzyme at the surface of the material. Three biological replicates were imaged at 40x, 100x, and 200x magnification to determine the localization of MPO. MPO, stained brown with DAB, is present along the outer edge of the explanted material and is both intra and extracellular (Fig, 2.14A-C). Co-localization of MPO with the cellular layer surrounding the explant is apparent with the hematoxylin counterstain. These results demonstrate MPO staining on the surface of the BP explants.

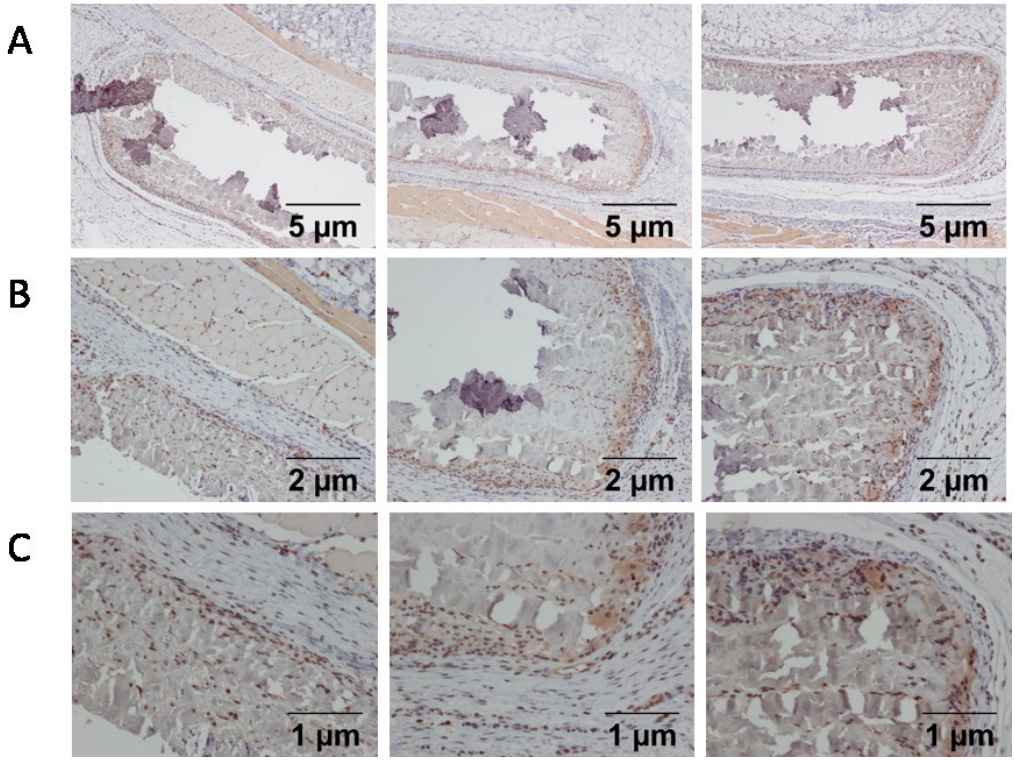

Fig. 2.14 MPO in 21 day rat subermal explants. (A) 40x (B) 100x (C) 200x.

To further assess the inflammatory response to BP rat subdermal explants, en bloc sections were stained with Masson's Trichrome to visualize the fibrous capsule. The longer time point explants (21 and 90 day) were used in this study since the formation of a fibrous capsule occurs later in the foreign body reaction. The formation of a fibrous capsule is evident in both the 21 day and 90 day explants, with the 90 day explants having a much thicker capsule (Fig. 2.15). These results demonstrate that the rat subdermal implant model with BP recapitulates the later phase of the foreign body reaction.

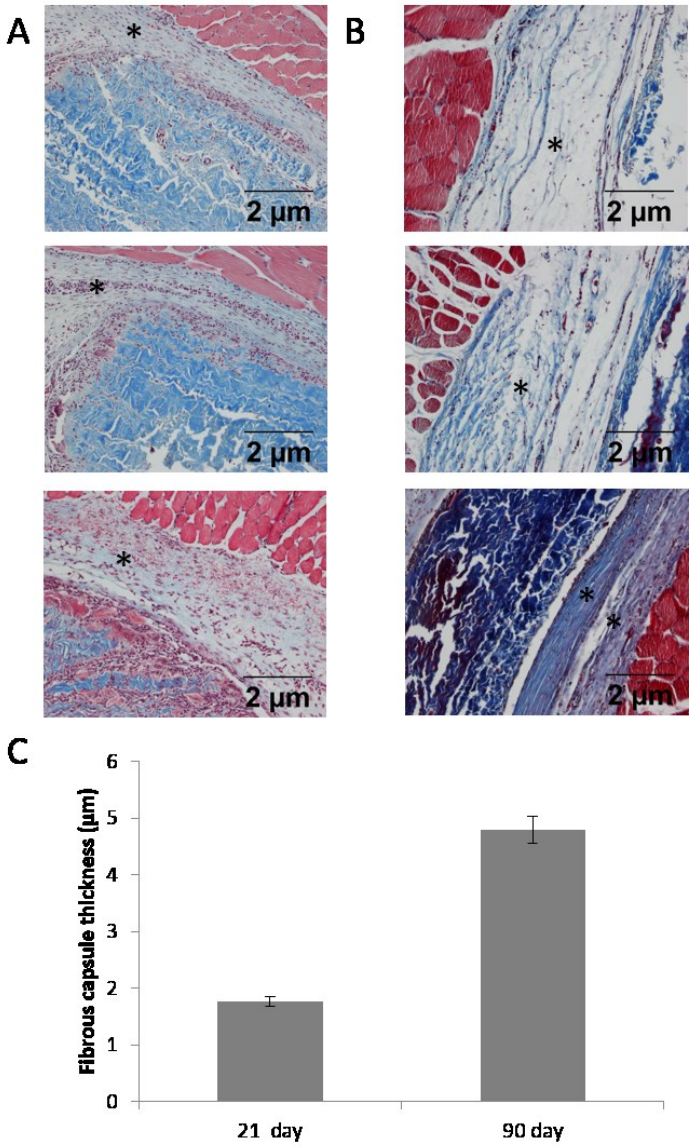

Fig. 2.15 Fibrous capsule of rat subdermal explants. (A) 21 day explants (B) 90 day explants, 100x, * indicates fibrous tissue. (C) Quantification of capsule thickness.

Oxidation and calcification of explants from sheep circulatory model

Since the oxidized amino acid levels in BP rat subdermal explants did not correlate with the levels found in clinical BHV explants despite the robust inflammatory response, we proposed that this may be due to a lack of direct circulation exposure as well as mechanical forces. To test this hypothesis, BJV BHV explants from 3 month sheep pulmonary arteries were analyzed for oxidized amino acids as well as calcification and morphological changes to determine the type of structural degeneration affecting these materials. Similar to the PAV and BP explants, the collagen structure of the BJV explants was not significantly deteriorated (Fig. 2.16A-D). Calcification was assessed qualitatively with Von Kossa staining of explanted BJV cusps (Fig 2.16E-F). None of the BJV explants displayed significant calcium accumulation. These results indicate that the BJV explants were not highly degraded, either by calcification or collagen damage.

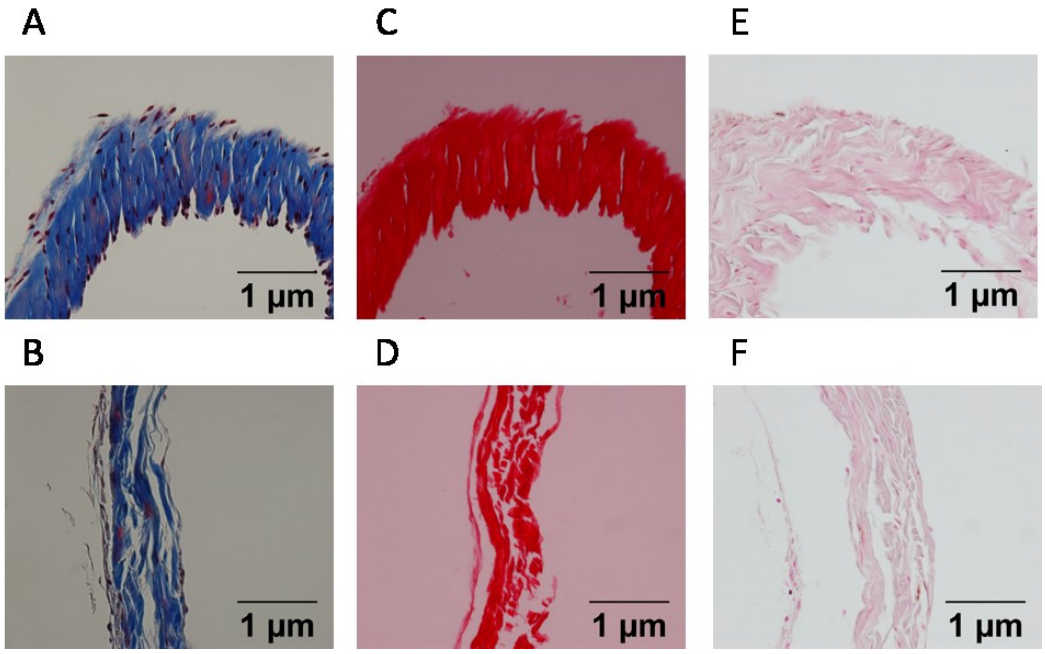

Fig. 2.16 Sheep pulmonary artery BJV BHV explant morphology and calcification. Masson's trichrome staining of non-implanted BJV (A) and BJV explant (B). Picrosirius red staining of non-implanted BJV (C) and BJV explant (D). Von Kossa staining of non-implanted BJV (E) and BJV explant (F).

Oxidized amino acids were quantified in explants to determine if these explants had higher levels of oxidized amino acids than subdermal explants. The main adduct of interest was dityrosine, however, the whole panel of 6 oxidized amino acids were analyzed for comparison. Meta-tyrosine, nitrotyrosine, and bromotyrosine were lower in explanted materials than in non-implanted BJV (Fig. 2.17A, C, F). Ortho-tyrosine and chlorotyrosine were higher in explanted materials (Fig. 2.17B, E). Similar to the clinical BP and PAV BHV explants, dityrosine was only detectable in the explanted materials and at levels that correlated with the clinical explants (Fig. 2.17D). These results demonstrate that dityrosine is accumulated in these circulatory explants therefore suggesting that circulation exposure is involved in the oxidation of BHV.

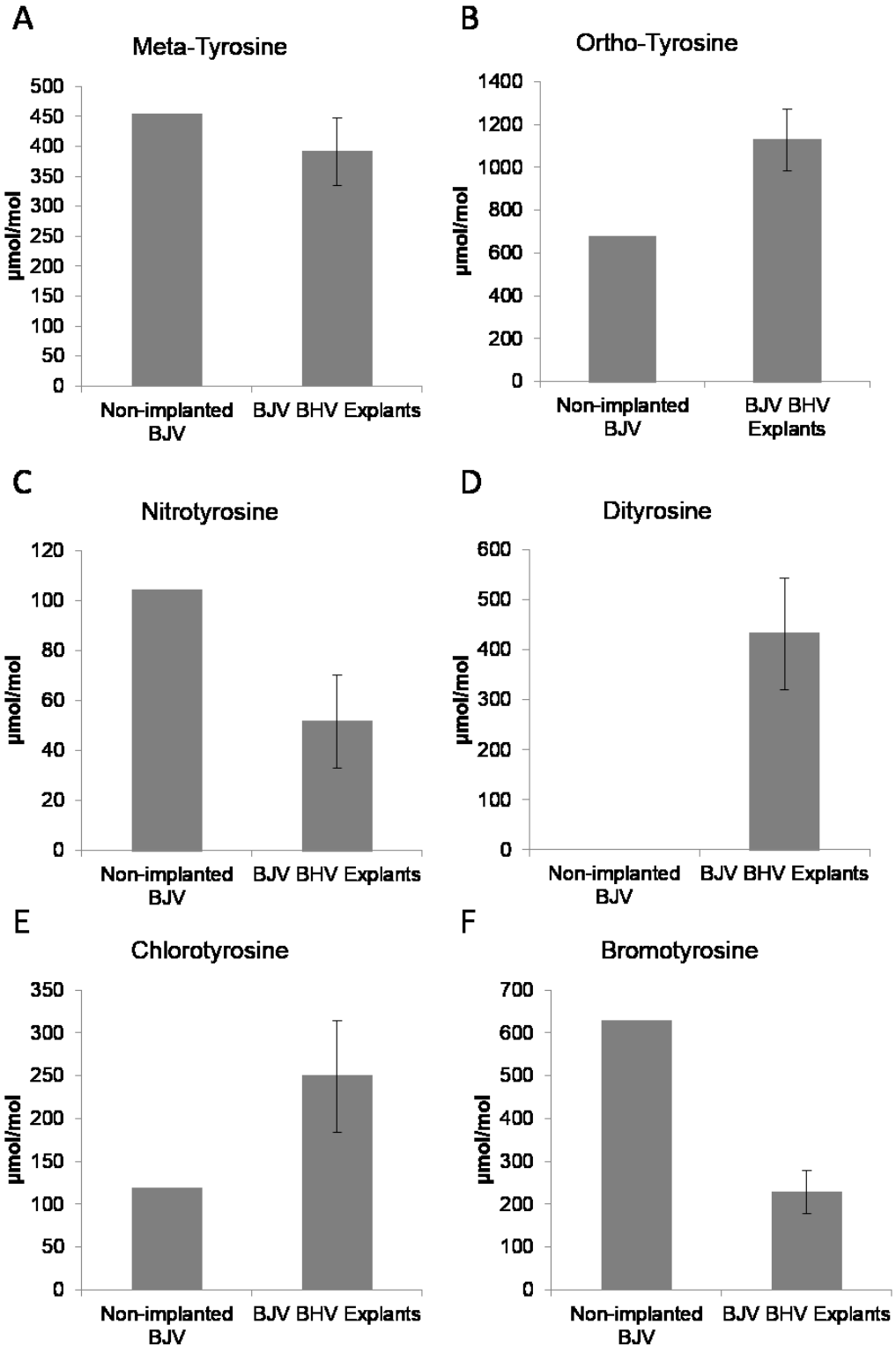

Fig. 2.17. Sheep pulmonary artery BJV BHV explants oxidized amino acids. Meta-tyrosine (A), ortho-tyrosine (B), nitrotyrosine (C) dityrosine (D), chlorotyrosine (E), and bromotyrosine (F) levels for non-implanted BJV (n=1) and BJV explants placed in sheep pulmonary arteries.

2.5 Discussion

Clinical BHV explants have an accumulation of dityrosine, thereby supporting the hypothesis that BHV are susceptible to oxidation. Furthermore, accelerated oxidation of the BHV leaflet material BP demonstrates that oxidation can lead to structural degeneration including a breakdown of glutaraldehyde cross-links and an increase in proteolytic degradation. Together these results demonstrate that oxidative stress affects BHV and contributes to structural degeneration.

Clinical BHV explants were obtained from patients requiring a replacement aortic valve due to the failure of the previous BHV. Characterization of these explants demonstrated a high percent of calcified valves with little or no structural disruption as assessed by morphology. Based on the high calcium accumulation, it was expected that the collagen structure of the explanted materials would display disorganization such as fibril fragmentation, but this was not observed. It is possible that with higher imaging magnification such as transmission electron microscopy, such fragmentation may be observed despite its absence with light microscopy analysis since it has previously been documented [72]. These findings are important since they demonstrate that despite clinical failure and calcium accumulation, there is no significant structural deterioration at the microscopic level.

The oxidized amino acids meta-tyrosine, ortho-tyrosine, nitrotyrosine, dityrosine, chlorotyrosine, and bromotyrosine were tested as markers of BHV oxidation since these adducts are formed through reactions by common oxidants such as hydroxyl radicals and peroxynitrite [84]. In addition, these adducts involve protein oxidation rather than DNA or lipid oxidation; this is important since BHV materials are primarily protein (collagen) based due to the glutaraldehyde and ethanol material treatments. Meta-tyrosine and ortho-tyrosine are formed by oxidants capable of phenylalanine hydroxylation [84]. Nitrotyrosine is a major product of reactions with peroxynitrite [96]. Dityrosine is formed through tyrosyl radicals, which are the product of various oxidants [78, 83]. Chlorotyrosine is formed through the production of hypochlorus acid by MPO whereas bromotyrosine is formed from the production of hypobromous acid by eosinophil peroxidase [77, 85]. With the exception of dityrosine, all oxidized amino acids analyzed were present in both non-

implanted PAV and BP at variable levels. For some oxidation products, such as nitrotyrosine, the level was lower in the BHV explant as compared to the non-implanted material which would suggest a reversal of the modification; however, a biochemical process for such a reversal has not been identified. Due to processing or animal variability, meta-tyrosine, ortho-tyrosine, nitrotyrosine, chlorotyrosine, and bromotyrosine do not seem to be specific to BHV oxidation that occurs in a patient. However, for both PAV and BP BHV, dityrosine was not present in the non-implanted tissues but was elevated in the BHV explants. Dityrosine therefore may be a specific marker of BHV oxidation. The elevation of dityrosine in the clinical BHV explants demonstrates that both PAV and BP BHV are subject to oxidation.

Dityrosine, unlike the other oxidized amino acids assessed in BHV explants, is a protein cross-link that forms as a result of oxidation [83, 97]. In addition to being a marker of BHV oxidation, dityrosine could represent a functional consequence of BHV oxidation since the introduction of new material cross-links could alter the mechanical and structural properties of the material. For BHV, additional cross-linking may cause material stiffening, leading to impaired opening and closing of the valve and subsequent mechanical failure. However, at this time it is unclear whether dityrosine represents a functional consequence of BHV oxidation rather than just a marker of BHV susceptibility to oxidation.

A system of accelerated material oxidative damage was used to examine potential functional consequences of BHV oxidation. Since BHV structural damage occurs on a time scale of years it was necessary to develop a system to test oxidation-mediated structural degradation in an experimental setting. Exposure of BP to oxidizing conditions resulted in significant destruction of the collagen fibrils as well as mass loss, increased susceptibility to collagenase degradation, and a loss of glutaraldehyde. Each of these findings could potentially result in structural degradation and mechanical dysfunction of a BHV. The significant structural deterioration was not surprising since BHV materials are tissue-derived and these oxidizing conditions greatly exceed physiological conditions. However, both the collagenase and glutaraldehyde findings are particularly important since each of these results have been documented in previous studies. Oxidation of soluble or purified collagen has been shown to increase the susceptibility to proteolytic digestion due to a

breakdown of collagen cross-linking [28, 30, 31]. Loss of glutaraldehyde cross-linking of BHV materials has been reported for rat subdermal explants of BP cross-linked with ^{3}H-glutaraldehyde [98, 99]. Based on evidence of collagenase digestion and loss of glutaraldehyde cross-links, it can be concluded that oxidation of BHV results in structural degeneration.

The rat subdermal implant model is the widely accepted animal model of BHV calcification [93, 100]. Juvenile rats are used since they have more active calcium metabolism with higher circulating levels of alkaline phosphatase as well as calcium and phosphate; therefore contributing to the accelerated implant calcification [68]. This model was evaluated for its representation of oxidation-mediated BHV degradation to determine whether it also recapitulates non-calcific BHV degradation. The mass loss that occurs in the accelerated oxidation model does not occur with rat subdermal implantation, therefore additional endpoints of BHV oxidation were assessed in the rat explants due to the difference in degree of material damage. Hydroxyproline is an amino acid found abundantly in collagen and rarely in other proteins, therefore the levels of hydroxyproline in a BP sample correlates directly with overall collagen content [95]. Hydroxyproline content was found to be significantly lower in both 21 and 90 day BP rat subdermal explants, which indicates a loss of collagen. This measurement may not be specific to collagen oxidation since collagen is also susceptible to degradation by proteolytic enzymes in vivo [23]. In addition, the loss of hydroxyproline correlated with higher calcium levels, therefore the accumulation of calcium may also result in a loss of collagen content. Similar to the accelerated oxidation model, collagenase digestion and picrosirius red were used to analyze BP rat explants. Although 21 day explants did show an increase in collagenase digestion compared to non-implanted materials, this difference was not significant. Furthermore, the 90 day explants were less susceptible to collagenase than 21 day explants. This finding may be due to the high calcium content in the 90 day explants which reduces collagen content and therefore the substrate of collagenase. Material cross-linking was assessed with DSC in non-implanted and 90 day BP explants to determine whether there was any change in overall material stability. Prior to glutaraldehyde fixation, the shrink temperature of BP is approximately 63 °C [101]. After glutaraldehyde fixation the shrink temperature was 87 °C; the 90 day explants had a shrink temperature of 84 °C, which is significantly lower than the non-

implanted glutaraldehyde fixed BP, but significantly higher than that of non-glutaraldehyde fixed BP. The reduction in shrink temperature in the rat subdermal implants from the non-implanted glutaraldehyde fixed BP could contribute to material failure related to a weakening of the material. Potentially all of the endpoints assessed for rat subdermal BP implants could lead to material degradation and eventual failure for BHV.

In order to correlate the rat subdermal model with the clinical BHV explants, oxidized amino acids were quantified in the BP rat subdermal explants. Previously, we identified dityrosine as the most reliable marker of BHV oxidation due to its absence in non-implanted materials; however, the whole panel of oxidation products were quantified in rat explants to fully characterize these explants. For meta-tyrosine, ortho-tyrosine, bromotyrosine, nitrotyrosine, and chlorotyrosine the trends seen with the clinical BHV were similar with the BP explants. Dityrosine was present in 21 day but not 7 day explants and at levels a magnitude lower than the clinical values. Together with the previous oxidation assessment of rat subdermal explants, the dityrosine results indicate that the rat subdermal implant model does not correlate well with oxidation of clinical BHV explants and an alternative animal model should be used.

In order to explain how the rat subdermal implant model represents BHV calcification but not oxidation, additional studies were performed to focus on BP inflammation in this model. We hypothesize that the major factor of BHV oxidation is the production of ROS/RNS from inflammatory cells, therefore, this model would need to produce a robust inflammatory response. The results of the inflammation studies demonstrated an active inflammatory response characterized by cellular recruitment, MPO, and fibrous capsule formation. Therefore, since the rat subdermal implant model does involve significant implant inflammation there must be other factors that drive BHV oxidation such as blood contact or exposure to mechanical stresses.

The availability of BJV BHV explants from a 3 month sheep circulatory model allowed for the assessment of two critical factors of BHV oxidation: direct blood flow and mechanical forces. The BJV BHV explants analyzed were obtained from three months old sheep studies of catheter-deployed BHV in the pulmonary arteries. These BJV BHV explants had dityrosine levels similar to the clinical BHV explants despite the short implantation period. A comparison of the rat and sheep

model therefore demonstrates that circulation is necessary for BHV oxidation since dityrosine levels were very low in the rat model. The rat subdermal implant model lacks direct blood flow and mechanical forces that BHV normally experience. Since exposure to shear stress has been found to increase oxidative damage [86, 87], it is likely that both direct circulatory exposure and shear stress are involved in BHV oxidation. Therefore, a short-term circulatory model may be the most useful system for studying BHV oxidation in a non-clinical setting.

Clinical BHV explants are susceptible to oxidative stress as indicated by the elevation of dityrosine. Oxidation of the BHV material BP in an accelerated system demonstrated that oxidation can lead to material degradation including collagen deterioration, loss of glutaraldehyde cross-links, and an increase in degradation by proteolytic enzymes. Although the rat subdermal implant model results in an inflammatory response to the BP implant, the oxidation endpoints are only modestly represented. However, in a short term sheep circulatory model, oxidation of BJV BHV was observed, which supports the hypothesis that in addition to inflammation, shear stress, and direct circulation exposure accelerate BHV oxidation. Since BHV have the advantages over the alternative mechanical valves of a lower risk of device-associated thrombosis, significant emphasis has been placed on improving BHV durability with a specific focus on calcific structural degeneration. Although BHV inflammation has been characterized, previous studies did not address mechanisms of ROS/RNS induced BHV degeneration resulting from the activation of inflammatory cells. Therefore, these studies identify a previously overlooked mechanism of BHV structural degeneration arising from oxidation-mediated material damage.

Chapter 3: Covalent modification of BHV with DBP to mitigate BHV oxidation

This chapter has been published:

Christian AJ, Lin H, Connolly JM, Alferiev IS, Ferrari G, Hazen SL, Ischiropoulos H, Levy RJ. The susceptibility of bioprosthetic heart valve leaflets to oxidation. *Biomaterials*. 2014; 35:2097-102.

3.1 Abstract

Clinical BHV are subject to oxidative modification that can lead to structural degeneration through the loss of material cross-linking and increased degradation by proteolytic enzymes. We hypothesized that this process could be mitigated by modifying BHV materials with an antioxidant to prevent the reaction of oxidants with the material. The oxidant scavenger 3-(4-hydroxy-3,5-di-tert-butylphenyl) propyl amine (DBP) was covalently immobilized to BP through a carbodiimide-driven conjugation reaction. DBP attachment to BP, which was confirmed with ^{14}C labeled DBP, did not affect mechanical properties of BP. The ability of DBP to mitigate oxidative degradation of BP was assessed through exposure of BP and DBP modified BP to oxidizing conditions (1% H_2O_2/100 μM $FeSO_4$) as well as in a rat model of BHV degeneration. With exposure to oxidizing conditions, DBP effectively reduced BP oxidative degradation as measured by loss of glutaraldehyde cross-links and susceptibility to collagenase digestion. In the rat subdermal implant model, DBP attenuated the reduction of material cross-linking associated with implantation, but did not affect the accumulation of oxidized amino acids including dityrosine, which was only modestly elevated in the explanted materials. In addition, DBP modified BP had significantly less calcium accumulation as compared to unmodified explants. These studies demonstrate that modification of BHV materials with the oxidant scavenger DBP mitigates BHV degradation resulting from material exposure to oxidizing conditions and may prevent BHV degradation associated with calcification and oxidation in the rat subdermal implant model.

3.2 Introduction

BHV are susceptible to oxidative stress, as indicated by elevated dityrosine in clinical BHV explants and structural degeneration resulting from exposure to oxidizing condition, which includes loss glutaraldehyde cross-links and increased digestion by proteolytic enzymes [102]. Strategies to prevent or mitigate oxidation-mediated structural degeneration of BHV have not been developed. In these studies we investigated the hypothesis that modification of BHV materials with an oxidant scavenger could prevent structural degeneration resulting from oxidative stress.

Studies with polymeric biomaterials, such as polyurethane, have demonstrated that antioxidant material modifications can attenuate material oxidative degradation [27, 33-35]. A common approach for modifying a polymeric biomaterial with an antioxidant is to dissolve the compound, such as α-tocopherol or Santowhite, in the polymer solution prior to casting [33]. In addition, surface modifications of the polymer have been done following casting through covalent modification such as bromoalkylation of the polymer followed by a reaction with a thiol-containing antioxidant [27]. It may be possible to use a variation of both methods, either passive incorporation by incubating the material in a solution containing the antioxidant or covalent modification, to modify BHV materials with an antioxidant. Covalent modification was tested as our first approach for modifying BHV materials to create a model oxidation resistant material, which was chosen based on the experience in the Levy lab with this type of modification of biomaterials.

Glutaraldehyde-fixed heterograft tissues are used in the fabrication of BHV. These materials are comprised primarily of collagen and other extracellular matrix proteins. Due to the composition of these materials, there are some limitations in the types of conjugation chemistries that could be used to attach an antioxidant. The functional groups found in collagen are amines from lysine and asparagine, and carboxylic acids from glutamate and aspartate [103]. In addition, harsh solvents cannot be used since they would severely damage the tissue. Amines are involved in glutaraldehyde cross-linking [40], therefore carboxylic acids are the available functional groups for conjugation. We first aimed to covalently link an antioxidant containing a reactive amine to carboxylic acids of the BHV materials through a carbodiimide-driven reaction.

The requirements of an antioxidant for conjugation through carbodiimide-driven chemistry are a reactive amine that is not necessary for antioxidant activity and compound stability at slightly acidic pH which is used in the carbodiimide activation of carboxylic acids. Based on previous studies by the Levy lab with di-tert-butylphenol derivatives [27, 36], which are based on the commercially used antioxidant BHT, we proposed the use of an analogue of these compounds containing the appropriate reactive amine. The compound must contain an accessible amine therefore an alkyl chain and terminal amine were added to the compound, resulting in the compound 3-(4-hydroxy-3,5,-di-tert-butylphenyl)propyl amine (DBP).

DBP was reacted with the BHV material BP according to the proposed carbodiimide-driven reaction to determine the efficiency of DBP conjugation to BP. In addition, DBP modified BP was characterized in terms of mechanical properties as well as oxidant scavenging capacity of DBP in order to assess whether the modification chemistry had any negative impact on BP or DBP. To address our initial hypothesis that BHV materials modified with DBP would be less susceptible to oxidative degradation, BP with and without DBP was assessed for oxidative degradation resulting from either exposure to oxidizing conditions or subdermal implantation in rats.

Here we developed an antioxidant modification of the BHV material BP using DBP, which is structurally-similar to BHT, and a carbodiimide-driven conjugation reaction for immobilization of DBP to the carboxylic acid groups of BP. DBP modified BP was assessed for material properties and resistance to oxidative damage.

3.3 Materials and Methods

Materials

Biosol and Bioscint were purchased from National Diagnostics (Atlanta, GA). Amplex Red was purchased from Life Technologies (Philadelphia, PA). Glutaraldehyde was purchased from Polysciences, Inc (Warrington, PA). ^{3}H-glutaraldehyde and [2,3-^{14}C]-methyl acrylate were purchased from American Radiolabeled Chemicals (St. Louis, MO). All chemicals unless otherwise specified were purchased from Sigma Aldrich (St. Louis, MO).

Synthesis of DBP

DBP was synthesized by Dr. Ivan Alferiev through the reaction of 2,6-di-tert-butylphenol with methyl acrylate under catalysis with a mixture of NaOH and KOH. The resulting methyl 3-(4-hydroxy-3,5,-di-tert-butylphenyl)propionate was reduced with lithium aluminum hydride in ethyl ether to 3-(4-hydroxy-3,5,-di-tert-butylphenyl)propanol, which was transformed into the mesylate by treatment with methanesulfonyl chloride and triethylamine in dichloromethane. The mesylate was reacted with phthalimide potassium salt in 1-methylpyrrolidinone and the phthalimide derivative was cleaved with hydrazine in ethanol to DBP-amine base, which was finally transformed into its water-soluble hydrochloride (Fig. 3.1).

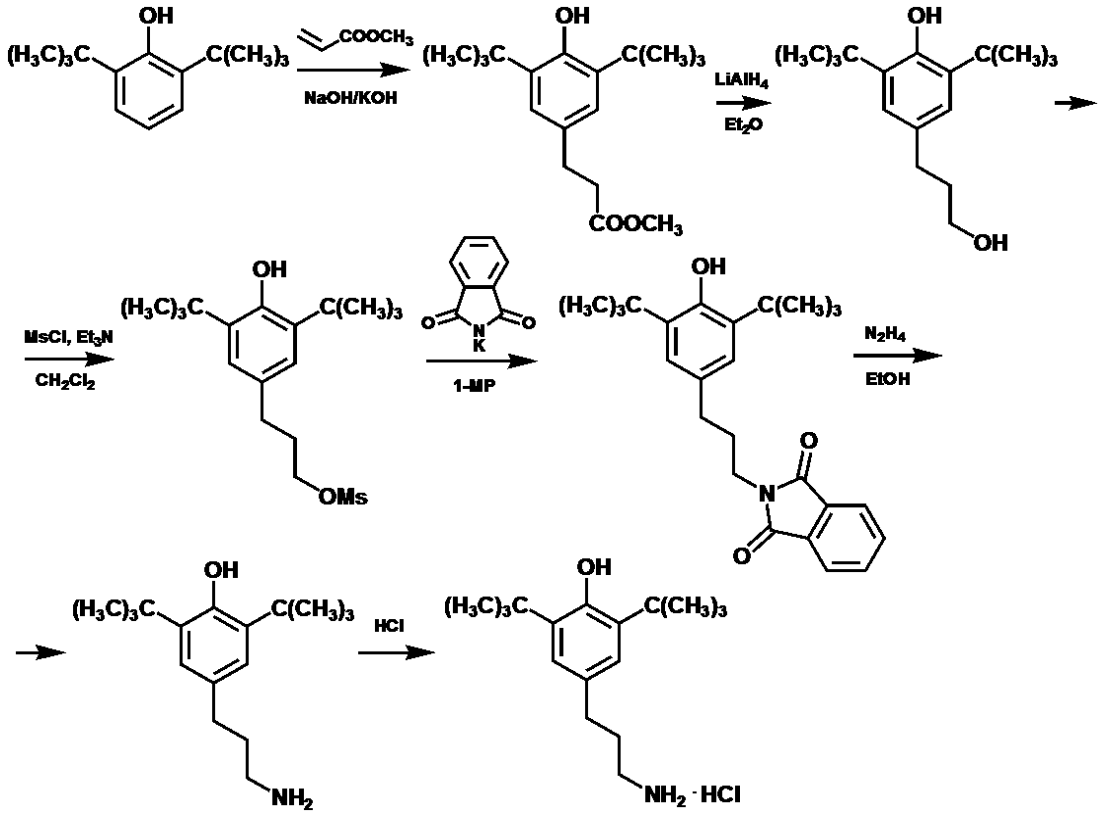

Fig. 3.1 DBP synthesis. The synthesis of DBP from the precursor 2,6-di-*tert*-butylphenol.

^{14}C-DBP hydrochloride (7 µCi/mmol) was prepared similarly to non-labeled DBP, using [2,3-^{14}C]-methyl acrylate (10 – 20 mCi/mmol) diluted with the non-labeled compound. The only difference between this radiolabeling synthesis and the non-radioactive procedure was at the first step, where an excess of 2,6-di-tert-butylphenol was applied to react the labeled acrylate as completely as possible.

BP treatments and DBP modification

Fresh BP obtained from an abattoir was treated with 0.625% glutaraldehyde or 0.625% ^{3}H-glutaraldehyde (specific activity 24 µCi/mmol) in HEPES buffer pH 7.4 for 7 days at room temperature with gentle shaking. BP was then modified with DBP through a carbodiimide-driven conjugation reaction (Fig. 3.2). The DBP modification reaction was prepared as two solutions: 42 mM DBP in 100% ethanol and 43 mM N-hydroxysuccinimide (SuOH) in deionized H_2O. Immediately before adding BP, the two solutions were combined and 65 mM 1-ethyl-3-(3-dimethylaminopropyl)carbodiimide hydrochloride (EDC) was added. The reaction proceeded for 24 hours at room temperature with gentle shaking. DBP modified BP was rinsed for 10 minutes in 100% ethanol to remove precipitate formed during the reaction. The required length of the ethanol rinse was determined experimentally through UV monitoring of the wash solution; the precipitate is rapidly solubilized in ethanol, therefore only a short reaction time is necessary. As a control for the effects of DBP, BP was treated with the carbodiimide reaction with the exclusion of DBP (Glut-EDC/SuOH). All BP samples were stored in 0.2% glutaraldehyde.

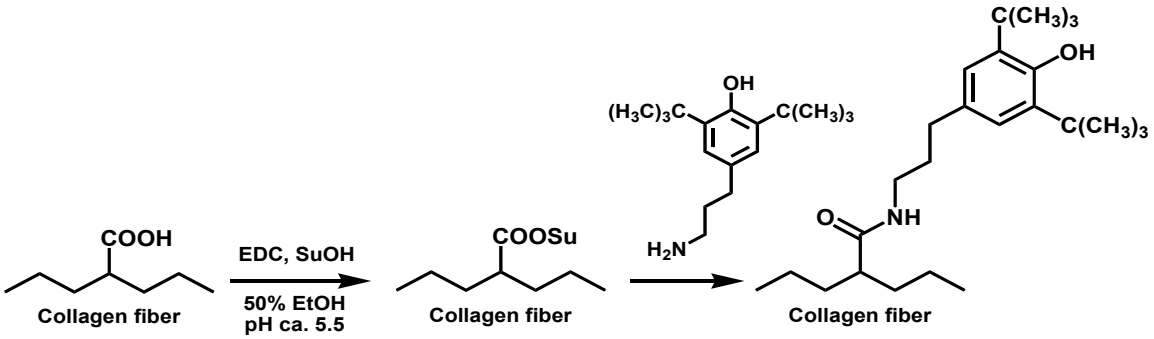

Fig. 3.2 DBP modification scheme. Carboxylic acids are activated with the carbodiimide EDC in the presence of SuOH to form stable N-succinimidyl ester intermediates that can then react with the amine of DBP to form an amide bond.

Glutaraldehyde fixed BP was reacted with [bis(trifluooacetoxy)iodo]benzene (BTI) to convert asparagine (Asn) and glutamine (Gln) residues to diaminopropionic acid and diaminobutanoic acid, respectively, and prevent the conversion of Asn to aspartic acid (Asp) and Gln to glutamic acid (Glu) during acid hydrolysis [104]. BTI derivatization was performed in 5 M guanidine-HCl and 10 mM trifluoroacetic acid for 4 hours at 60ºC [105]. BP was then hydrolyzed in 6 N HCl, dried under air at 60 °C, and reconstituted for amino acid analysis by HPLC at the CHOP Metabolomics Core Facility.

BP was modified with ^{14}C-DBP through the carbodiimide-driven reaction to quantify the attachment of DBP to BP. Lyophilized ^{14}C-DBP modified BP was solubilized with Biosol at 50 °C with shaking for 72 hours. Solubilized tissues were added to Bioscint and analyzed by liquid scintillation counting.

Material properties of DBP BP

Material cross-linking of DBP modified pericardium was determined using differential scanning calorimetry (DSC) to measure thermal denaturation temperature [91]. A 2 mm tissue biopsy punch was used to prepare pericardium samples for DSC analysis. The samples were hermetically sealed in aluminum pans then analyzed using a Perkin Elmer DSC 7. The sample temperature was increased from 25 °C to 100 °C at 10 °C/min. The endothermic peak was calculated using Pyris software.

DBP modified pericardium was subjected to uniaxial tensile testing to determine the effects of the DBP modification on material flexibility and strength. Samples were cut to dimensions of 8 mm width and 25 mm length. Semi-circular sections were cut from the middle of the sample to obtain a bone-like shape. The samples were tested using an Instron machine with assistance from Dr. Alex Radin at the University of Pennsylvania. The samples were placed in pneumatic grips and stretched at a crosshead speed of 100 mm/min until failure. Young's elastic modulus, ultimate tensile strength, and maximum elongation were determined from the load-displacement data obtained during testing.

Oxidation capacity of DBP BP

The oxidation reporter molecules dihydrorhodamine 123 (DHR123) and Amplex Red were used to determine the oxidant scavenging capacity of DBP modified BP in a system containing MPO (1 μg/mL), H_2O_2 (10 μM), and either Cl^- (120 mM NaCl) or NO_2^- (100 μM $NaNO_2$) ions [106]. Amplex red (50 μM) or DHR123 (25 μM) was added to the BP samples immediately after adding H_2O_2, MPO and either NaCl or $NaNO_2$. Fluorescence of the solution was determined 30 minutes after adding Amplex Red or DHR123 in order to quantify the corresponding oxidation products resorufin or rhodamine, respectively. Fluorescence was measured an excitation/emission of 560/590 nm for resorufin and 536/500 nm for rhodamine.

For a cell-based system of oxidation, HL-60 (ATCC) were differentiated to a neutrophil-like phenotype in 1.25% DMSO in IMDM/20% FBS/penicillin/streptomycin for 3 days at 37 °C in 5% CO_2 [107-109]. Differentiated HL-60 (1 x 10^5 cells) were seeded on 4 mm BP samples in a solution containing 4 U/mL horseradish peroxidase, 5 μM Amplex Red or DHR123, and 500 ng/mL phorbolmyristylacetate (PMA). Resorufin or rhodamine fluorescence was read 30 minutes after the addition of PMA.

Accelerated oxidative damage model

BP samples were placed in PBS or 1% H_2O_2/100 μM $FeSO_4$ for 7 days with solution changes every 2-3 days. Lyophilized samples were weighed at the start and end of treatments. The same endpoints described in Chapter 2 were used to assess the effect of DBP in this system.

Rat subdermal implants

Three week old male Sprague-Dawley rats (60-90 grams) were used for the subdermal implantation studies as previously described in Chapter 2. The animals were sacrificed at 7, 21, or 90 days and the materials were explanted for further analysis. The implants were removed and either fixed in neutral buffered formalin for paraffin embedding or acid hydrolyzed for calcium analysis. Heparinized blood was taken from rats at the 90 day time point to measure toxicity.

Toxicity

Toxicity was assessed by measuring levels of alkaline phosphatase (ALP), creatinine, and aspartate transaminase (AST) in plasma of rats with implants for 90 days [110, 111]. Creatinine was measured using a creatinine assay kit (Cayman Chemical). AST was measured with the Abnova AST kit. ALP activity was through a reaction of serum samples with the ALP substrate p-nitrophenylphosphate disodium salt hexahydrate (10 mM); the formation of p-nitrophenol was monitored by absorbance and compared to a standard curve of p-nitrophenol. All kits were used according to manufacturer instructions

Statistical Methods

Results are shown as the mean ± standard error for the mean. Single ANOVA with Tukey's test or a two tailed t-test were used to determine significance, which was defined as a p value less than 0.05.

3.4 Results

Attachment of DBP to BP

To estimate the maximum binding capacity of DBP to BP, total amino acid composition was determined by HPLC (Fig. 3.3A). The major amino acids of BP are glycine, alanine, and not measured here, proline and hydroxyproline [103]. Since the carbodiimide reaction involves the activation of carboxyl in BP, the molar concentration of Asp and Glu residues in acid-hydrolyzed BP samples is of importance to the theoretical maximum binding of DBP to BP. A BTI derivatization step was included for quantification of Asp and Glu in order to convert asparagine (Asn) and glutamine (Gln) residues to diaminopropionic acid and diaminobutanoic acid, respectively, and prevent the conversion of Asn to aspartic acid (Asp) and Gln to glutamic acid (Glu) during acid hydrolysis. There are 196 ± 7 nmol Asp/mg dry BP and 303 ± 10 nmol Gln/mg for a total of 499 ± 17 nmol of terminal carboxyl-containing amino acid residues per mg of BP (Fig. 3.3B). Therefore the maximum attachment of DBP is 500 nmol/mg based on amino acid composition.

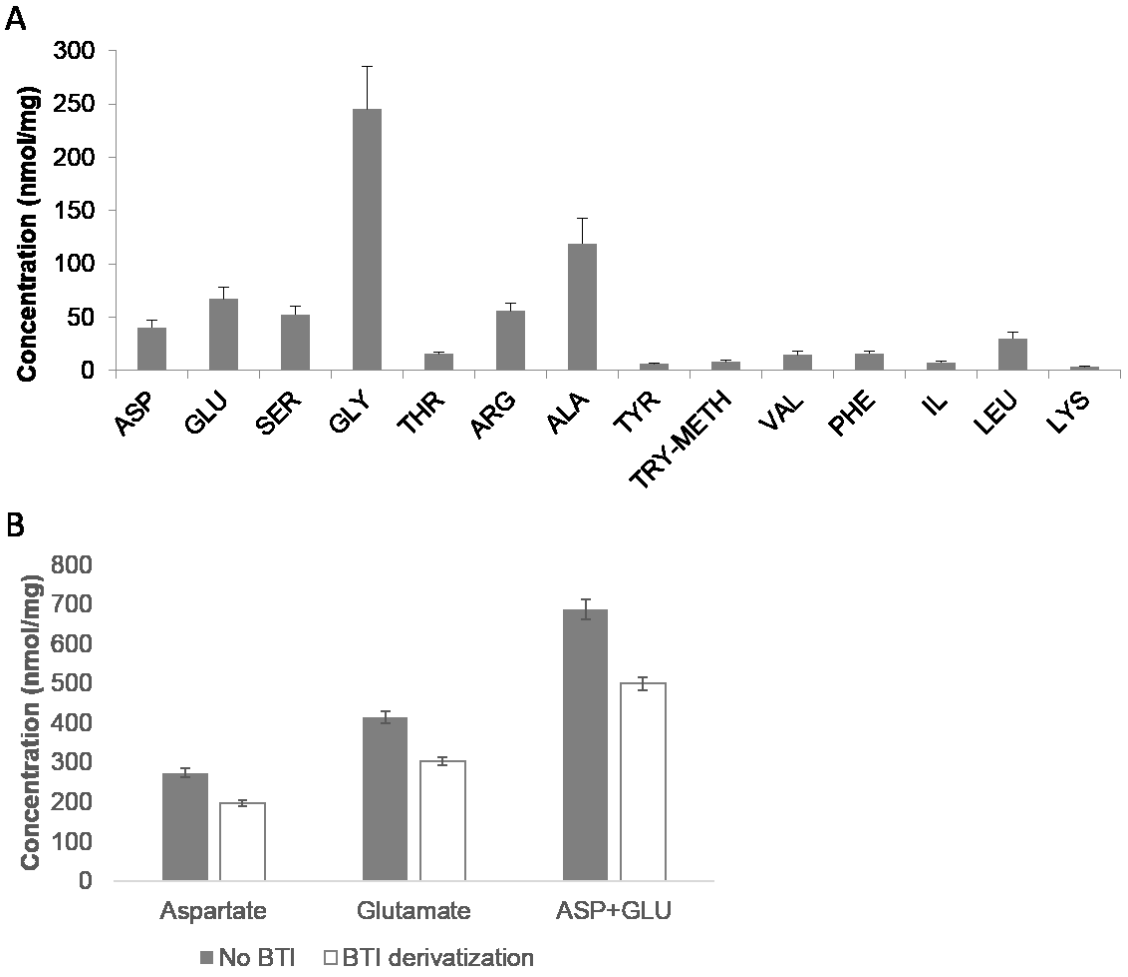

Fig. 3.3 Amino acid composition of BP. (A) Full amino acid composition (B) Asp and Glu quantification with BTI derivatization.

The attachment of DBP to BP was quantified using ^{14}C-labeled DBP. A dose curve of DBP modified BP was generated through dilutions of the DBP reaction solution in 50% ethanol (Fig. 3.4). The amount of DBP attached to BP using the undiluted reaction solution was 439 ± 8 nmol/mg. This result demonstrates that the reaction of DBP with BP results in nearly maximum attachment of DBP to BP based on the predicted binding determined by Asp and Glu quantification.

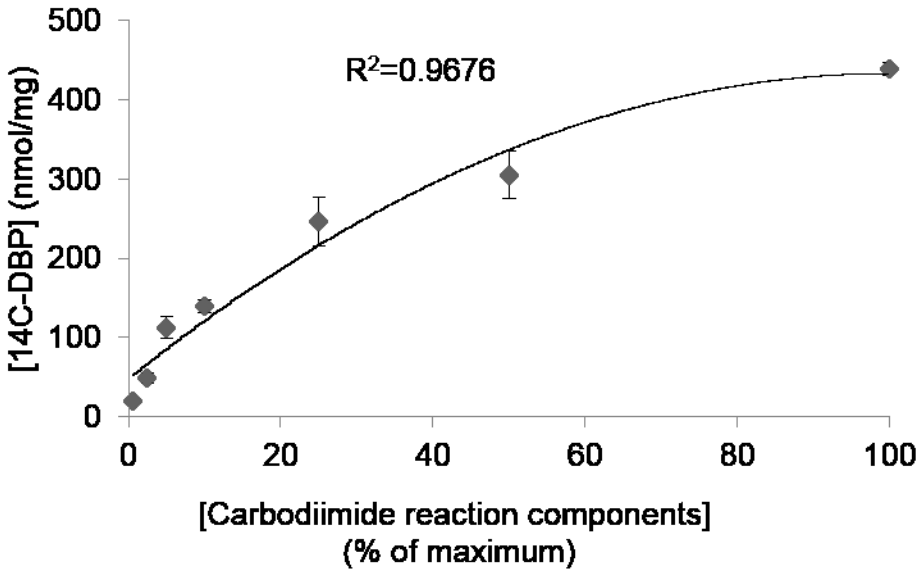

Fig. 3.4 ^{14}C-DBP binding to BP. Dose curve generated by dilution of reaction components in 50% ethanol.

Material properties of DBP BP

To assess whether the DBP modification affects the material properties of BP, uniaxial tensile testing and DSC were performed on unmodified and DBP modified BP. A representative stress-strain curve is shown for both groups (Fig. 3.5). Ultimate tensile strength, maximum strain, and Young's elastic modulus were calculated from tensile testing. The tensile properties of DBP modified BP did not differ significantly from unmodified BP (Table 3.1). The shrink temperature of pericardium was not affected by the DBP modification (Table 3.1). These results demonstrate that the DBP modification does not change the material properties of BP.

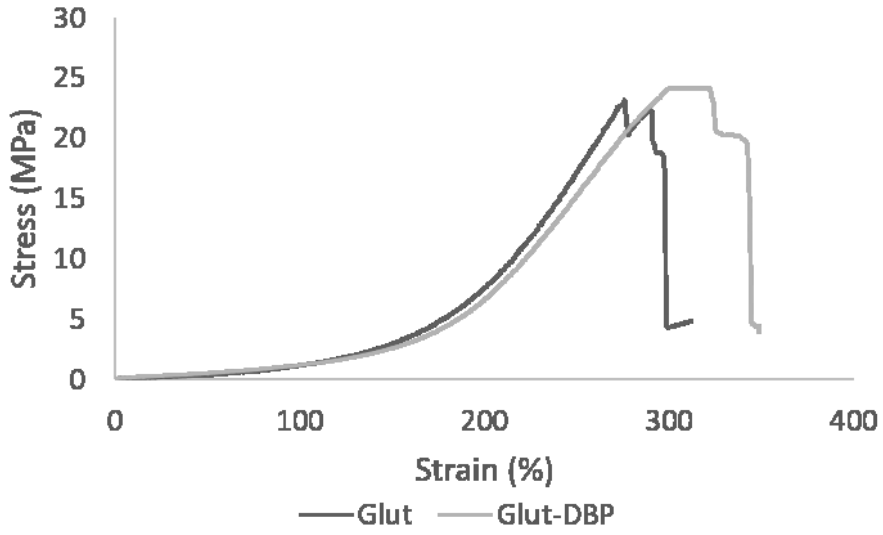

Fig. 3.5 Stress-strain response. Tensile testing of glutaraldehyde fixed BP with and without the DBP modification. Representative curves shown for n=5.

	Glut Pericardium	Glut-DBP Pericardium	p-value
Shrink temperature (Celsius)	88.3 ± 0.4	87.1 ± 0.2	0.089
Young's elastic modulus (kPa)	127 ± 14.8	117.8 ± 6.5	0.202
Ultimate tensile strength (MPa)	21.1 ± 0.7	17.5 ± 1.7	0.104
Elongation (%)	328.9 ± 11.7	339.8 ± 5.7	0.434

Table 3.1. **Mechanical properties of BP**. Shrink temperature determined by differential scanning calorimetry. Elastic modulus, ultimate tensile strength, and elongation determined from stress-strain curves generated from tensile tests.

Oxidant scavenging capacity of DBP BP

The oxidation reporter molecules Amplex Red and DHR123 were used to determine the oxidant scavenging capacity of DBP modified BP. Oxidants generated by MPO in the presence of hydrogen peroxide and either chloride or nitrite or by PMA activated HL-60 were used to oxidize Amplex Red to resorufin and DHR123 to rhodamine. Significantly less Amplex Red and DHR123 were oxidized in the presence of DBP modified BP as compared to unmodified BP in the cell-free systems (Fig. 3.6), which demonstrates that DBP scavenges oxidants after immobilization to BP. In the HL-60 ROS/RNS producing system, DBP modified BP had less oxidation of both Amplex Red and DHR123, but these differences were not significant which could be due to biologic variability or for DHR123, intracellular oxidation since DHR123 crosses the cell membrane. These results demonstrate that DBP modified BP has oxidant scavenging activity.

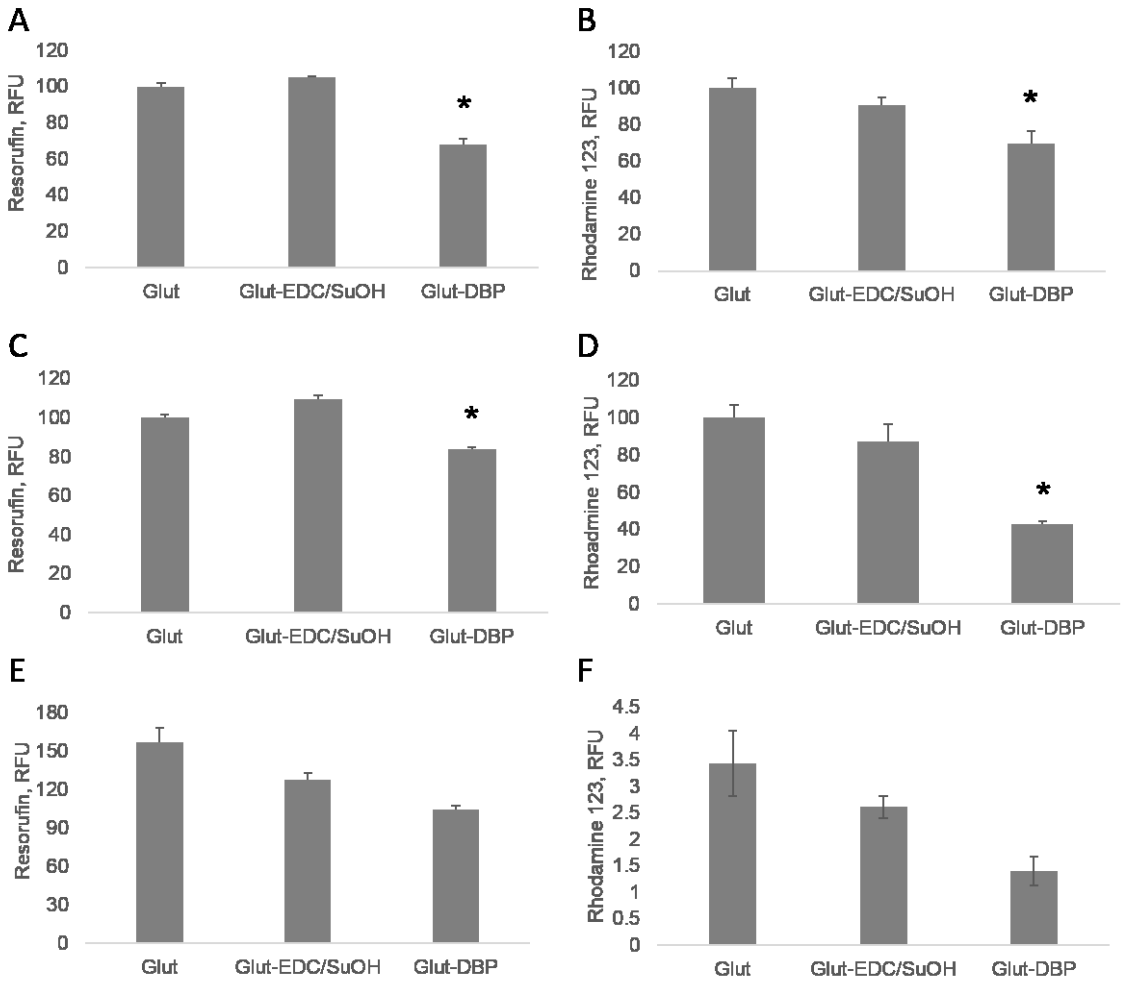

Fig. 3.6 Oxidant scavenging capacity of DBP modified BP. MPO/H_2O_2/Cl oxidation of Amplex red (A) and DHR123 (B). MPO/H_2O_2/NO_2 oxidation of Amplex red (C) and DHR123 (D). HL-60 respiratory burst oxidation of Amplex red (E) and DHR123 (F). * $p<0.05$ vs unmodified (Glut) BP.

DBP mitigates BP oxidation in experimental oxidizing conditions

Previously it was shown that oxidation of BP by a well-known oxidizing system results in significant material destruction as shown by picrosirius red staining, material weight loss, collagenase digestion, and loss of ^{3}H-glutaraldehyde cross-links (Fig. 2.3). When exposed to the same oxidizing conditions, DBP modified BP had significantly less oxidative damage than unmodified BP as shown by picrosirius red staining (Fig. 3.7A-D) and total mass loss, 20.2 ± 2.6% dry weight loss vs. 94.1 ± 0.8% (Fig. 3.7E). DBP modified BP was also less susceptible to digestion by collagenase than unmodified BP ($p = 0.01$) (Fig. 3.7F) and had decreased release of ^{3}H-glutaraldehyde than unmodified BP ($p < 0.01$ (Fig. 3.7G). For all endpoints, the chemically treated BP control (Glut-EDC/SuOH) had no effect on preventing oxidative damage thereby demonstrating that DBP rather than the carbodiimide-driven conjugation reaction is responsible for the attenuation of material oxidative damage.

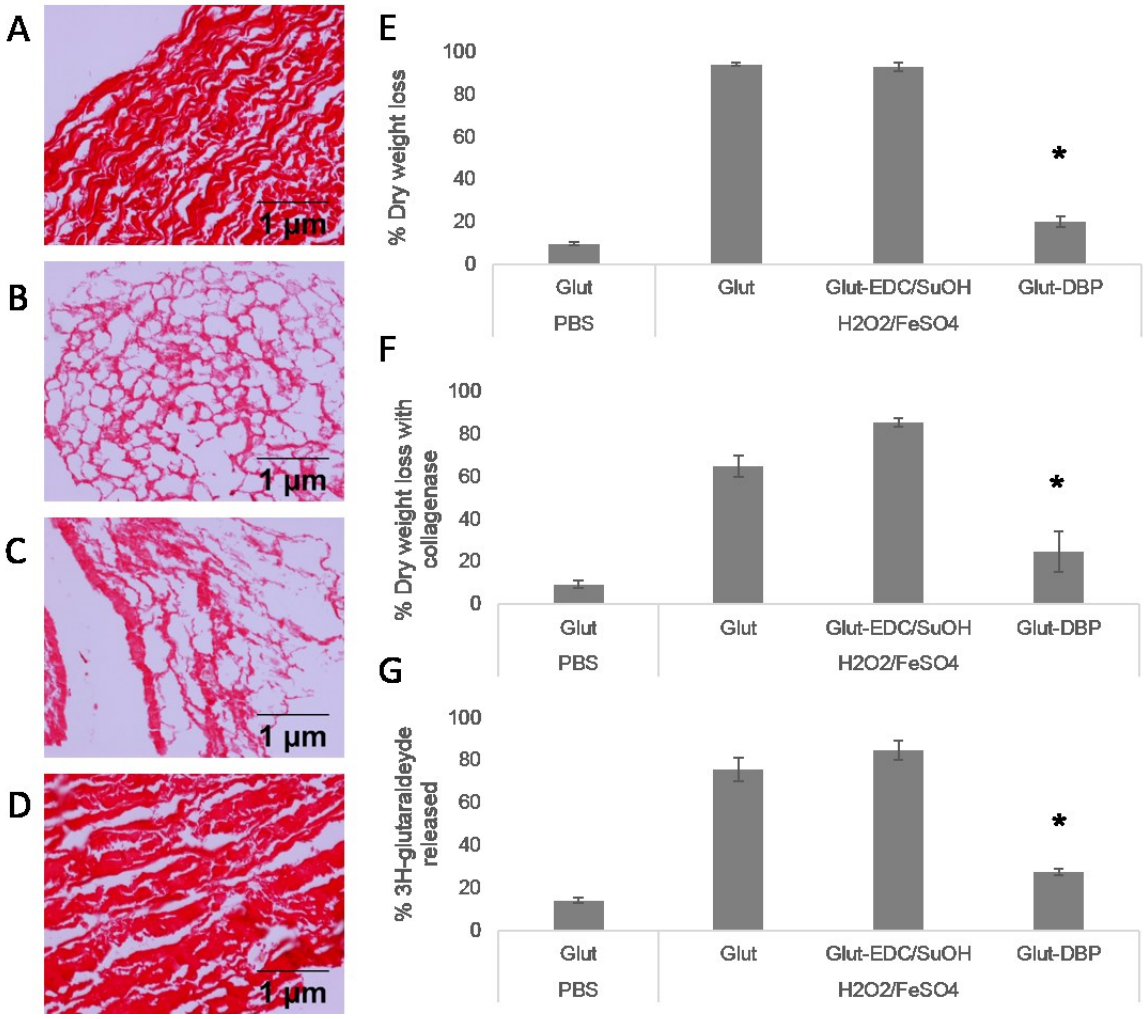

Fig. 3.7 BP oxidation with H_2O_2 and $FeSO_4$. (A-D) Picrosirius red staining of collagen (A) Glut pericardium no treatment (B) Glut pericardium oxidized (C) Glut-EDC/SuOH oxidized (D) Glut-DBP oxidized (E) Dry weight loss of pericardium (F) Collagenase treatment of oxidized pericardium. (G) Stability of ^{3}H-glutaraldehyde cross-linking in PBS and oxidizing conditions. ^{3}H-glutaraldehyde released into solution and ^{3}H-glutaraldehyde bound to tissue at end of treatments. * $p < 0.05$ vs Glut.

Toxicity

Systemic toxicity of DBP modified BP was assessed through measurement of ALP, AST, and creatinine in serum of rats with 90 day BP implants. ALP, AST, and creatinine levels from rats with unmodified BP implants were within or slightly below the reported normal range [110, 111], indicating that the presence of BP alone does not cause systemic toxicity. Both DBP modified BP (Glut-DBP) and carbodiimide reacted BP (Glut-EDC/SuOH) did not cause a significant change in serum ALP, AST, or creatinine (Table 3.2), thereby demonstrating that the DBP modification does not cause systemic toxicity in rats. In addition to the DBP modified and chemistry control samples, the ethanol groups (Glut-EtOH (10 min), Glut-EtOH, and Glut-DBP-EtOH), which were included to assess calcification did not cause systemic toxicity.

	Creatinine (µmol/L)	ALP (U/L)	AST (U/L)
Glut	49.2 ± 2.7	37.8 ± 3.1	21.5 ± 4.1
Glut-DBP	34.8 ± 11.3	39.4 ± 8.8	20.7 ± 1.4
Glut-EDC/SuOH	36.2 ± 12.3	39.2 ± 8.5	34.5 ± 9.3
Glut-EtOH (10 min)	35.7 ± 11.7	58.2 ± 6.5	40.0 ± 16.4
Glut-EtOH	70.9 ± 12.7	50.1 ± 9.1	20.7 ± 7.4
Glut-DBP-EtOH	51.4 ± 4.0	53.0 ± 7.1	35.9 ± 1.9
Normal	50-70 umol/L	~ 100 U/L	30-50 U/L

Table 3.2 Toxicity in rat subdermal implant model. Serum toxicity markers in rats with subdermal BP implants for 90 days.

Calcification

Calcification of BP was assessed in 21 day and 90 day rat subdermal explants to determine the effect of the DBP modification on calcium accumulation since calcification is a significant cause of structural deterioration of BHV. BP that was exposed to 100% ethanol (Glut-EtOH) was used as a positive control for mitigating BHV calcification since this material treatment is used in some clinical grade valves [79]. The DBP modification involves carbodiimide-driven chemistry as well as exposure to ethanol, therefore additional experimental groups were included in this study to control for anti-calcification effects of either the chemistry or ethanol. The mean calcium level in Glut BP explants was 59.4 ± 10.0 μg calcium/mg tissue for 21 day explants (Fig. 3.8A) and 334.6 ± 24.8 μg calcium/mg tissue for 90 day explants (Fig. 3.8B). Calcium levels were significantly lower than Glut for Glut-EtOH 10 minutes, Glut-EtOH, and Glut-DBP-EtOH 21 day explants ($p<0.05$). Glut 21 day explant calcium levels were higher than those of Glut-DBP and Glut-EDC/SuOH (30.3 ± 1.5 μg calcium/mg tissue and 31.9 ± 8.9 μg calcium/mg tissue, respectively), but these differences were not statistically significant. The 21 day results indicate that ethanol exposure provides more resistance to calcification than the DBP modification or carbodiimide chemistry, but these treatments also reduced calcium accumulation. In 90 day explants, Glut-DBP, Glut-EDC/SuOH (carbodiimide chemistry control), and Glut-DBP-EtOH had significantly lower calcium levels than Glut, but Glut-EtOH did not (Fig. 3.8B). Interestingly, the fold increase in calcium from 21 to 90 days was significantly higher in the Glut-EtOH group as compared to all other experimental groups (Fig. 3.8C). This result demonstrates significant breakthrough calcification for this clinically-used anti-calcification strategy. Interestingly, the DBP modification and carbodiimide control did not demonstrate this significant increase in calcification from 21 to 90 days. These results demonstrate that the DBP modification mitigates calcification of BP, but this effect may be due to the carbodiimide chemistry and ethanol exposure rather than the antioxidant activity of DBP.

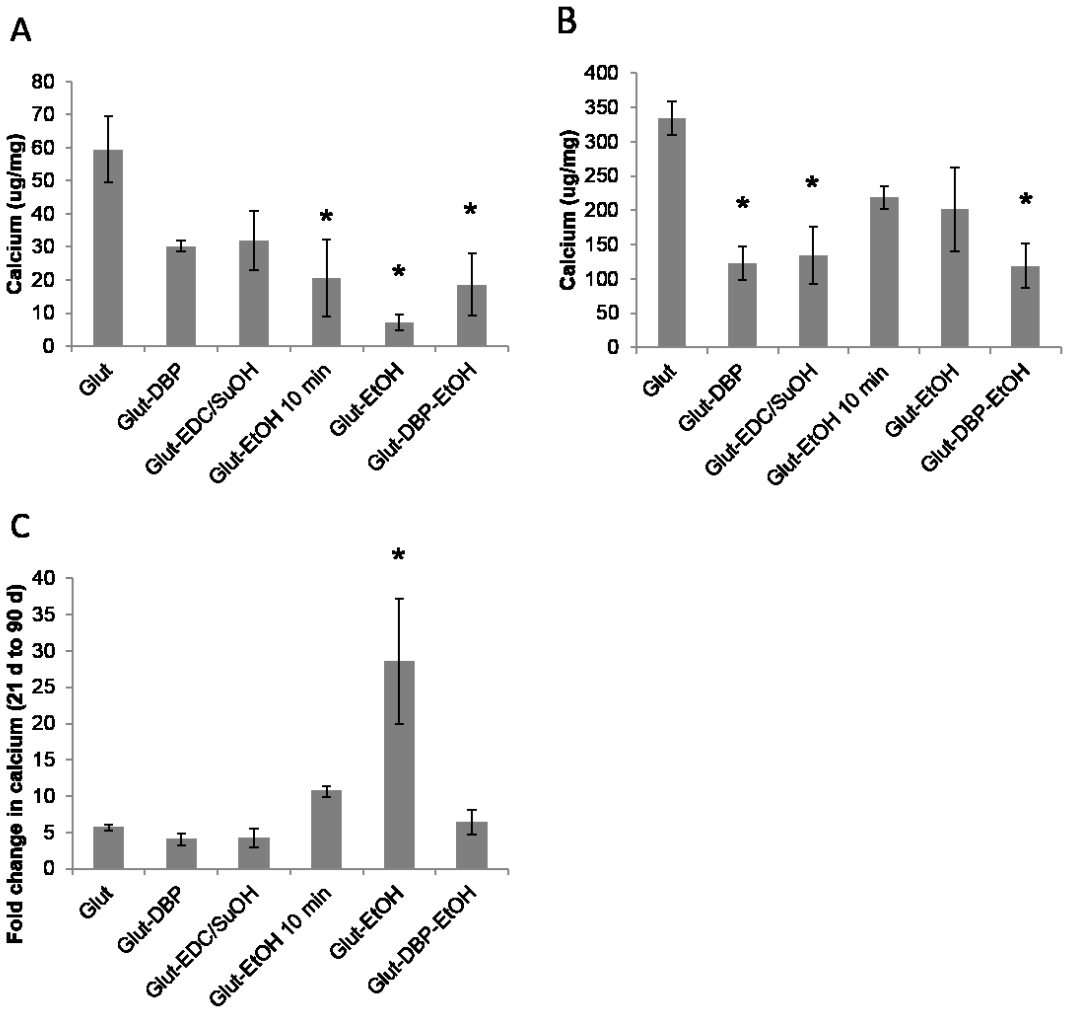

Fig. 3.8 Calcification in rat subdermal implant model. 21 day (A) and 90 day (B) explants. Fold change in calcium levels from 21 to 90 days.

Oxidation

Several endpoints were used to assess BHV oxidation, including hydroxyproline loss, collagenase digestion, shrink temperature, and oxidized amino acids. We previously demonstrated that 90 day BP explants have a significant loss of hydroxyproline, indicating a loss of collagen content. This effect may result from oxidation as well as proteolytic degradation or calcification. Hydroxyproline content was assessed in DBP modified BP explants in order to assess whether DBP has a protective effect against collagen loss. Neither DBP nor the EDC/SuOH control mitigated the loss of hydroxyproline (Fig. 3.9A) thereby demonstrating that DBP does not specifically prevent collagen loss.

Collagenase digestion was significantly increased in BP following exposure to oxidizing conditions, therefore this endpoint was used as a measure of oxidation in 90 day BP explants. The 90 day BP explants were more susceptible to collagenase digestion than non-implanted control tissue, but this difference was not significant by ANOVA ($p=0.075$) (Fig. 3.9B). DBP BP explants were less, but not statistically significant, susceptible to collagenase digestion than unmodified and carbodiimide reacted BP (Glut 13.5 ± 1.8, Glut-DBP 8.1 ± 1.6, Glut-EDC/SuOH 10.4 ± 2.9) (Fig. 3.9C). These results indicate that although the 90 day explants are slightly more susceptible to collagenase digestion than non-implanted materials, DBP does not have a significant effect on proteolytic degradation.

Shrink temperature, as determined by DSC, is used as a measure of material cross-linking, which could be disrupted by oxidative stress. Therefore, the shrink temperatures of BP explants were assessed to determine whether this endpoint could be used as an in vivo marker of oxidative stress. Unmodified (87.1 ± 0.5 °C control vs 84.4 ± 0.6 °C explant)and carbodiimide reacted BP (90.1 ± 0.1 °C control vs 87.4 ± 0.1 °C explant) had significantly lower shrink temperatures than non-implanted controls ($p=0.031$ and $p=0.0012$, respectively). The shrink temperatures of non-implanted DBP and DBP explants were not significantly different ($p=0.65$) (Fig. 3.9C). These results demonstrate that BP material cross-linking is affected during implantation as indicated by a decrease in shrink temperature and DBP can mitigate this effect, thereby demonstrating a protective effect in vivo.

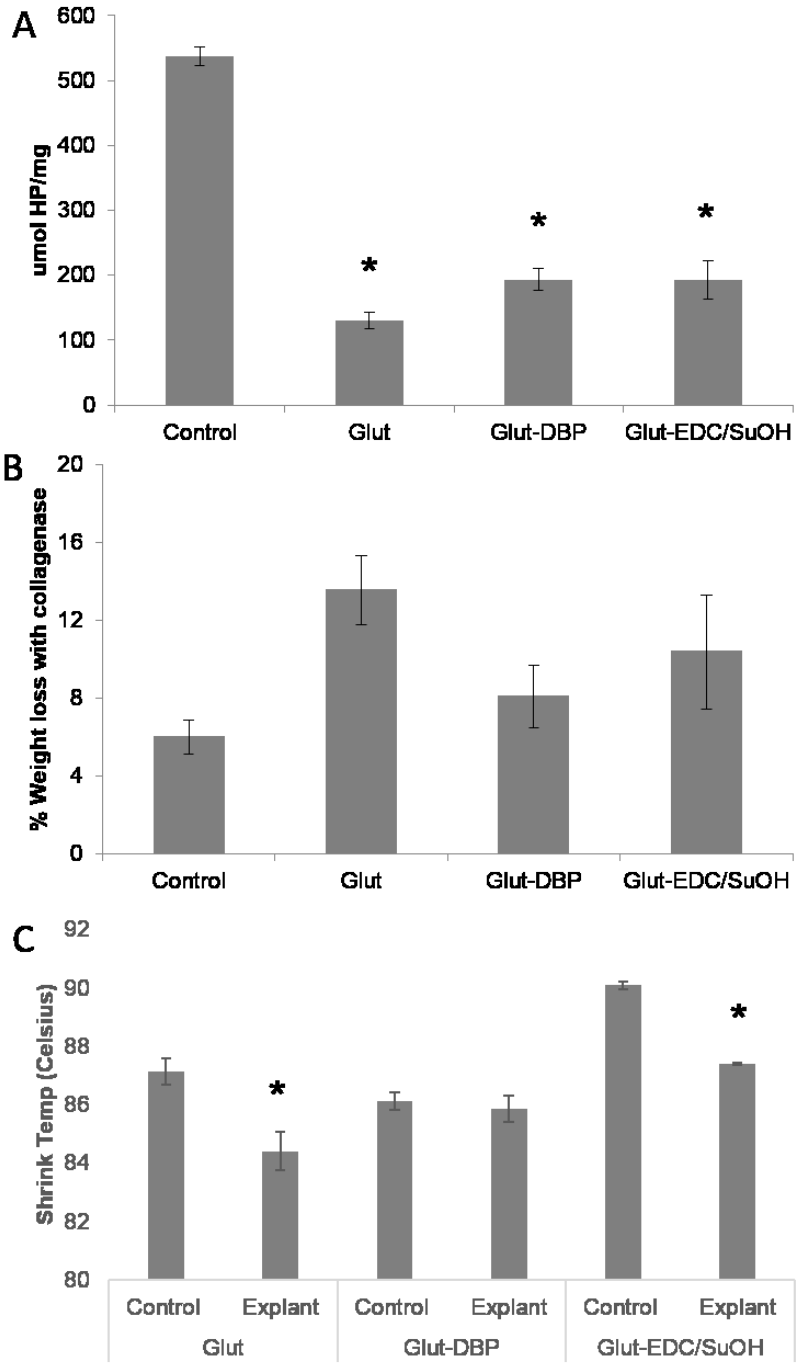

Fig. 3.9 Oxidation of rat subdermal explants. Loss of hydroxyproline in 90 day explants as compared to non-implanted BP (control) (A). Collagenase digestion of 90 day explants and non-implanted BP (B). Shrink temperature differences between controls and explants (C). * $p<0.05$ vs control.

In previous studies, the levels of oxidized amino acids in 7 and 21 day rat subdermal implants were shown to be only mildly elevated as compared to non-implanted materials (Fig. 2.5). However, since it was not feasible to test the effect of the DBP modification in a different animal model, such as a sheep circulatory implant, the rat subdermal implant model was used to assess the effect of DBP on this oxidative endpoint. Dityrosine levels are shown for the rat subdermal explants since this adduct was found only in clinical BHV explants and not in control non-implanted tissues. Dityrosine was detected in some but not all 21 day explants; 3 of the 5 DBP modified explants had measurable levels of dityrosine (Fig. 3.10). Due to the low levels of dityrosine in the explants, it was not possible to fully assess whether DBP had an effect on the accumulation of this adduct.

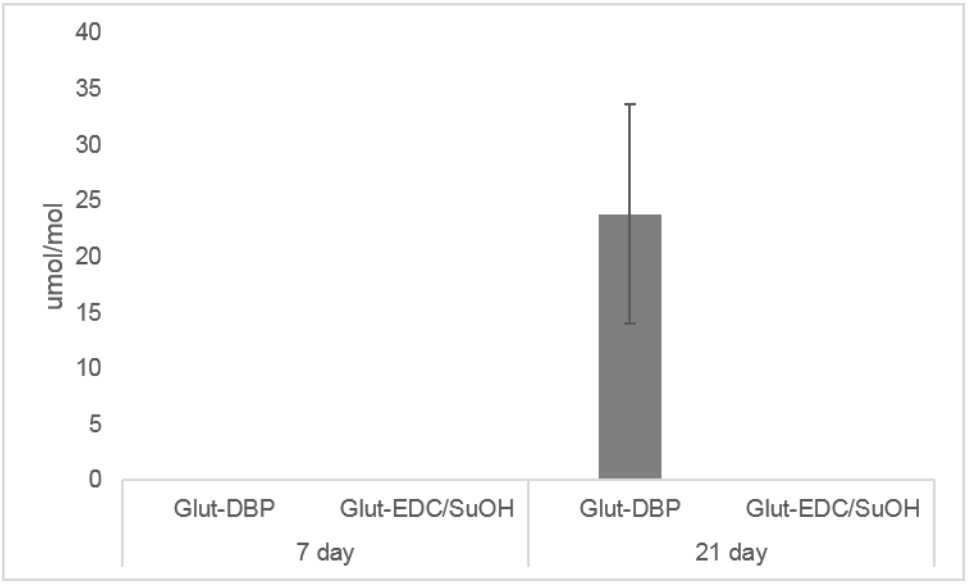

Fig. 3.10 Dityrosine in rat subdermal explants. Dityrosine levels in 7 and 21 day Glut-DBP and Glut-EDC/SuOH rat subdermal explants.

3.5 Discussion

BHV have been shown to be susceptible to oxidative degradation; therefore, the use of antioxidants may prevent BHV degeneration. As a strategy to mitigate oxidation-mediated degradation of BHV, the BHV material BP was modified with the antioxidant DBP. After confirming the attachment of DBP to BP, we demonstrated that the modification does not alter the mechanical or material properties of BP, which could otherwise affect hemodynamic properties. The oxidant scavenging activity of DBP following immobilization to BP was characterized, thereby demonstrating that DBP retains antioxidant activity. Subsequently, DBP mitigated oxidative damage of BP in an accelerated model. To translate these findings to an animal model, DBP modified BP was subject to the rat subdermal implant system. DBP attenuates the loss of material cross-linking normally seen with unmodified BP explants. In addition, DBP combined with the carbodiimide chemistry and ethanol treatment, reduced the progression of calcification to a greater extent than ethanol pretreatment alone. These studies demonstrate that an antioxidant modification of BHV materials can reduce BHV structural degeneration.

Since previous pretreatment and local delivery strategies for BHV have not involved incorporation of a compound in the BHV leaflets, a major component of these studies was the optimization of the reaction used for immobilizing DBP to BP. Carbodiimide-driven reactions have previously been used in the context of BHV, but for the purpose of additional material cross-linking rather than immobilizing an active compound such as DBP [39, 45]. The efficiency of the carbodiimide-driven reaction used to immobilize DBP to BP was assessed by first determining the theoretical maximal binding of DBP, which is mediated through reactions with carboxylic acids provided by aspartate and glutamate residues of BP. Aspartate and glutamate composition was then compared to the actual binding of DBP as determined with ^{14}C labeled DBP. Based on this comparison, we determined that the attachment of DBP to BP is nearly maximized. It was therefore not necessary to further optimize the modification reaction for DBP attachment.

A major advantage of BHV over mechanical prosthetic valves is the blood-material properties which result in a lower risk of thrombosis [112, 113]. Therefore, any material modifications involving the BHV leaflet materials should not alter these properties. To demonstrate

that DBP modified BP leaflets would have similar properties to unmodified BP leaflets, uniaxial tensile testing was performed. Uniaxial tensile stress is only one of the types of mechanical stresses affecting BHV leaflets. In addition, BHV leaflets are subject to cyclical flexural and shear stresses [16, 114]. Only uniaxial tensile testing was performed due to a lack of availability for a mechanical testing system that could asses all types of mechanical stresses affecting BHV leaflets. The tensile properties as well as material cross-linking were not affected by DBP, therefore indicating that the DBP modification would be unlikely to affect hemodynamic properties of a BHV leaflet. However, future studies should address the performance of DBP modified BHV both under other forms of mechanical stress such as flow conditions or cyclical fatigue, and ideally in vivo inthe circulation with blood-material interactions.

The structure of DBP is based on the widely used antioxidant BHT [48]. BHT scavenges and removes oxidants through oxidation of the hydroxyl group to form phenoxyl radicals that can be oxidized to various structures through reorganization of the free radical [49]. Since DBP differs from BHT only due to the addition of a propyl amine, not directly next to the hydroxyl group or the *tert*-butyl hindering groups, it is unlikely that the antioxidant activity of these compounds would be significantly different [115]. However, since DBP is immobilized rather than free in solution, we confirmed the scavenging activity of DBP following attachment to BP. DBP modified BP has scavenging activity against both ROS and RNS, which establishes that DBP retains scavenging activity after immobilization to BP. Multiple oxidant generating systems, including a cell-based system, were used to demonstrate that DBP is a broad acting oxidant scavenger, which is important since tyrosyl radicals, which can result in dityrosine formation as found in clinical BHV explants [102], can be produced by a range of oxidants.

DBP modified BP was subject to an accelerated model of BHV oxidative degradation in order to determine the ability of DBP to mitigate oxidative damage of BP. DBP mitigated all parameters of BHV oxidation including collagenase digestion, ^{3}H-glutaraldehyde release, and general collagen degradation. This model has previously been used to assess biomaterial oxidative degradation, but does require the use of non-physiologic conditions, therefore comparison with additional models should be used. Furthermore, it is striking that DBP was able

to protect BP from oxidative degradation in this model due to the severity of the oxidizing conditions. Although additional studies using either animal models or physiologic conditions should be used to corroborate these findings, the accelerated model of oxidative degradation demonstrated significant efficacy of DBP in mitigating BP oxidative degradation.

The rat subdermal implant model is one of the established animal systems for testing BHV degradation. In particular, this model results in accelerated calcification of BHV materials, which has been shown to be caused by several factors including elevated levels of serum calcium and phosphorus in juvenile rats as well as higher alkaline phosphatase activity [68]. It has not been directly studied whether the location of the implant (subdermal) also contributes to accelerated calcification. Such a study would be technically challenging, if not impossible. As expected for this model, the unmodified BP implants had significant calcium accumulation at both 21 days and 90 days. Previously these levels have been correlated with mean calcium levels seen in explanted clinical BHV [68]. Somewhat surprisingly, DBP modified BP rat subdermal explants were less calcified than unmodified BP at the 90 day time point. Additionally, the clinically-used anti-calcification pretreatment of 24 hour ethanol exposure did not have significantly lower calcium accumulation than unmodified BP at 90 days; thereby demonstrating that the DBP modification may be superior to ethanol treatment in preventing long-term calcification. However, it is unclear if DBP alone mitigates BHV calcification, since the chemistry control group also had significantly less calcium accumulation. The combination of the scavenging activity of DBP and the carbodiimide-driven chemistry may be an effective anti-calcification strategy. Future studies should address whether oxidation is directly involved with BHV calcification and whether the antioxidant activity or the carbodiimide-driven chemistry is more important for the anti-calcification effect observed with DBP modified BP.

Some compounds that have antioxidant activity also possess anti-inflammatory activity due to the involvement of oxidants in various signaling pathways such as nuclear factor kappa B-mediated production of inflammatory cytokines and subsequent cellular recruitment and activation [116, 117]. Therefore, we hypothesized that DBP may have an effect on the overall inflammatory response to BHV leaflets. This hypothesis was tested in the rat subdermal implant model for

endpoints including cellular recruitment, cytokine production and myeloperoxidase expression (data not shown). Unfortunately, we did not observe anti-inflammatory properties for DBP; therefore suggesting that the major mechanism of action for DBP is its oxidant scavenging properties.

Oxidation of BHV materials has not previously been assessed by other research groups in the rat subdermal implant model. Furthermore, the major focus of this system is calcification over other mechanisms of BHV degeneration. We sought to determine whether this model could recapitulate the oxidative degradation endpoints we identified in both clinical BHV explants, specifically dityrosine, or in the accelerated oxidative degradation system. Previously we used histology to demonstrate a breakdown of BP collagen structure following exposure to oxidizing conditions. In the rat subdermal implant model, the destruction of the collagen structure was not as obvious, therefore we added material cross-linking as a measurement of BP degradation. Unmodified BP explants from the rat model had a loss of material cross-linking as demonstrated by a decrease in shrink temperature, which was not observed with the DBP modification. This suggests that DBP may prevent BHV degeneration associated with a breakdown of cross-linking. Additionally, loss of BHV cross-linking could be associated with calcification progression since the growth or expansion of calcium phosphate crystals would either breakdown normal material cross-linking, or physically expand in weakened areas due to oxidative damage to crosslinks [13]. Therefore, the DBP effect on cross-linking may also be related to calcification prevention.

Dityrosine formation in rat subdermal BP explants was previously found to poorly correlate with the levels measured in clinical BHV explants (Chapter 2). However, we did assess the effect of DBP on dityrosine simultaneously with the unmodified explants. DBP did not affect dityrosine, which can likely be attributed to the rat subdermal implant model rather than a lack of activity by DBP since there is only a modest elevation in dityrosine and inconsistently across explants. This model was used for assessment of DBP in an animal system since it provides a low cost and technically simple model for testing BHV materials. However, this model lacks direct blood flow and mechanical forces that BHV normally experience and exposure to shear stress has been found to increase oxidative damage [87]. In earlier studies, it was shown that the sheep explants had

dityrosine levels similar to those in clinical BHV explants despite the short implantation period. It was not possible to test DBP modified BP in a large animal model. Future studies with DBP should focus on large animal models that involve direct blood contact and exposure to mechanical stress.

Covalent modification of the BHV material BP with DBP mitigated oxidative damage in the accelerated model. In addition, this modification did not adversely affect the material properties of BP or the scavenging activity of DBP. Although the covalent attachment of DBP to BHV did not prevent dityrosine formation in the rat subdermal implant model, it did mitigate calcium accumulation as well as cross-linking breakdown. Thus, these results demonstrate in both the accelerated model and the rat subdermal implant model that an antioxidant modification of BHV materials, specifically with DBP, effectively attenuates structural degeneration associated with oxidative stress.

Chapter 4: Attenuation of BHV oxidation with superoxide dismutase mimetics

Manuscript in preparation:

Christian AJ, Garofolo S, Tovmasyan A, Batinic-Haberle I, Bianco R, Ischiropoulos H, Levy RJ. Mitigation of bioprosthetic heart valve oxidation with a superoxide dismutase mimetic.

4.1 Abstract

Previously, we demonstrated that the oxidant scavenger DBP is capable of mitigating BHV oxidation. In order to improve upon the DBP modification strategy, we proposed the use of a class of catalytic antioxidants, MnPyP SOD mimetics. SOD mimetics such as MnPyP are able to remove oxidants in a non-stoichiometric manner; therefore, unlike DBP, they may be able to provide sustained antioxidant protection for BHV. Three MnPyP SOD mimetics, MnTE-2-PyP, MnTnOct-2-PyP, and MnTnOct-3-PyP, were compared for use with BHV in terms of efficiency in passive, or non-covalent, uptake into the BHV material BP. MnTnOct-2-PyP and MnTnOct-3-PyP had greater retention in BP than MnTE-2-PyP. Since MnTnOct-2-PyP is a more potent SOD mimetic than MnTnOct-3-PyP, it was identified as the best candidate for use with BHV. In addition, we tested whether MnTnOct-2-PyP could be packaged in liposomes for targeted drug delivery; based on the high retention of MnTnOct-2-PyP in BHV we expected that the compound would be a good candidate for this purpose. We demonstrated that MnTnOct-2-PyP is efficiently incorporated into liposome drug carriers. MnTnOct-2-PyP loaded BP was tested in the rat subdermal implant model as well as in a sheep circulatory model to assess its effect on BP degradation. Calcification, which remains a significant issue with BHV durability, was not significantly affected by the presence of MnTnOct-2-PyP in BP. In the sheep patch implant model, which provides both exposure to blood flow and mechanical forces, MnTnOct-2-PyP demonstrated SOD activity following implantation which indicates stable retention of MnTnOct-2-PyP in BP. The effect of MnTnOct-2-PyP on BHV oxidation as measured by dityrosine is pending the completion the analysis of these materials. These studies demonstrate that MnPyP SOD mimetics can be stably incorporated in the BHV material BP, as well as liposomes, without covalent or other active conjugation while maintaining SOD activity and may provide sustained antioxidant protection for BHV.

4.2 Introduction

Antioxidants such as DBP are limited in their oxidant scavenging capacity since they react with oxidants in a stoichiometric nature [49]. Compounds such as SOD mimetics scavenge oxidants through redox cycling of a metal center, undergoing reversible reduction and oxidation while removing potentially damaging oxidants [62]. This mechanism of redox cycling provides catalytic activity with the potential for long-term antioxidant activity since the original compound is not irreversibly reduced or oxidized in the process of removing oxidants. We hypothesized that a catalytic antioxidant such as an SOD mimetic could improve upon the previous DBP strategy for mitigating oxidation-mediated BHV degradation by providing sustained antioxidant protection.

SOD has the physiological role of controlling superoxide ($O_2^{-\bullet}$) concentration by catalyzing its dismutation into molecular oxygen and hydrogen peroxide [118]. Superoxide is normally formed through mitochondrial electron leak or by inflammatory and endothelial cells [118]. Superoxide is involved in various signaling events and in the activation of redox sensitive transcription such as hypoxia factor 1 (HIF-1) and nuclear factor kappa B (NF-κB) which are involved in processes such as cellular proliferation and neutrophil recruitment and activation [62, 63, 119]. In situations of excessive superoxide production such as in acute inflammation, without removal by SOD, superoxide could cause damage to DNA, lipids, or proteins [118]. Superoxide is capable of oxidative protein fragmentation at proline residues, which is relevant to the degradation of BHV since collagen has a significantly higher percent of proline residues (16% of all amino acids) as compared to the average protein (5.6%) and may therefore be more susceptible to superoxide-mediated damage [55]. Although superoxide is able to direct damage proteins [28, 56], it has been proposed that the major deleterious effects of superoxide overproduction or loss of SOD function are mediated through the production of other more reactive oxidants from superoxide [55, 118]. Superoxide is involved in the production of peroxynitrite (ONOO-) from nitric oxide [58] as well as hydrogen peroxide and subsequently hydroxyl radicals through Fenton chemistry[120]. The use of SOD or an SOD mimetic may effectively mitigate BHV oxidation by controlling the formation of other oxidants as well as preventing direct damage by superoxide.

The clinical use of native SOD is limited by its size, susceptibility to proteolytic degradation leading to a short circulating half-life, antigenicity, and the expense of large-scale protein production [54]. Due to these limitations as well as the significance of SOD in various disease states including atherosclerosis, cancer, and amyotrophic lateral sclerosis [62], synthetic compounds that are capable of mimicking the activity of SOD have been developed. At this time there are numerous classes of SOD mimetics available. The consistent structural feature of the SOD mimetics is a redox reactive metal center, typically manganese, iron, or copper [54, 63]. The most potent SOD mimetics also have a ring structure and cationic substituents to provide electrostatic guidance for superoxide towards the metal center [62, 64]. SOD mimetics dismutate superoxide through the same mechanism as native SOD: oxidation M^{n+1}-SOD+ $O_2^{-\bullet} \rightarrow M^n$-SOD + O_2 and reduction M^n-SOD + $2H^+ + O_2^{-\bullet} \rightarrow M^{n+1}$-SOD + H_2O_2 [62]. Some of the important features of an SOD mimetic are the reduction potential of the metal center which should equally favor both reduction and oxidation, the catalytic rate constant for superoxide dismutation, and stability of the metal center [60, 62, 121]. The reduction potential of the metal center for native SOD is +300 mV vs. normal hydrogen electrode (NHE); this value is nearly evenly between the potential for superoxide oxidation (-160 mV) and reduction (+890 mv), thereby not favoring one reaction [62]. Loss of the metal center can occur for compounds that favor the oxidation reaction and the lower oxidation state of the metal [62].

MnPyP are a class of SOD mimetics that have been widely studied and optimized for SOD activity, lipophilicity, and bioavailability and are therefore good candidates for clinical use. MnPyP SOD mimetics have additional antioxidant functions including scavenging of peroxynitrite and peroxyl radicals [54, 64]. A broad acting antioxidant is favorable for use with BHV since there are a variety of reactive species produced during inflammation and in normal physiology. The MnPyP SOD mimetics are also capable of scavenging H_2O_2 [54] by mimicking catalase: Mn(III)-PyP + H_2O_2 + $2H^+ \rightarrow$ Mn(IV)-PyP + $2H_2O$ and Mn(IV)-PyP + $H_2O_2 \rightarrow$ Mn(III)-PyP + O_2 + $2H^+$ [122] or peroxidase Mn(III)-PyP + H_2O_2 + $AH_2 \rightarrow$ Mn(III)-PyP + A + $2H_2O$, where A is an oxidizable substrate [123]. The catalase and peroxidase activity of the SOD mimetics is an important function since H_2O_2 is produced through the dismutation of superoxide [62]. Therefore, a specific SOD mimetic that

lacked any catalase or peroxidase activity could be potentially damaging through this pro-oxidant activity of producing H_2O_2 [124]. By using SOD mimetics that can scavenge other oxidants, particularly H_2O_2, it may be possible to avoid the deleterious effects of H_2O_2 production from superoxide dismutation.

In addition to antioxidant activity, the MnPyP SOD mimetics are cationic and possess hydrophobic alkyl chains that may mediate uptake into a tissue such as BP [46, 119]. Hydrophobic compounds are able to partition through lipid membranes, thereby resulting in higher cellular or tissue uptake [119]. Thus, a hydrophobic compound such as a MnPyP is expected to have more efficient uptake into a BHV material. The charge of the compound may also contribute to the distribution of a compound within a tissue or cell. Collagen contains both negatively and positively charged residues [125], therefore a charged compound may be able to interact with these regions to facilitate stable incorporation through ionic interactions. Both electrostatic and hydrophobic interactions may facilitate uptake and retention into tissues thereby avoiding the use of a chemically-driven reaction and the exposure to additional reagents that may affect the activity of the MnPyP or the integrity of the BHV material.

A compound that has efficient uptake into a tissue such as BHV heterograft materials may also be efficiently incorporated into lipid-based drug carriers or liposomes for targeted drug delivery [126]. There are numerous applications including solid tumor cancers and inflammatory conditions in which targeted drug delivery may be advantageous in either altering pharmacokinetic properties, reducing toxicity, or improving efficacy [127]. In addition, targeted delivery of antioxidants such as SOD mimetics may be useful in treating conditions involving oxidative stress such as endothelium dysfunction related to acute lung injury [128-131].

Three manganese pyridyl porphyrin SOD mimetics were provided by the Batinic-Haberle group of Duke University: MnTE-2-PyP, MnTnOct-2-PyP, and MnTnOct-3-PyP. The two ortho substituted compounds (MnTE-2-PyP and MnTnOct-2-PyP) have stronger SOD activity than the meta substituted compound (MnTnOct-3-PyP) as determined by the rate constant for superoxide dismutation, $\log k_{cat}$, which have been reported as 7.76, 7.71, and 6.53, respectively [61]. In addition to differences in SOD activity, the compounds also differ in lipophilicity as determined by both the

thin layer chromatography retention factor (R_f) and the octanol-water partition coefficient ($logP_{OW}$), with MnTnOct-3-PyP being most lipophilic (R_f 0.656, $logP_{OW}$ not reported), followed by MnTnOct-2-PyP (R_f 0.644, $logP_{OW}$ -2.32), and MnTE-2-PyP (R_f 0.156, $logP_{OW}$ -7.79) [61, 132]. Here we assessed the incorporation of MnPyP SOD mimetics into the BHV material BP and the effect of these compounds on BHV oxidation.

4.3 Materials and Methods

Materials

MnTE-2-PyP, MnTnOct-2-PyP, and MnTnOct-3-PyP were provided by Ines Batinic-Haberle (Duke University, Durham, NC). Phospholipids were purchased from Avanti Polar Lipids (Alabaster, AL). All chemicals unless otherwise specified were obtained from Sigma Aldrich (St. Louis, MO).

Spectroscopy

The manganese pyridyl porphyrin SOD mimetics absorb in the visual spectrum, which allows for quantification by spectroscopy. The three SOD mimetics tested have a maximum absorbance at 455 or 460 nm [132, 133]; these wavelengths were used for measuring the concentration of a compound in solution.

Incorporation of SOD mimetics in BP

BP samples were incubated in aqueous solutions of MnTE-2-PyP, MnTnOct-2-PyP, or MnTnOct-3-PyP for 18-24 hours overnight at 37 °C with shaking. At the end of the incubation, the concentration of unreacted compound was determined by absorbance of the reaction solution at the maximum absorbance, 455 or 460 nm. BP samples that had been incubated with SOD mimetics were placed in 5 mL PBS for release at 37 °C with shaking. PBS solutions were changed after 2 and 4 hours then every 24 hours for 5 days at which point no measurable amount of compound released was measured. A455 or A460 was used to measure the amount of compound released from BP. The amount of SOD mimetic retained within the BP sample was determined by

subtracting the amount of compound in the wash steps and 5 day release period from the total compound reacted. Samples were stored at 4°C in PBS for future use.

SOD activity of drug loaded BP

The nitroblue tetrazolium (NBT) reduction assay was adapted to measure SOD activity of SOD mimetics incorporated in BP (Fig. 4.1) as previously described [134]. BP samples (4 mm) were incubated in nitroblue tetrazolium salt (10 mg/mL) for 20 minutes at room temperature. The samples were then rinsed before adding a solution containing xanthine (59 μM), followed by xanthine oxidase. The reaction proceeded overnight at room temperature. The samples were washed and imaged. Image analysis was done with ImageJ. Mean gray value of the images were used to determine NBT reduction; mean gray value is reported as a fold change from the same tissue before exposure to NBT.

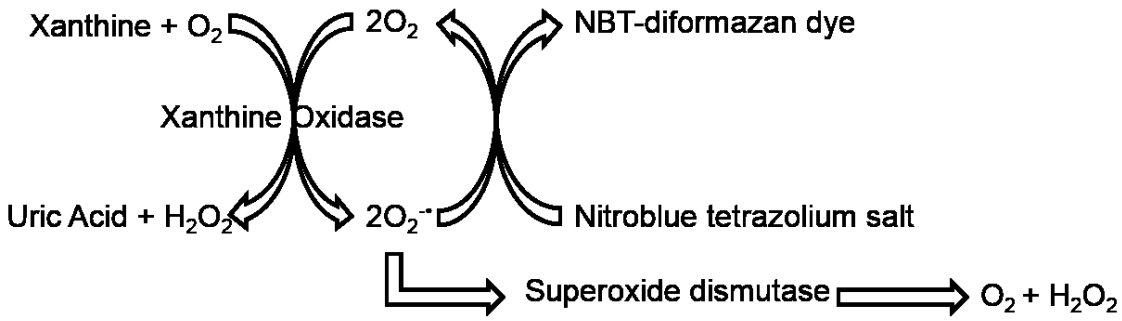

Fig. 4.1 NBT reduction assay. The reaction of xanthine oxidase with xanthine produces superoxide as well as uric acid and hydrogen peroxide. NBT is reduced to NBT-diformazan dye in the presence of superoxide. When superoxide dismutase or SOD mimetics are present, NBT is not reduced since SOD dismutates superoxide to oxygen and hydrogen peroxide.

Rat subdermal implants

Three week old male Sprague-Dawley rats (60-90 grams) and 1 cm^2 BP samples were used for the rat subdermal implantation studies as previously described [68]. A loading dose of 150 μg MnTnOct-2-PyP was used for each 1 cm^2 BP section. Following the standard uptake protocol, the implants were washed in PBS for up to 7 days to avoid leaching of MnTnOct-2-PyP from the BP sample. The animals were sacrificed at 90 days and the explanted BP samples were processed for either paraffin embedding, acid hydrolysis, or the NBT assay. Paraffin embedding

was performed following fixation in neutral buffered formalin. Acid hydrolysis was performed on lyophilized tissues for calcium quantification. The NBT assay was done as previously described with 4 mm sections.

Sheep patch implants

Sheep patch surgeries were done in collaboration with Professor Richard Bianco and colleagues in the Department of Surgery at the University of Minnesota. Two loading doses of MnTnOct-2-PyP were used to determine the effective dose range for MnTnOct-2-PyP. Either 15 µg or 150 µg MnTnOct-2-PyP was added to 1 cm^2 BP sections for low and high doses, respectively. Loaded samples were then washed for up to 7 days in PBS prior to implantation. The patches were also washed in 4% paraformaldehyde for sterilization. Six BP patches, either control or MnTnOct-2-PyP loaded were sewn into the walls of the aorta, left atrium, or pulmonary artery of each sheep. Previous studies have used similar patch models for exposing BHV materials to blood flow [71, 135]. In the left atrium and aorta, 1 control and 1 high dose MnTnOct-2-PyP patches were placed at each site. In the pulmonary artery, 1 control and 1 low dose MnTnOct-2-PyP patches were placed. A total of 4 sheep were included in this study. After 90 days, the animals were sacrificed and the patches were removed en bloc. The primary endpoint for analysis was oxidized amino acid quantification, which was performed on paraffin sections. Remaining tissue was acid hydrolyzed for calcium quantification. The NBT assay was performed on only the aortic patches from 2 animals due to the availability of explanted tissue.

Liposome preparation and characterization

For proof of principle studies with a targeted liposomal drug delivery system and MnPyP, liposomes were conjugated to an endothelial antibody, platelet endothelial cell adhesion molecule (PECAM), for formulation studies with SOD mimetics, through collaboration with Vladimir Muzykantov, Melissa Howard, and Elizabeth Hood at the University of Pennsylvania. The PECAM antibody was thiolated with SATA for covalent interaction with maleimide, which was introduced into the lipid bilayer as DSPE-PEG-maleimide, thereby also providing a PEG linker. Liposomes were prepared by dehydration and extrusion. Briefly, 1,2-dipalmitoyl-sn-glycero-3-phosphocholine

(DPPC), 1-hexadecanoyl-sn-glycero-3-phosphocholine (PC), L-α-phosphatidylglycerol (PG), cholesterol, and 1,2-distearoyl-sn-glycero-3-phosphoethanolamine-N-[maleimide(polyethylene glycol)-2000] (ammonium salt) (DSPE-PEG(2k)-maleimide) in chloroform were combined for a molar ratio of 4.47:2.16:1.00:1.34:0.38:0.1 as previously described [129, 130]. The lipid solution was dehydrated overnight, leaving a solid lipid film. The film was resuspended through shaking in an aqueous solution of MnTnOct-2-PyP. The rehydrated, drug-containing films, were subject to three cycles of freeze-thawing to improve drug loading efficiency. The lipid films were then extruded 10 times through 200 nm filters using an Avanti mini extruder to generate uni-lamellar liposomes. Rat IgG and PECAM antibodies were thiolated with N-Succinimidyl S-Acetylthioacetate (SATA) then added to the lipid films afer extrusion. The liposomes were purified by ultracentrifugation and resuspended in PBS. To determine antibody conjugation efficiency, 10% I^{125} labeled-IgG was added to liposome preparations for quantification with a gamma counter; this small percent of radiolabeled antibody was used to avoid false positives from unbound antibodies. Size and polydispersity of the liposomes was assessed with dynamic light scattering. Loading efficiency of MnTnOct-2-PyP was determined both by A455 by disrupting the liposomes in 1% Triton X-100 as well as by SOD activity with the cytochrome c assay. Liposomes were tested intact and disrupted (with 1% Triton X-100) to measure SOD activity by the cytochrome c reduction assay (Fig. 4.1) as previously described [136, 137]. A reaction buffer consisting of xanthine (59 μM), cytochrome c (23.5 μM), 50 mM potassium phosphate,100 μM EDTA, pH 7.8 was added to the liposome samples. To initiate the production of superoxide, xanthine oxidase was added to all samples. Absorbance at 550 nm was monitored for the reduction of cytochrome c (Fe^{3+}) to cytochrome c (Fe^{2+}), which absorbs at 550 nm.

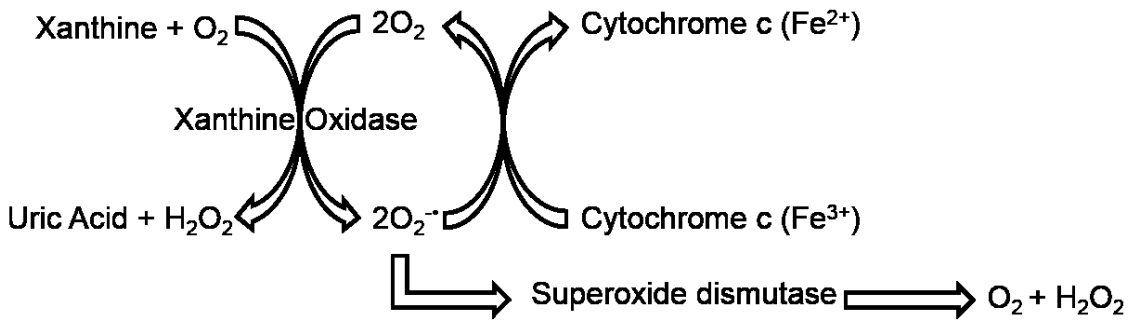

Fig. 4.2 Cytochrome c reduction assay. The reaction of xanthine oxidase with xanthine produces superoxide as well as uric acid and hydrogen peroxide. Cytochrome c (Fe^{3+}) is reduced to cytochrome c (Fe^{2+}) in the presence of superoxide. When superoxide dismutase or SOD mimetics are present, cytochrome c (Fe^{3+}) is not reduced to cytochrome c (Fe^{2+}) since SOD dismutates superoxide to oxygen and hydrogen peroxide.

Targeting of the PECAM-liposomes was compared to the IgG-liposomes by incubating the liposomes with PECAM-expressing cells, human umbilical vein endothelial cells (HUVEC). Cells were blocked with 3% bovine serum albumin before adding the liposomes. Liposomes were left on the cells for 30 minutes. Liposome binding was assessed by gamma counting of I^{125} in the cell pellet as compared to the supernatant.

4.4 Results

Characterization of SOD mimetics

Since the analysis of the MnPyP relied heavily on their quantification from absorbance, both the structures and absorbance spectra of MnTE-2-PyP, MnTnOct-2-PyP, and MnTnOct-3-PyP are shown in Fig. 4.3A-D. The compounds display a maximum spectral peak between 455 and 460 nm, whose intensity is dependent on the concentration of compound (Fig. 4.3D). Absorbance at the spectral peak can be used to determine the concentration of the compound in solution from a standard curve (Fig. 4.3E).

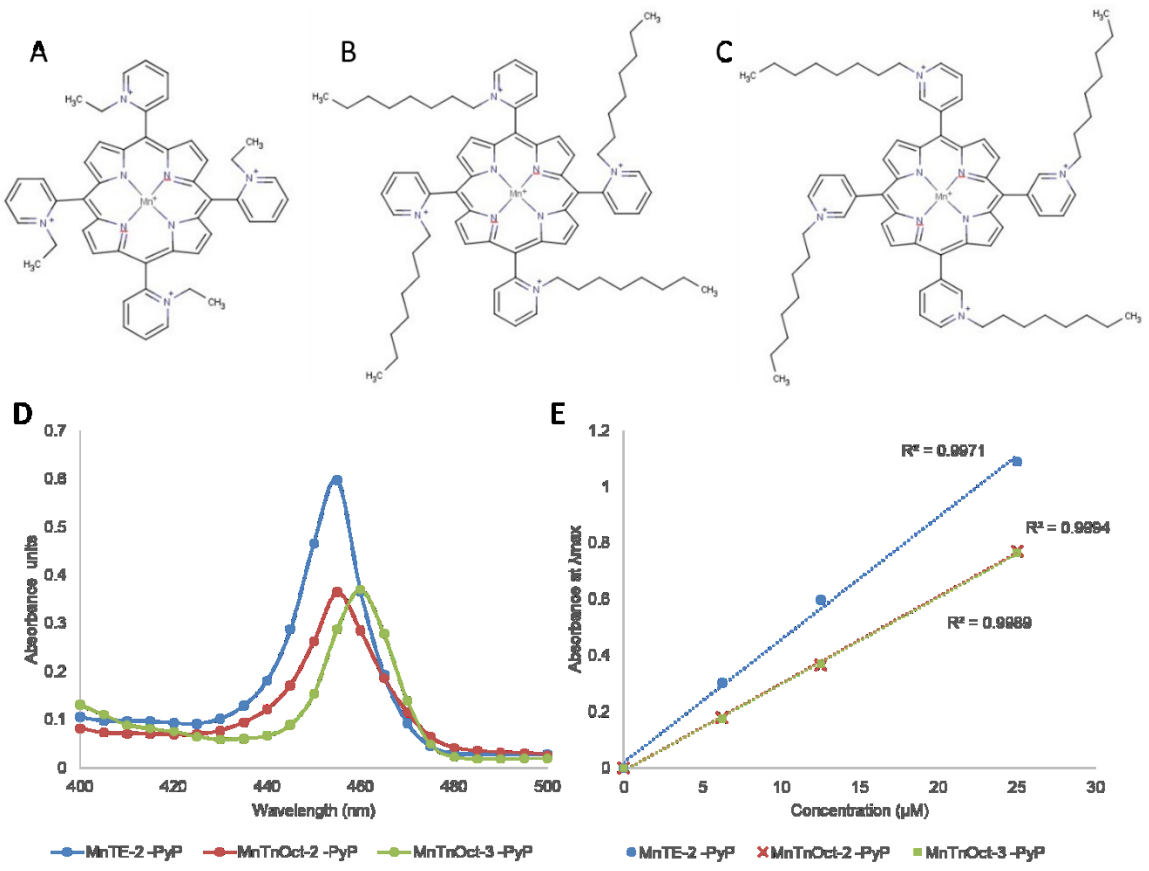

Figure 4.3 Characterization of MnPyP. (A) MnTE-2-PyP, (B) MnTnOct-2-PyP, (C) MnTnOct-3-PyP. (D) Spectra for each compound at 12.5 μM. (E) Standard curve for each compound of absorbance at maximum wavelength vs. concentration.

Uptake of Mn porphyrins in BP

To determine whether the MnPyP SOD mimetics could be incorporated in BP without an active reaction such as a covalent modification and to identify the MnPyP SOD mimetic with the greatest uptake, BP sections were incubated in each of the three compounds and uptake was assessed 24 hours later with A455 or A460. For comparing MnTE-2-PyP and MnTnOct-2-PyP, 32.5 µg of compound was added to the BP sections. The uptake of MnTE-2-PyP was 29% of the amount added or 9.4 µg whereas 77% or 24.9 µg of MnTnOct-2-PyP was taken up by BP (Fig. 4.4A). Since the major difference between the two compounds is the length of the alkyl chain, these results suggest that the longer alkyl chain of MnTnOct-2-PyP facilitates greater uptake in BP.

In order to assess the effect the position of the substituted alkyl chain (meta or ortho) on the uptake of an MnPyP SOD mimetic to BP, MnTnOct-3-PyP (meta) and MnTnOct-2-PyP (ortho) were compared. MnTnOct-3-PyP had higher uptake than MnTnOct-2-PyP at the three loading doses tested, but this difference was only significant at the highest dose (200 µg) and not the lower loading doses (50 µg and 100 µg) (Fig. 4.4B). The percent uptake for both compounds, a measure of uptake efficiency, decreased with the increasing loading dose (Fig. 4.4B). This suggests that there may be a saturation point for loading MnPyP compounds in BP. Together, these results demonstrate that the meta substituted MnPyP MnTnOct-3-PyP has higher uptake than MnTnOct-2-PyP, but the uptake of both of these compounds does not increase linearly with an increase in loading dose.

Since it was observed that an increase in loading dose does not correspond to a linear increase in MnPyP uptake, higher doses of MnTnOct-3-PyP, which had the highest uptake of the three compounds tested, were added to BP to identify the saturation point of uptake as well as to assess whether it would be possible to add 10x more MnTnOct-3-PyP than MnTnOct-2-PyP to account for the 10x lower SOD potency. With increasing amounts of MnTnOct-3-PyP, a significantly lower percent of compound is taken up by BP (Fig. 4.4C). The loading efficiency significantly decreases over the range of 200-1300 µg with the maximum uptake being 300 µg, which requires the 1300 µg loading dose (Fig. 4.4C). Based on the inefficiency of uptake at these high loading doses, it would be optimal to use a lower starting dose, between 100 and 200 µg in

order to maximize the uptake without wasting a significant amount of compound. For MnTnOct-2-PyP, approximately 75% of the compound is taken up at both the 100 and 200 µg, thereby providing high doses of MnTnOct-2-PyP in BP while conserving the amount of compound added to BP (Fig. 4.4B). These results indicate that the octyl substituted MnPyP have higher uptake into BP than MnTE-2-PyP. Since the ortho substituted MnPyP SOD mimetics have 10x the SOD activity than the meta substituted as determined by the rate constant for SOD dismutation, MnTnOct-2-PyP has been identified as the best candidate for use with BHV.

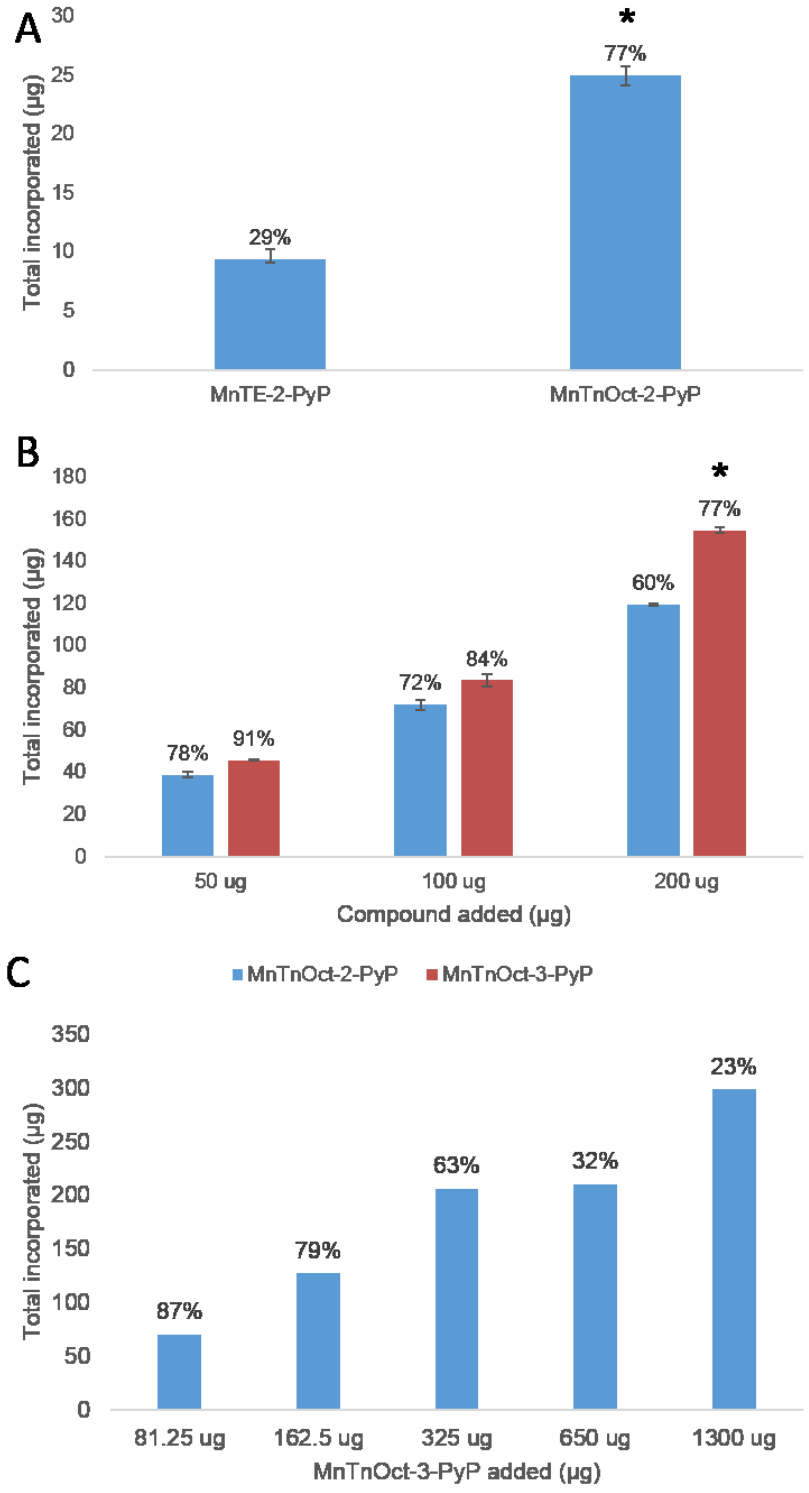

Figure 4.4 Uptake of MnPyP compounds in BP. (A) Ethyl vs octyl ortho analogues, 32.5 ug added, % uptake noted at each column. (B) Meta vs. ortho octyl analogues compared at three doses, 50, 100, or 200 ug, % uptake noted at each column. (C) High loading dose uptake of MnTnOct-3-PyP, % uptake noted at each column. * $p<0.05$ between compounds.

Stable incorporation of MnTnOct-2-PyP

Initial experiments with all three MnPyP SOD mimetics demonstrated that the compounds are taken up by BP without an active or driven reaction. However, these experiments did not address whether the compounds will remain retained in BP. Since MnTnOct-2-PyP was identified as the best candidate for use with BP, additional experiments were performed to assess the stability of the compound within BP. After an overnight incubation of either 50, 100, or 200 µg MnTnOct-2-PyP with BP at 37 °C with shaking, the BP samples were placed in 5 mL PBS at 37 °C with shaking to determine whether the compound was released from BP. The PBS solutions were changed frequently to avoid saturation of the solution. A 7 day release period resulted in a plateau of the release of MnTnOct-2-PyP from BP, thereby indicating that the compound retained in BP was stable (Fig. 4.5A). These results demonstrate that MnPyP SOD mimetics are retained in BP following the initial uptake stage and a prolonged release period.

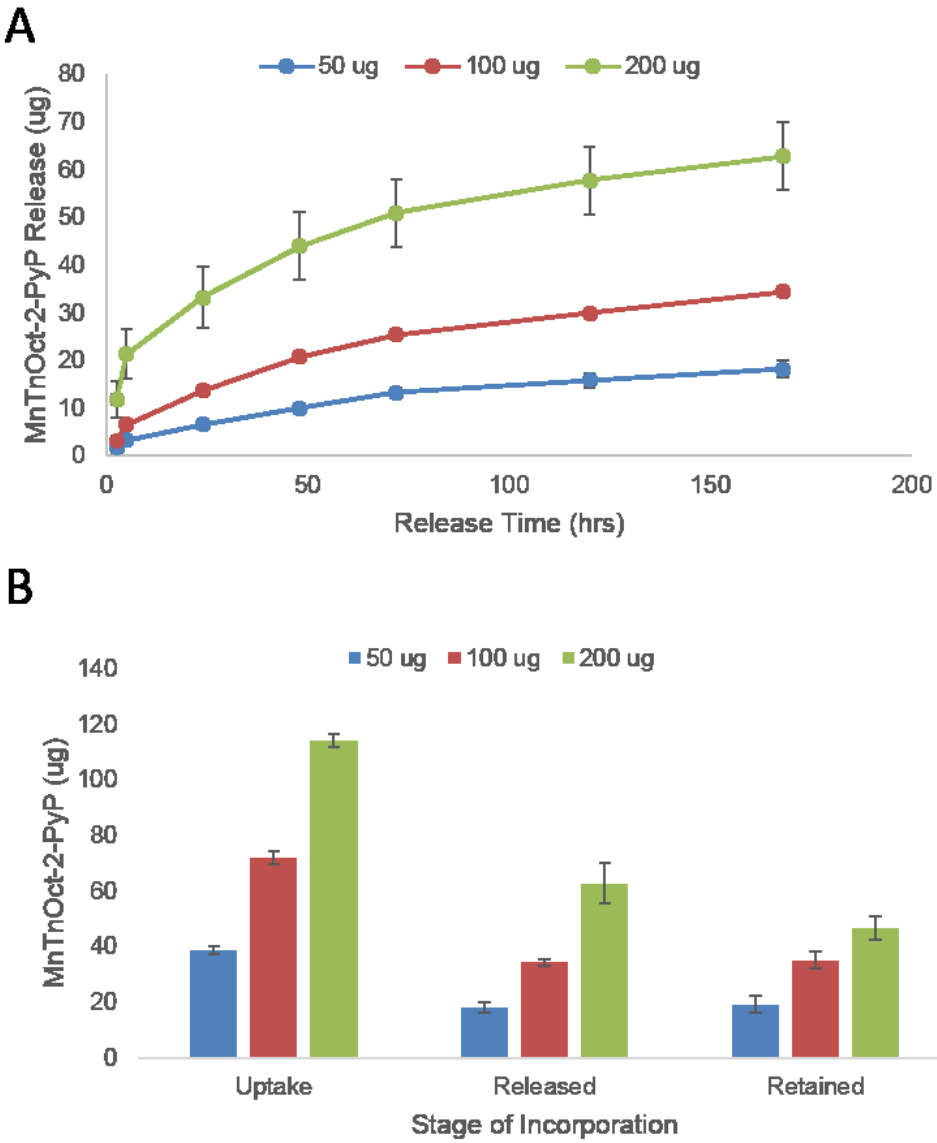

Fig. 4.5 Optimization of passive incorporation of MnTnOct-2-PyP. (A) Release of MnTnOct-2-PyP from BP at different loading concentrations (B) Uptake, total release, and MnTnOct-2-PyP retained in BP.

SOD activity of drug loaded BP

In addition to stable retention of MnTnOct-2-PyP in BP, the compound must still mimic SOD; therefore the SOD activity of drug loaded-BP was determined. The NBT reduction assay rather than the cytochrome c assay was used due to interference from BP with the kinetic A550 monitoring used with the cytochrome c assay. The NBT reduction assay uses the same reaction as cytochrome c to produce superoxide, but does not rely on the kinetics of the reduction of the reporter molecular. A specific concern with using NBT with MnTnOct-2-PyP loaded BP is the fact that high doses result in a color change of the tissue similar to the color of reduced NBT or NBT-formazan dye. Therefore, a low dose of MnTnOct-2-PyP (loading dose of 10 μg/8 mm tissue) was used to test the SOD activity of MnTnOct-2-PyP after incorporation into BP. NBT reduction was mitigated in BP loaded with MnTnOct-2-PyP as compared to non-drug loaded BP (Fig. 4.6A). The difference in NBT color change was analyzed in ImageJ by quantifying the mean gray value and normalized to the mean gray value of the same tissues prior to reacting with NBT (Fig. 4.6). These results demonstrate that MnTnOct-2-PyP retains SOD activity when incorporated in BP.

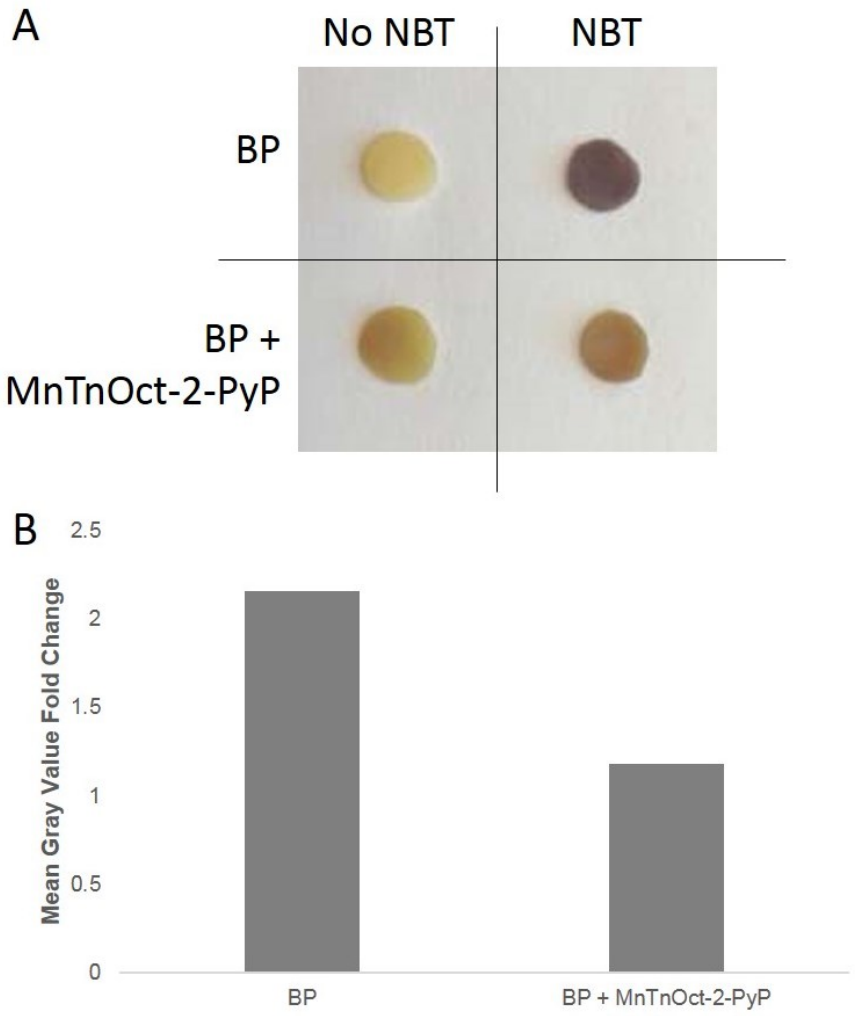

Fig. 4.6 SOD activity of BP loaded with MnTnOct-2-PyP. (A) MnTnOct-2-PyP BP reacted with xanthine oxidase/xanthine with or without NBT pre-incubation (B) Quantification of mean gray value from image analysis in ImageJ.

Rat subdermal implants of MnTnOct-2-PyP loaded BP

Rat subdermal implants of MnTnOct-2-PyP loaded BP were carried out for 90 days to determine whether MnTnOct-2-PyP retains SOD activity as well as its effect on calcification and dityrosine formation. MnTnOct-2-PyP loaded BP samples were prepared with a loading dose of 150 µg; following uptake and release approximately 70 µg MnTnOct-2-PyP were retained in the BP samples used for implantation (Fig. 4.7A). Each rat had a non-drug loaded and MnTnOct-2-PyP loaded BP sample to provide individual controls. The explanted BP samples were analyzed by the NBT assay to determine whether MnTnOct-2-PyP retained SOD activity following subdermal implantation. Compared to the non-drug loaded BP explants, the MnTnOct-2-PyP loaded BP explants had significantly less reduction of NBT (Fig. 4.7B), thereby demonstrating that MnTnOct-2-PyP loaded BP retains its activity following 90 day rat subdermal implantation.

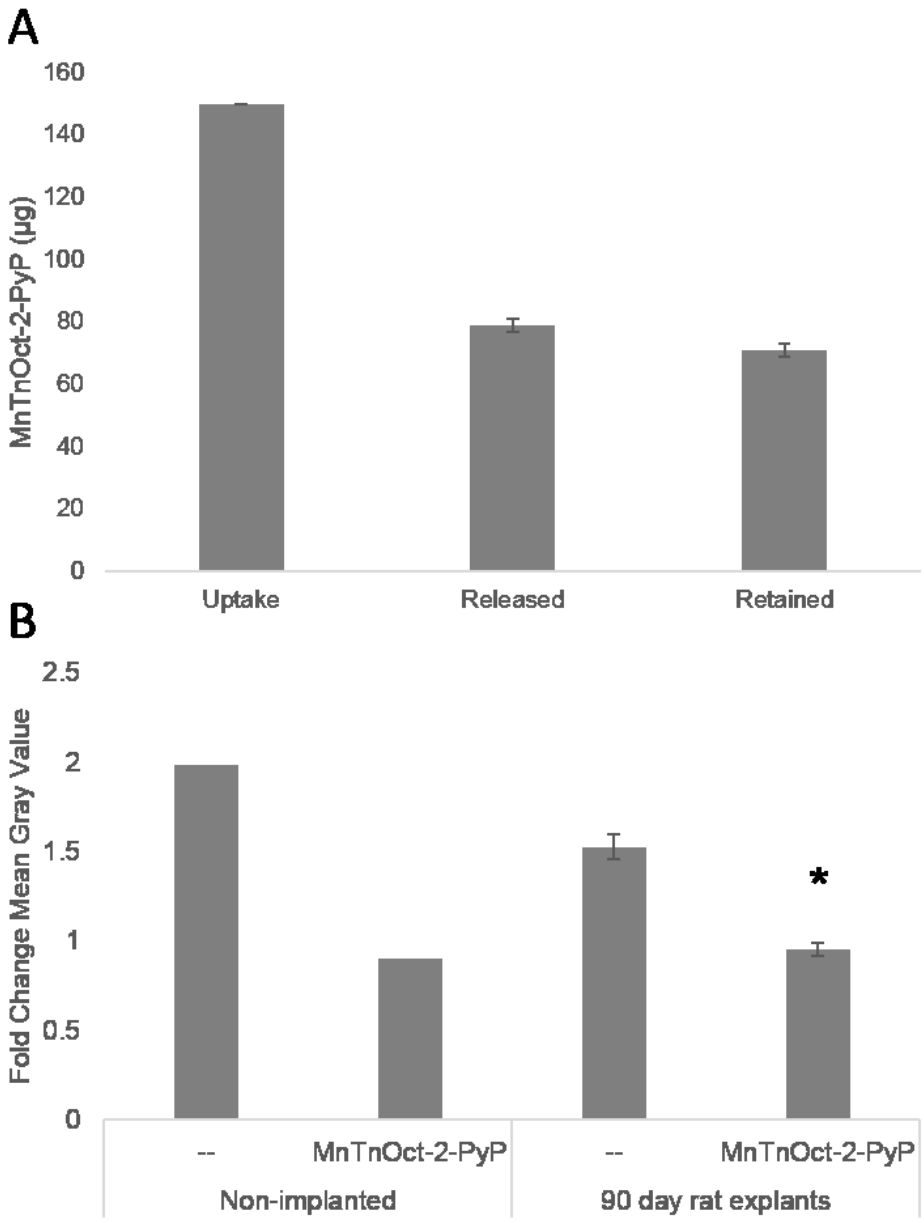

Fig. 4.7 Rat subdermal explants preparation and SOD activity. (A) Preparation of MnTnOct-2-PyP loaded BP for implantation. (B) NBT assay with 90 day BP explants, MnTnOct-2-PyP and non-drug loaded. *p<0.05 vs non-drug loaded.

The effect of MnTnOct-2-PyP on calcification of the 90 day rat subdermal implants was assessed since calcium accumulation contributes to BHV degradation. In addition to unmodified BP controls, BP that was exposed to pH 6.5, the pH of the MnTnOct-2-PyP loading solution, was included to control for potential effects of the process of drug incorporation on BHV degradation. The 90 day BP explants had mean calcium accumulation of 309.8 ± 18.4 μg calcium/mg tissue (Fig. 4.8). MnTnOct-2-PyP loaded BP had less calcium accumulation than non-drug loaded BP explants with a mean of 267.8 ± 23.7 μg calcium/mg tissue (Fig. 4.8). Surprisingly, the pH control had significantly less calcium than both the non-drug loaded and MnTnOct-2-PyP loaded samples with a mean of 119.9 ± 28.9 μg calcium/mg tissue (Fig. 4.8). Acidic conditions are necessary to extract calcium from tissues therefore it may be that this slightly acidic pH interfered with the initiation of calcium phosphate formation [138]. It was expected that the SOD mimetic could decrease calcification since oxidation has been shown to promote calcification in certain situations such as vascular calcification or atherosclerosis [139-141]. However, the effect of MnTnOct-2-PyP on calcification was very modest.

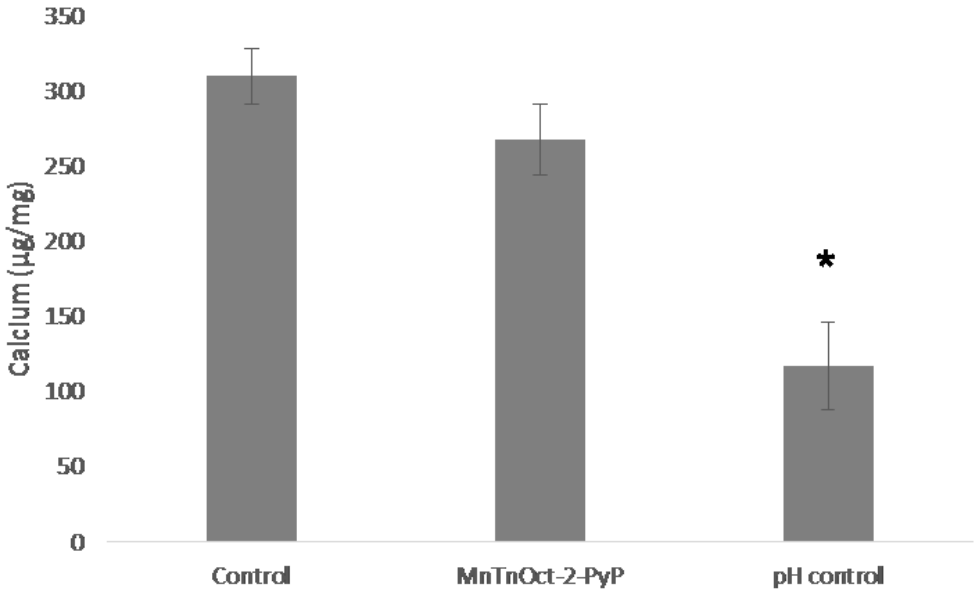

Fig. 4.8 Calcification of rat subdermal explants loaded with MnTnOct-2-PyP. 90 day BP explants control (unmodified), MnTnOct-2-PyP, and pH 6.5 control. *p<0.05 vs both control and MnTnOct-2-PyP by one-way ANOVA with Tukey's test.

Sheep patches of MnTnOct-2-PyP loaded BP

In order to assess MnTnOct-2-PyP loaded BP samples in an animal model that provides both exposure to blood flow and mechanical (shear) stress, a sheep implant model was performed through collaboration with Professor Richard Bianco of the University of Minnesota. A total of 4 juvenile sheep and 24 BP patches were used in this experiment. BP samples were sewn into the walls at three locations in the heart: ascending aorta, pulmonary artery, and left atrium. Two BP patches, both non-drug loaded and MnTnOct-2-PyP loaded, were placed at each location and retrieved after 90 days. At the end of the study, all 24 patches were intact and later successfully removed from the surrounding tissue (Fig. 4.9).

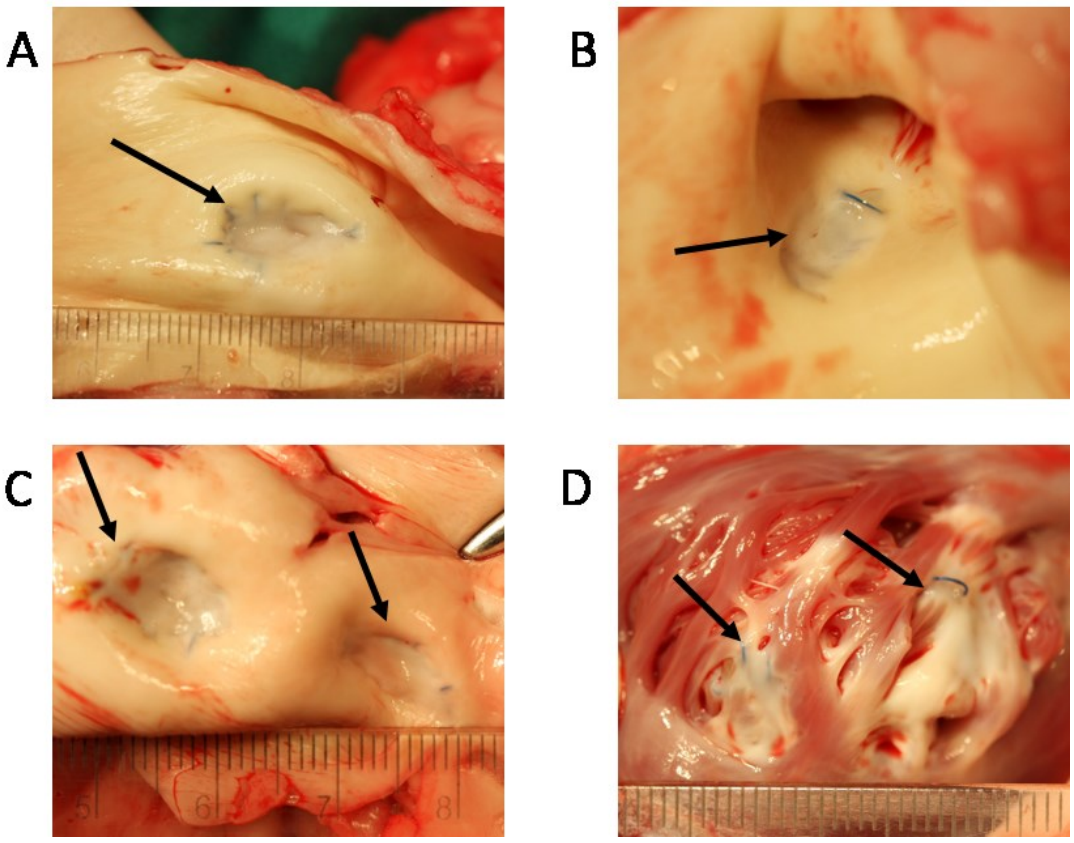

Fig. 4.9. Gross anatomy of sheep patch implants. (A) Distal ascending aorta. (B) Ascending aorta. (C) Pulmonary artery. (D) Left atrium. Patches identified with arrows.

Two doses of MnTnOct-2-PyP were analyzed in order to determine a dose range for activity of MnTnOct-2-PyP towards oxidative and calcific damage. The low dose was prepared by adding 15 μg whereas the high dose was prepared with 150 μg MnTnOct-2-PyP. Following uptake and release, 11 μg and 70 μg MnTnOct-2-PyP were retained in the low and high dose samples, respectively (Fig. 4.10A). The SOD activity of non-implanted and explanted patches was assessed by the NBT assay to determine whether exposure to circulation in the sheep model reduced SOD activity of the MnTnOct-2-PyP loaded BP samples. Due to the availability of explanted material, only 2 control and 2 MnTnOct-2-PyP loaded explants from the aortic position were analyzed. The MnTnOct-2-PyP loaded explants had a lower, but statistically insignificant, fold change in mean gray value, which suggests that the SOD activity of MnTnOct-2-PyP is retained (Fig. 4.10B). A larger sample size is necessary to determine statistical significance; however, these results are encouraging in that MnTnOct-2-PyP seems to retain SOD activity after in vivo exposure.

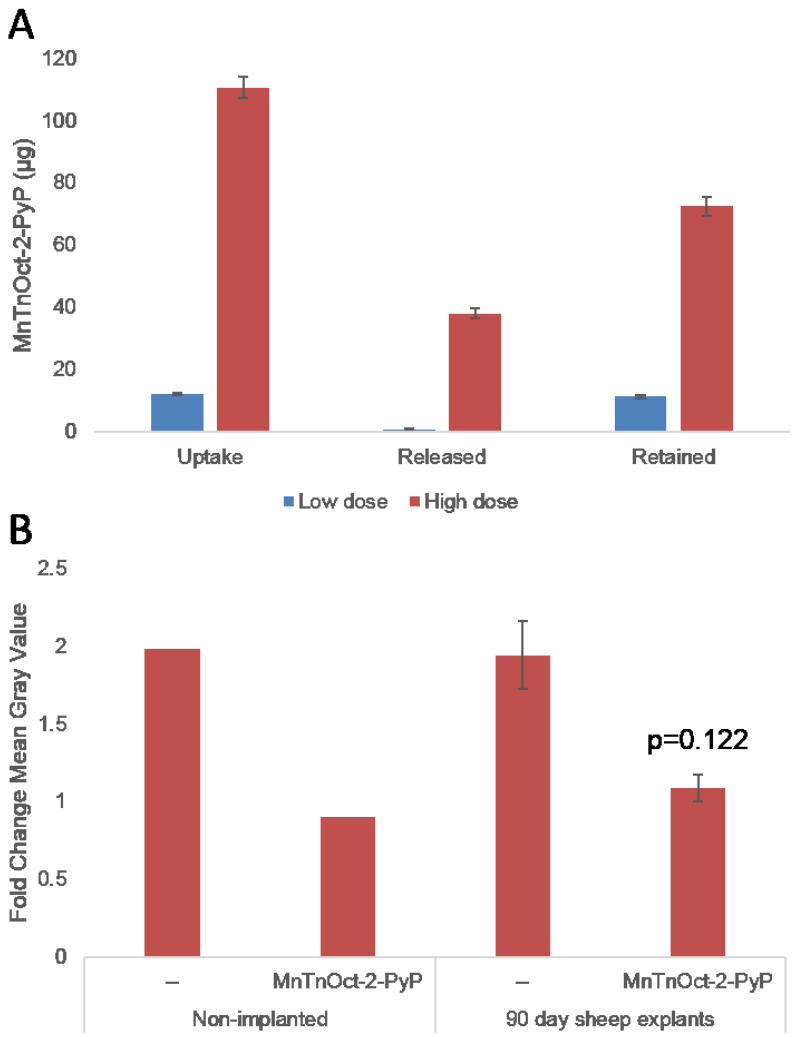

Fig. 4.10. Sheep patch implants preparation and SOD activity. (A) Preparation of low and high dose MnTnOct-2-PyP BP patches. (B) SOD activity as determined by the NBT assay of non-implanted and explanted patches; n=2 for explanted samples, aortic patches from animals CAV3 and CAV4.

Since BHV calcification is an important mechanism of BHV failure, calcium and phosphorus, which comprise the calcium phosphate deposits, were quantified in the sheep patch explants. Both calcium and phosphorus levels were close to the non-implanted levels (3.57 μg calcium/mg tissue and about 0 phosphorus) for all but two patch explants (Fig, 4.11A). In one animal ("CAV2"), the calcium levels of two drug loaded patches were much higher than all other patches, but this was not seen in patches from any of the other three animals. Mean calcium levels were highest in the left atrial patches (Fig, 4.11B) whereas mean phosphorus was highest in the pulmonary artery patches (Fig. 4.11C), but with high variation. This result is not surprising due to the short implantation period. The duration of 90 days was chosen since the primary end point of interest was oxidation rather than calcification and previous studies with catheter-deployed BJV BHV in the pulmonary arteries demonstrated elevated dityrosine after only 90 days (Fig. 2.16). These results therefore demonstrate low calcium and phosphorus accumulation in the sheep patch implant model and no significant effect of MnTnOct-2-PyP.

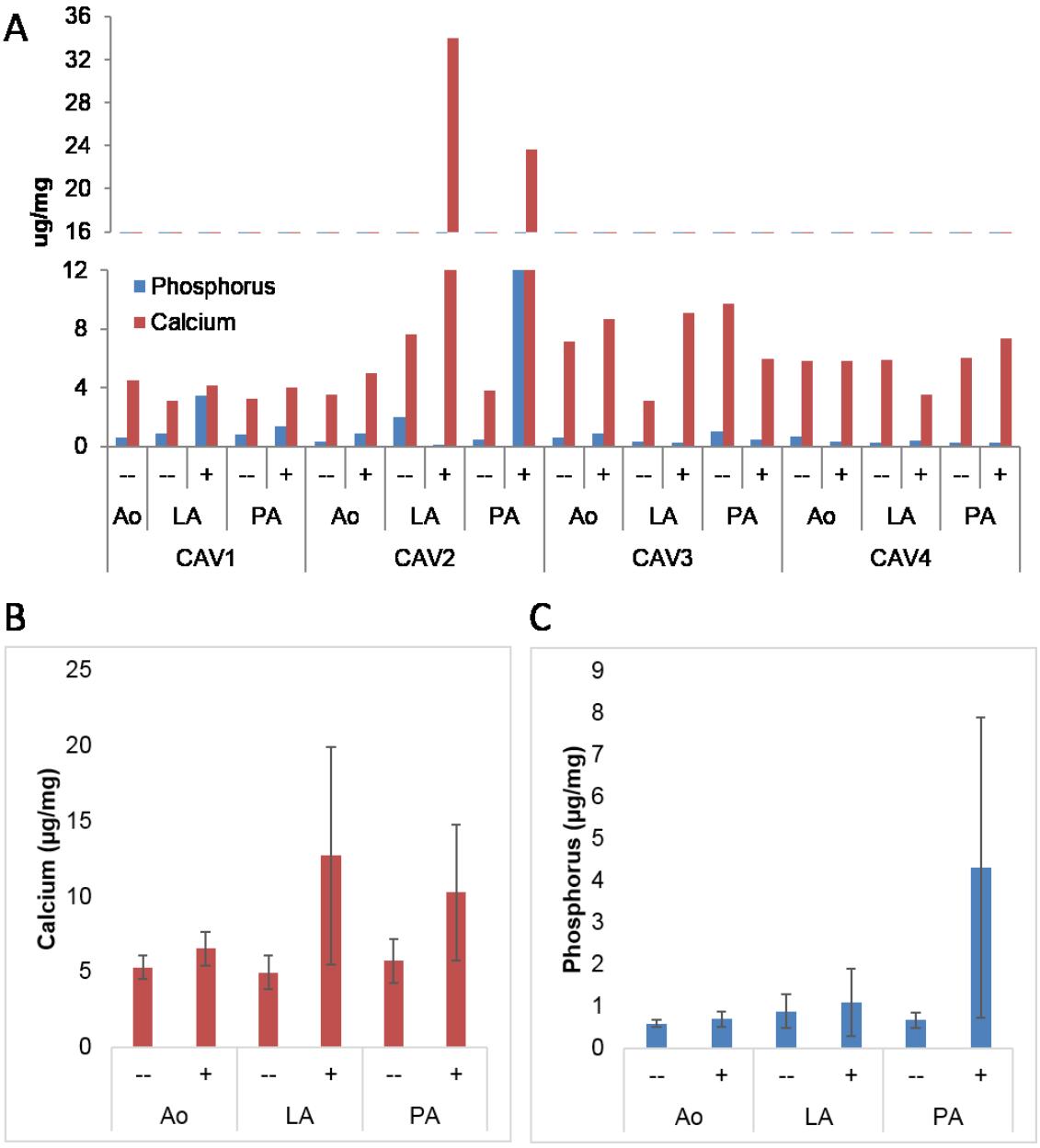

Fig. 4.11 Calcification of sheep patch explants loaded with MnTnOct-2-PyP. (A) Calcium and phosphorus values for individual patches and samples; CAV1-4 indicate the individual animals. (B) Mean calcium levels by patch location. (C) Mean phosphorus levels by patch location. Ao: aorta, LA: left atrium, PA: pulmonary artery, "--": control, "+": MnTnOct-2-PyP.

Liposomal delivery of SOD mimetics

Studies with the MnPyP SOD mimetics and BP demonstrated that these compounds readily partition into tissue primarily through hydrophobic interactions since the octyl substituted compounds have higher uptake than the ethyl substituted. In order to determine whether these compounds would be useful in a targeted delivery application, antibody-conjugated liposomes, MnTnOct-2-PyP-loaded liposomes were prepared (Fig. 4.12).

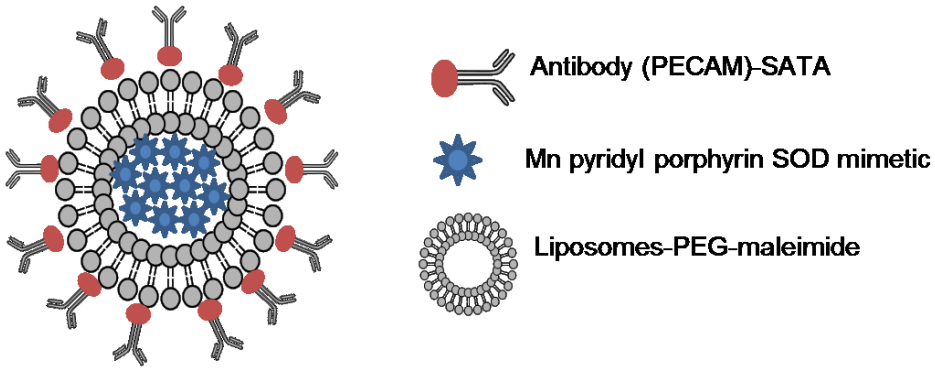

Fig. 4.12 MnPyP SOD mimetic antibody-conjugated liposomes. MnPyP SOD mimetics were loaded in the aqueous core created by the lipid bilayer. Maleimide-SATA modified antibody (PECAM) will be used to conjugate the antibody to the surface of the liposome.

MnTnOct-2-PyP was chosen over MnTE-2-PyP and MnTnOct-3-PyP based on its high partitioning efficiency in BP and potent SOD activity. Drug encapsulation efficiency, liposome size, and antibody binding were determined for MnTnOct-2-PyP liposomes (Table 4.1). The drug loading efficiency is high with approximately 70%, as determined by A455. The antibody binding was lower than previously described, but could be due to procedural differences rather than the presence of MnTnOct-2-PyP [129]. The size of the liposomes corresponds with previous formulations of these liposomes containing other drug cargo [129, 130]. These results demonstrate that MnTnOct-2-PyP is efficiently encapsulated in liposomes conjugated with antibodies for targeted delivery.

Antibody	% Drug Loading (A_{455})	% Antibody Binding	Size (nm)
PECAM	69.5 +/- 2.7	44 +/- 3.7	184 +/- 12
IgG	63.3 +/- 7.6	48 +/- 7.7	170 +/- 8

Table 4.1 MnTnOct-2-PyP liposome formulation. Both PECAM and IgG liposomes were prepared containing MnTnOct-2-PyP. Drug loading, antibody binding, and liposome size were assessed to characterize the liposomes.

Targeting of the PECAM-conjugated liposomes to HUVECs was done to determine whether the PECAM-conjugated liposomes are still able to bind endothelial cells with MnTnOct-2-PyP as the drug cargo. More PECAM conjugated liposomes were bound to HUVECs than IgG conjugated liposomes, demonstrating liposome targeting specific to endothelial cells through the PECAM antibody (Fig. 4.13). This result demonstrates that there is PECAM antibody binding to endothelial cells for liposomes loaded with MnTnOct-2-PyP.

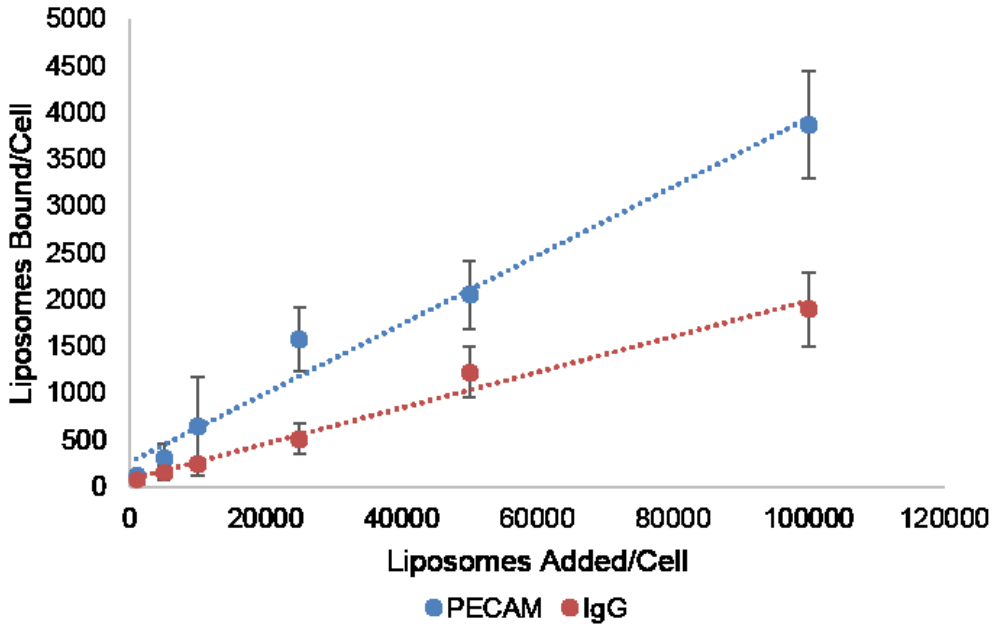

Fig. 4.13 Binding of PECAM and IgG liposomes to HUVEC. Liposomes loaded with MnTnOct-2-PyP and conjugated to either IgG or PECAM antibodies were incubated with HUVECs to determine targeting of PECAM for cell binding.

The SOD activity of the MnTnOct-2-PyP antibody-conjugated liposomes was determined with the cytochrome c reduction assay in order to demonstrate that MnTnOct-2-PyP retains its SOD activity after encapsulation. SOD activity was assessed in both intact as well as Triton-disrupted liposomes to determine whether the liposome must be degraded for MnTnOct-2-PyP to have activity. Cytochrome c reduction by superoxide was monitored by absorbance at 550 nm over 250 seconds (Fig. 4.14A). SOD activity was calculated from the curves in Fig. 4.14A by determining the slope of the linear region (Fig. 4.14B), which can be converted to units of SOD activity per mL of liposome preparation. The disrupted liposomes have more SOD activity as would be expected if MnTnOct-2-PyP is loaded in the aqueous core; however, the intact liposomes also had SOD activity, which suggests that some of the MnTnOct-2-PyP is loaded in the lipid bilayer. These results demonstrate that both the intact and disrupted MnTnOct-2-PyP liposomes maintain SOD activity, but degradation of the liposomes or release of the drug cargo results in the highest activity.

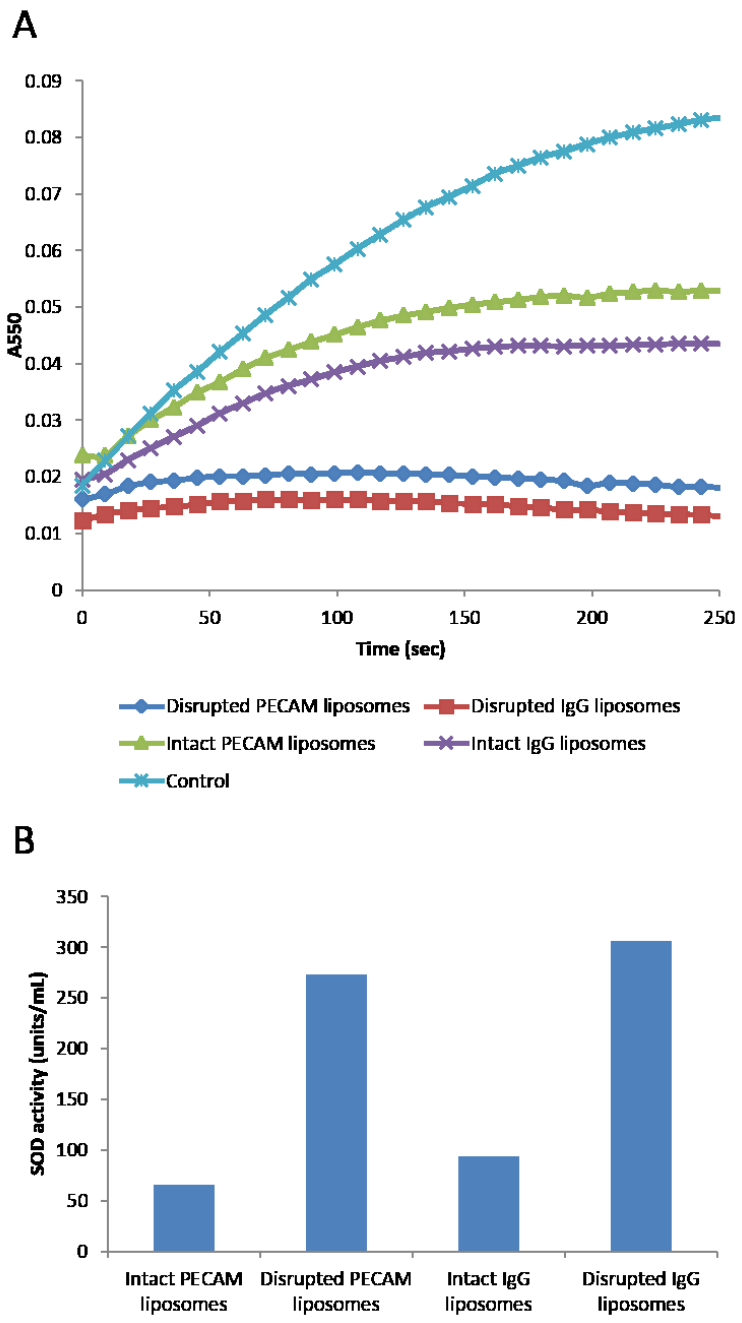

Fig. 4.14 SOD activity of MnTnOct-2-PyP PECAM and IgG conjugated liposomes. (A) Time course of cytochrome c reduction by superoxide generated from xanthine/xanthine oxidase in the presence of intact or 1% Triton X-100 disrupted liposomes. (B) Quantification of SOD activity from slope of time course.

4.5 Discussion

MnPyP SOD mimetics are good candidates for mitigating oxidative damage of a long-term implant such as BHV due to efficient partitioning into the BHV material BP and potent catalytic antioxidant activity. Three MnPyP SOD mimetics were selected for potential use with BHV in order to determine whether the length or position (meta vs ortho) of the alkyl chain affected uptake into BHV materials. Longer meta-substituted alkyl chains were shown to be most efficiently incorporated into BP. However, the meta-substituted compounds have 10-fold lower SOD activity, which could not be compensated for by loading more compound into BP. Therefore, MnTnOct-2-PyP (ortho substituted octyl) was identified as the lead candidate for an SOD mimetic drug delivery strategy for BHV. MnTnOct-2-PyP retained SOD activity following incorporation in BP. MnTnOct-2-PyP loaded BP was tested in two animal models, both the rat subdermal implant model of calcification and a sheep patch implant model that provided exposure to blood flow. MnTnOct-2-PyP did not affect calcification of the implanted materials, but did retain SOD activity following implantation. These studies demonstrate that the use of a MnPyP SOD mimetic, MnTnOct-2-PyP, provides a simple method of drug delivery and may attenuate BHV oxidation.

Numerous studies have focused on the structure-function relationships of MnPyP SOD mimetics, therefore MnTE-2-PyP, MnTnOct-2-PyP, and MnTnOct-3-PyP were specifically selected as a group for optimization in delivery to BHV materials. The ortho-substituted compounds (MnTE-2-PyP and MnTnOct-2-PyP) have the most favorable electrostatic and SOD activity based on the reduction potential of the manganese center as well as the catalytic rate constant for superoxide dismutation [61, 132]. However, it was expected that the more important characteristic for incorporation would be lipophilicity or potential hydrophobic interactions. Both MnTnOct-2-PyP and MnTnOct-3-PyP are significantly more lipophilic than MnTE-2-PyP. MnTnOct-3-PyP, the meta analogue, has been shown to be more lipophilic and have more conformational flexibility than the ortho analogue, which results in greater cellular accumulation [142]. In these studies, the differences in incorporation efficiencies of the meta and ortho analogues was only evident at very high concentrations where the maximum drug loading capacity was met. By comparing the three

compounds, we concluded that the incorporation is likely due to hydrophobic interactions, potentially through hydrogen bond formation between the octyl side chains and collagen. Our findings that the efficiency of uptake into BP increased from MnTE-2-PyP to MnTnOct-2-PyP to the highest with MnTnOct-3-PyP was not surprising. However, it would only be advantageous to use MnTnOct-3-PyP over MnTnOct-2-PyP if the uptake was 10x greater to account for differences in SOD activity. Interestingly, there is a saturation point for MnPyP uptake into BP, which appears to be around 300 μg/8 mm BP section, but additional studies and replicates, which would require significant amounts of the compounds, would be necessary to specifically identify this point. Thus, MnTnOct-2-PyP was selected as the optimal candidate for incorporation into BHV materials due to its efficient uptake and potent SOD activity.

Although MnPyP SOD mimetics are taken up by BP, all is not stably retained in the tissue as determined by the release of compound into PBS. After determining that the compound released from BP plateaus after 5-7 days, this step was added prior to any additional experiments, particularly the rat and sheep models. Even with the release period, up to 40% of the compound originally added to BP is retained. Based on the potency of the activity of these compounds as well as the local delivery to the material since the compound is present at the site of oxidant production or attack, we predict that this strategy would provide significant protection for BHV materials from oxidation.

It was not expected that the incorporation of MnTnOct-2-PyP into BP would affect its SOD activity since this was a passive process; however, SOD activity was confirmed to address this potential issue. Determining SOD activity in a drug-loaded tissue was challenging since traditional SOD activity assays could not be used due to the nature of the sample. The cytochrome c reduction assay relies on spectrophotometric measurements on a short (less than 1 minute) time scale; the presence of the tissue interfered with these measurements and was therefore unreliable. It was not possible to quantify the SOD activity in terms of the catalytic rate constant in the NBT assay since this assay uses an endpoint measurement rather than kinetics. Therefore, it was only possible to demonstrate that the MnTnOct-2-PyP loaded BP tissues did have SOD activity in that there was less NBT reduction as compared to the non-drug loaded samples. Additional studies could address

methods to quantify the activity of the compounds after incorporation in order to determine if the activity is affected. An additional unknown is the amount of compound that needs to be loaded into the BHV material to effectively interfere with material oxidation.

Earlier studies with the DBP modification and rat subdermal implant model demonstrated only modest oxidation of BHV as measured by the formation of dityrosine, thereby indicating that this model does not fully represent BHV oxidation since it does not produce dityrosine levels corresponding with clinical or sheep explants. However, this model is useful in assessing BHV calcification since it is accelerated. Oxidative stress has been shown to drive calcification in certain situations such as vascular calcification [140] or atherosclerosis [87]. The clinical use of antioxidants in atherosclerosis prevention has been studied based on this relationship. Therefore, we hypothesized that in addition to mitigating BHV oxidative damage, an SOD mimetic may also reduce calcification of BHV. In the previous studies with DBP it was not possible to directly assess the effect of an antioxidant on BHV calcification since the DBP chemistry involves exposure to ethanol, a known anti-calcification agent [88]. Calcification of MnTnOct-2-PyP rat subdermal explants was surprisingly not significantly less than the unmodified explants and was actually higher than the pH control, which was used at the same pH as MnTnOct-2-PyP. A possible explanation for the apparent anti-calcification effect of the pH control is that if the slightly acidic pH (6.5) was maintained during implantation, this could prevent calcium phosphate deposition since acids are used to solubilize these crystals [138] It is still possible that an antioxidant could mitigate BHV calcification, however, MnTnOct-2-PyP does not have this effect. A possible explanation for this finding is that the specific antioxidant MnTnOct-2-PyP did not affect BHV calcification due to its properties, in particular, the manganese center. Manganese supplementation is used to promote bone health, which was based on early studies demonstrating a positive effect of manganese diet supplementation on bone growth and strength [143]. Therefore, future work should directly address the relationship between oxidation and calcification without the confounding variables of a specific antioxidant.

Testing BHV leaflet materials in a large animal valve replacement model is expensive and requires significant resources including surgical facilities, surgeons, and clinical-grade valves. The

sheep patch implant model provides an alternative that still exposes the materials to blood and mechanical stresses; two factors that are not represented in the rat subdermal implant model However, the mechanical forces that the patches are exposed to are primarily shear whereas the normal heart valves are exposed to additional including flow and flexural stresses [144]. This model also allowed for testing a high number of samples per animal since multiple locations in the heart could be used. It is likely that the short implant duration (90 days) was the major contributor to the low levels of both calcium and phosphorus in the samples. Although MnTnOct-2-PyP did not affect calcification in this model or in the rat model, a longer sheep calcification study should be performed to ensure that MnTnOct-2-PyP does not accelerate calcification.

Dityrosine was selected as the endpoint for implant oxidation since it is present in clinical BHV explants but not in non-implanted materials and potentially represents a functional effect of BHV oxidation. Dityrosine cross-links could cause stiffening of the valve material, which may affect mechanical properties. Quantification of dityrosine levels in the MnTnOct-2-PyP BP explants are pending.

Liposomal formulations of MnTnOct-2-PyP were prepared to demonstrate that MnTnOct-2-PyP is a good candidate for targeted liposomal delivery. In these studies, the liposomes were conjugated to PECAM, which is used for targeting to the endothelium. However, there are many possible applications for targeted delivery of MnPyP SOD mimetics including cancer chemo or radiosensitizers [124, 145] and inflammation related to acute lung injury [127, 128]. The goals of these studies were to provide proof of principle that MnPyP SOD mimetics could be delivered via a liposomal system without affecting liposome structure or in this situation, antibody binding. The use of liposomal delivery rather than systemic delivery of MnPyP has the potential to increase the dose at the necessary site and to prevent toxicity related to off-target effects.

For most liposomal drug delivery systems, the drug cargo is loaded either into the aqueous core or the lipophilic shell, depending on the water solubility of the particular drug [126, 146]. In some instances, the drug cargo may load in both areas. It is interesting for the case of MnTnOct-2-PyP liposomes that the intact carriers had significant SOD activity. It is expected that MnTnOct-2-PyP would be localized to the aqueous core since it is a water soluble drug; however, as was

demonstrated with BP, the alkyl chains are hydrophobic and could facilitate uptake into the lipophilic shell of the liposomes. This could explain the efficient drug loading as well as the SOD activity of the intact liposomes. In addition, having MnTnOct-2-PyP accessible from the surface of the liposome could accelerate the action of the drug once it has reached the target site since the liposomes do not require internalization and complete degradation for SOD activity. MnTnOct-2-PyP loaded liposomes therefore represent an interesting possibility for targeted drug delivery given the appropriate model or disease state.

In conclusion, we show that MnPyP SOD mimetics can be incorporated in BP, which is likely mediated through hydrophobic interactions with the four alkyl substituents. These interactions provide stable retention of the compound within the BHV material BP as well as in liposome drug carriers. The compounds retain their SOD potency after incorporation and may therefore prevent BHV oxidation in a sheep circulatory model. These results suggest future investigations of MnTnOct-2-PyP for preventing BHV oxidant-mediated degradation.

Chapter 5: Conclusions and Future Directions

Improving BHV durability would address a significant clinical need since currently 30% of BHV fail within 10 years of implantation [147] and the alternative, mechanical valves, require long-term anti-coagulation [1]. The primary aim of my dissertation was to explore the role of oxidative stress in BHV degradation with an additional goal being the development of potential therapeutic strategies targeting this process in an effort to improve BHV durability.

5.1 BHV susceptibility to oxidation

Through both the analysis of clinical BHV explants and the use of experimental systems of BHV oxidation, we determined that BHV are susceptible to oxidation and that this process can lead to material degeneration [102]. The major finding of our analysis of failed clinical BHV explants was the elevation of the tyrosine oxidation product dityrosine in these explants and the absence in non-implanted BHV materials. Tyrosyl radicals are formed through the oxidation of tyrosine by various oxidants; the reaction of two tyrosyl radicals can then result in the formation of dityrosine [78]. This is unlike many other oxidation products that involve a specific oxidation pathway, rather than a range of oxidants, such as with chlorotyrosine which is a product of hypochlorous acid that is produced by myeloperoxidase [148]. Dityrosine may also represent a functional effect of BHV oxidation since it is a protein cross-link that could affect the material properties of BHV [83, 97, 149]. Additional studies are needed to determine the specific functional effect of this increase in dityrosine in BHV, but based on these studies we have shown that dityrosine may be a marker of BHV oxidation.

Since BHV degradation occurs on a time scale of years, it was necessary to use accelerated experimental models to identify the structural effects of oxidation on BHV materials. The $H_2O_2/FeSO_4$ system, which was based on a model used to assess oxidative degradation of polymers [65, 66], demonstrated that oxidation of BP results in a breakdown of glutaraldehyde cross-links, an increase in susceptibility to digestion by collagenase, and disruption of the normal collagen structure [102]. Each of these effects could have the result of material deterioration. An

interesting finding from the $H_2O_2/FeSO_4$ system was that glutaraldehyde cross-links are lost with exposure to oxidizing conditions. A similar result using ^{3}H-glutaraldehdye to cross-link BP was reported from the rat subdermal implant model many years ago showing a significant loss glutaraldehyde in 21 day explants [37]. This study suggested that the result was mostly due to leaching of glutaraldehyde from BP, but with the 60% glutaraldehyde loss that was demonstrated, it is possible that other active mechanisms such as oxidation were involved. Glutaraldehyde cross-linking is an important property of BHV as it provides stability against proteolytic degradation, reduces immunogenicity, and improves mechanical properties [99]. It is possible that glutaraldehyde could even provide protection against oxidation through the introduction of additional cross-links. However, since glutaraldehyde is also susceptible to oxidation, any protection that would be conferred is likely transient since the glutaraldehyde cross-links are also susceptible to oxidation.

In order to corroborate the findings from the $H_2O_2/FeSO_4$ system with an in vivo system, the rat subdermal implant model was initially utilized but demonstrated poor representation of these endpoints, thereby suggesting that BHV oxidation may require both exposure to blood and mechanical forces, which this models lacks. A significant challenge in the field of BHV is the availability of animal models. The rat subdermal implant model has great value for the analysis of calcification since it provides an accelerated and technically simple system. However, as we learned with BHV oxidation, this system does not recapitulate other mechanisms of BHV degradation, which is likely due to the lack of blood flow exposure. We hypothesized that BHV oxidation would be represented in the rat model since the major source of ROS/RNS that is likely to cause BHV oxidation is inflammatory cells. Despite demonstrating that there is an intense inflammatory response to BHV materials in the rat subdermal implant model, BHV oxidation was modest. Therefore, it is likely that other factors, particularly blood exposure, drive BHV oxidation. Through our analysis of pulmonary artery, catheter-deployed BHV, we were able to determine that a short-term circulatory animal model does have dityrosine accumulation; therefore supporting the hypothesis that blood exposure is necessary for BHV oxidation. The sheep patch model used to assess the SOD mimetics strategy was useful in providing a simplified system with blood exposure,

but still required skilled surgeons and the expense of large animal care. Unfortunately, the use of non-animal models, such as in vitro circulatory models like the Chandler loop [150], are not a viable alternative due to the short-term nature and implant size constraints, which prevents the use of a full sized BHV. An ideal system would allow for testing of full sized BHV under physiologic forces and with exchange of blood flow for longer time points. Even with such a system, the gold standard will still be large animal valve replacement models [70].

It is not unexpected that oxidative stress affects BHV and may contribute to degradation since it was previously known that patients do have an inflammatory response to these devices [21, 151, 152]. It has been long recognized that even materials that are considered the most biocompatible still elicit a host response [24] and that this response can contribute to the degradation or eventual failure of the device [27, 67]. The role of the foreign body response and in particular oxidative stress has been very well characterized for the degradation of synthetic devices and we aimed to apply those methods to this different class of device, tissue-based prosthetic heart valves. Despite BHV being fabricated from non-synthetic materials, they are still foreign materials since they are derived from porcine or bovine and, in addition, are cross-linked with glutaraldehyde which is known to cause problems of its own including an exacerbation of BHV calcification. The major question in this area was not whether there is a host response to BHV, but whether this response then has any effect on the integrity of the material or function of the device. By identifying dityrosine in clinical BHV explants we were able to demonstrate that BHV are oxidized, likely as a result of inflammatory-produced ROS/RNS and the use of experimental models allowed for the identification of some effects of oxidation on a glutaraldehyde fixed BHV material.

In addition to ROS/RNS, activated inflammatory cells produce proteases such as matrix metalloproteinases (MMPs) that may be capable of degrading BHV [153]. Although glutaraldehyde fixation provides resistance to proteolytic degradation prior to implantation [42], we have shown that following implantation the materials become more susceptible to proteases. Therefore, MMPs may also have a role in the degradation of BHV. The use of an anti-inflammatory compound could mitigate BHV degradation by inhibiting the production of MMPs as well as ROS/RNS by reducing the activation or migration of inflammatory cells or by directly targeting ROS/RNS enzymes such

as NADPH oxidase [154]. With the antioxidant approach, the effects of ROS/RNS rather than their production are inhibited. The concerns with using a general anti-inflammatory agent are the systemic effects, but it may be possible to avoid these effects if the compound is immobilized within the BHV materials similarly to DBP.

The use of BHV in children and adolescents remains a significant challenge to this day, with reports of early failure still representing a major issue for the field [11, 155]. BHV in young patients have more rapid BHV calcification [12], which may be due to differences in calcium homeostasis or metabolism that drives this progression. It is possible that there are also differences in oxidation-mediated BHV leaflet deterioration based on age. Similarly, the general inflammatory response to the BHV or other medical device may differ between children and adults. A comparison of BHV oxidation and inflammation in children and adults could provide insight into the nature of BHV oxidation and the role of other factors such as patient age. These studies could help to address the need for improving BHV durability for both children and adults.

5.2 The DBP modification mitigates BHV oxidation in vitro

The first strategy we used for mitigating BHV oxidation was covalent modification of the BHV material BP with an oxidant scavenger DBP. In this strategy we were able to demonstrate that DBP could be efficiently immobilized to BP without affecting BP material properties or the oxidant scavenging activity of DBP. Most importantly, DBP showed efficacy in the H_2O_2/$FeSO_4$ system in that DBP modified BP had significantly less oxidative damage as determined by the previously identified endpoints. DBP was tested in the rat subdermal implant and was non-toxic as well as anti-calcific. It is likely that the anti-calcification effects of DBP are due to the brief exposure to ethanol [79] or the use of the carbodiimide-driven chemistry which may alter the cross-linking of the material [39, 45]. Ideally DBP modified BP would have been tested in a circulatory animal model where BHV oxidation may be better represented, but due to feasibility concerns as well as a concern of the long-term efficacy of a stoichiometric antioxidant such as DBP, these studies were not performed. The DBP modification strategy demonstrated proof-of-principle concepts that an antioxidant may improve the durability of BHV by preventing oxidative damage, thereby providing

a platform for future research in this area. Future studies should assess the behavior of DBP in the heart valve position as well as the effect on oxidative and calcific BHV degradation.

DBP was selected for modification of BHV based on previous studies from the Levy lab using similar BHT analogues [27]. Structure-function relationships were performed to identify the best candidate compound for use an antioxidant modification of biomaterials, initially polyurethane [36, 51]. Other common antioxidants such as α-tocopherol could not be used in place of DBP due to the lack of necessary functional groups. It may be possible to develop an antioxidant that can both be immobilized and have catalytic antioxidant activity in order to combine to the two features offered separately from the DBP and SOD mimetic approaches, but this would require significant time and expertise since to our knowledge, a compound with these characteristics is not commercially available.

Since BHV are long-term implants, some types of drug delivery methods cannot be used. In particular a strategy that involves drug release from the device, such as a drug-eluting stent, would not be a good system for BHV since the total amount of drug that can be delivered over the lifetime of the device is limited. For stents this is thought to be less of a concern since the drugs are used to target the acute inflammatory phase which can result in rapid restenosis [156, 157]. For BHV, it is likely that they are exposed to ROS/RNS throughout the lifetime of the device either through an active chronic inflammatory response to the device. Therefore, the amount of drug that could be delivered through a mechanism similar to a drug-eluting stent would have severe limitations in BHV applications. Similarly, intravenous delivery of drug carriers targeting the device, if possible, would require numerous administrations and would not be a feasible option from a patient convenience or cost perspective. The methods that have previously been used to provide local drug delivery to BHV involved some type of covalent modification; either through residual aldehyde groups [37] or through a modified version of the carbodiimide chemistry used to attach DBP [39]. As long as the drug being delivered remains attached and active, these approaches do have potential as clinical treatment. Unfortunately, many of the strategies that have been tested were targeting calcification of BHV and did not show significant efficacy. However, since we are targeting a different mechanism with DBP there is still promise for clinical efficacy.

5.3 SOD mimetics may provide sustained protection against BHV oxidation

Although the DBP strategy did show efficacy in experimental models, we sought to develop an improved strategy for mitigating BHV oxidation through the use of a catalytic antioxidant and the exclusion of additional chemistry such as the carbodiimide-driven reaction used with DBP. MnTnOct-2-PyP, a SOD mimetic, was efficiently incorporated into BP through passive interactions, likely hydrophobic interactions involving the alkyl substituents. MnTnOct-2-PyP retained SOD activity after incorporation. This strategy was tested in both the rat model and a sheep patch implant model in order to provide exposure to blood flow. MnTnOct-2-PyP did not affect calcification in either model. A promising finding from both animal models is that MnTnOct-2-PyP retained SOD activity after exposure to either a subdermal pouch or blood flow. This indicates that MnTnOct-2-PyP may provide sustained antioxidant protection.

The effect of MnTnOct-2-PyP on oxidation will be determined through the quantification of dityrosine, but these results are currently pending. We considered assessing other endpoints to determine the effect of MnTnOct-2-PyP on oxidation, but were limited in the available explant material as well as good alternative endpoints. Dityrosine is the best measure of oxidative stress we have found for BHV. We examined many other potential endpoints including histology for collagen damage, collagenase digestibility, and loss of collagen with hydroxyproline, but were only able to correlate the dityrosine finding with clinical BHV explants. Dityrosine quantification has the advantage in that it can be performed on paraffin-embedded sections, therefore other endpoints such as histology can also be assessed, but requires an established mass spectrometry method.

An area of concern with the SOD mimetics passive incorporation strategy is the true stability of this form of drug loading. Although we showed that after a 7 day release period the release of compound from BP cannot be measured and that the drug-loaded rat and sheep explants retain activity, the real test will be in a longer term valve replacement model where there are both flexural and shear stresses. It is possible that the interactions between the MnPyP SOD mimetics and the BHV leaflet materials are very stable, but this should be assessed in high flow model.

5.4 Future directions

The DBP and MnTnOct-2-PyP strategies could both be viable therapeutic options since they displayed different forms of efficacy. DBP significantly reduced BHV calcification and to a greater degree than the currently used ethanol anti-calcification treatment which had breakthrough calcification in the 90 day rat model [79, 88]. MnTnOct-2-PyP did not affect calcification, in a positive or negative manner, and did retain SOD activity, but dityrosine results are pending. Following the dityrosine results for the sheep patch model, the next step for both approaches is assessment in a large animal sheep valve replacement model to determine the mechanical properties as well as effect on degradation. It would be interesting to compare the durability of DBP and MnTnOct-2-PyP modified BHV leaflets to determine which strategy has a greater effect on overall BHV durability and performance.

Future studies should focus on identifying the specific factors that drive BHV oxidation in addition to inflammation and exposure to blood flow. One area that we were not able to fully explore was the time frame of oxidation. The foreign body reaction involves both acute and chronic inflammation, therefore BHV may be exposed to inflammatory cell ROS/RNS production throughout the lifetime of the device. However, it is also possible that more oxidative damage occurs in the acute phase due to a more robust inflammatory response; therefore, it would only be necessary to target this early stage rather than the entire lifetime of the device.

Since calcification remains a significant cause of BHV degradation, additional studies should focus on disseminating the relationship between oxidation and calcification since we now know that both processes do contribute to BHV degradation. We expect that oxidation would accelerate calcification since this is seen in both native vascular (atherosclerosis) and valvular calcification [140, 141, 158]. However, in these situations, the mechanism involves cellular activation or transdifferentiation such as the phenotypic switch of valvular interstitial cells from smooth muscle cells to pro-osteogenic cells in native aortic valve calcification [159, 160]. Since BHV materials are non-vital due to the decellularization by glutaraldehyde, the effect of oxidation on calcification may be a non-cellular mediated process or could involve inflammatory cells at the

material surface. It is also possible that oxidative and calcific degradation of BHV are not related. Assessment of the localization of both calcification and oxidation could help to determine if these processes are spatially related. For example, most calcification occurs on the circumferential edge of a BHV [93] whereas collagen degradation occurs in the center of the leaflet [14]. Analysis of clinical explants for dityrosine at the edge, circumferential, commissural, and center of explants could determine the localization of BHV oxidation which may provide additional insight into the relationship between oxidation and calcification.

Analysis of a larger set of clinical BHV explants could provide insight on the relationship between the various types of BHV degradation. We did evaluate the correlation between factors such as implant duration, dityrosine level, and calcification in our set of clinical BHV explants but were unable to draw any conclusions due to the small sample size. With a larger sample set, these relationships could be better studied with a greater statistical power.

BHV degradation is known to be caused by several mechanisms and the overlap of these processes has not been fully elucidated (Fig. 5.1). BHV calcification is driven by numerous factors, including serum calcium and phosphorous levels, alkaline phosphatase activity, and bone remodeling proteins such as osteocalcin and osteopontin, which are affected by age and co-morbidities such as renal failure [161]. Here we show that oxidation of BHV, likely resulting from the production of ROS/RNS by inflammatory cells, results in dityrosine formation, loss of glutaraldehyde cross-links, and increase in collagenase digestibility; all which may result in material deterioration. Structural damage to BHV may also occur through mechanical forces such as shear and flexural stresses [14]. Each of these processes may occur independently or influence each other and the progression to BHV failure.

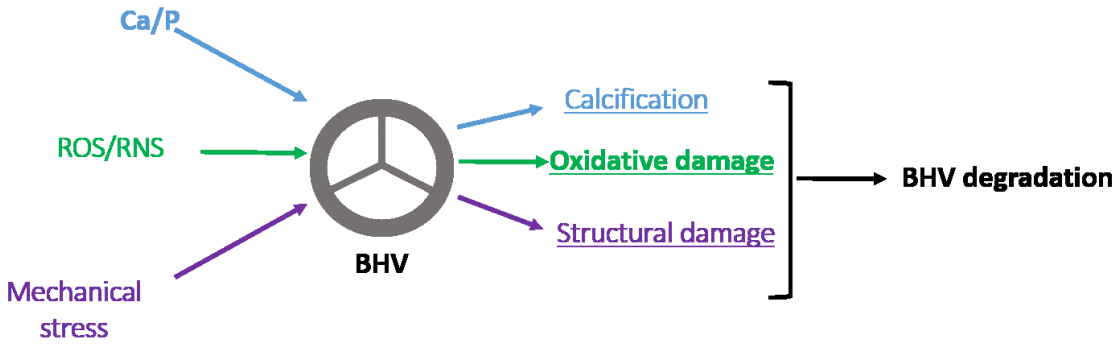

Fig. 5.1 Pathways of BHV degradation. Calcification and mechanical stress were previously known mechanisms of BHV degradation. Here we identified ROS/RNS oxidation of BHV as an additional mechanism of degradation.

The results presented here support the hypothesis that oxidative stress contributes to BHV degradation. Through modification of BHV materials with antioxidants, we show that this process of degradation may be mitigated through pharmacologic methods, with the hope of improving BHV durability.

References

1. Pibarot P, Dumesnil JG. Prosthetic heart valves: selection of the optimal prosthesis and long-term management. Circulation. 2009;119:1034-48.
2. Siddiqui RF, Abraham JR, Butany J. Bioprosthetic heart valves: modes of failure. Histopathology. 2009;55:135-44.
3. Leon MB, Smith CR, Mack M, Miller DC, Moses JW, Svensson LG, et al. Transcatheter aortic-valve implantation for aortic stenosis in patients who cannot undergo surgery. N Engl J Med. 2010;363:1597-607.
4. Otto CM, Bonow RO. Valvular Heart Disease. Braunwald's Heart Disease: A Textbook of Cardiovascular Medicine, 9th Ed2011. p. 1468-539.
5. Schoen FJ, Levy RJ. Calcification of tissue heart valve substitutes: progress toward understanding and prevention. Ann Thorac Surg. 2005;79:1072-80.
6. What is mitral valve prolapse? : MVP Resource; 2013 [cited 2014 January 9]. Available from: http://mvpresource.com/wp-content/uploads/2013/04/Heart-Valves-and-Chambers.png.
7. Bender JR. Heart Valve Disease. In: Zaret BL, Moser M, Cohen LS, editors. Yale University School of Medicine Heart Book: William Morrow & Co; 1992. p. 167-76.
8. Rajamannan NM, Evans FJ, Aikawa E, Grande-Allen KJ, Demer LL, Heistad DD, et al. Calcific aortic valve disease: not simply a degenerative process: A review and agenda for research from the National Heart and Lung and Blood Institute Aortic Stenosis Working Group. Executive summary: Calcific aortic valve disease-2011 update. Circulation. 2011;124:1783-91.
9. Bonow RO, Carabello BA, Chatterjee K, de Leon AC, Jr., Faxon DP, Freed MD, et al. 2008 focused update incorporated into the ACC/AHA 2006 guidelines for the management of patients with valvular heart disease: a report of the American College of Cardiology/American Heart Association Task Force on Practice Guidelines (Writing Committee to revise the 1998 guidelines for the management of patients with valvular heart disease). Endorsed by the Society of Cardiovascular Anesthesiologists, Society for Cardiovascular Angiography and Interventions, and Society of Thoracic Surgeons. J Am Coll Cardiol. 2008;52:e1-142.
10. Zilla P, Brink J, Human P, Bezuidenhout D. Prosthetic heart valves: catering for the few. Biomaterials. 2008;29:385-406.
11. Saleeb SF, Newburger JW, Geva T, Baird CW, Gauvreau K, Padera RF, et al. Accelerated Degeneration of a Bovine Pericardial Bioprosthetic Aortic Valve in Children and Young Adults. Circulation. 2014.
12. Sanders SP, Levy RJ, Freed MD, Norwood WI, Castaneda AR. Use of Hancock Porcine Xenografts in Children and Adolescents. Am J Cardiol. 1980;46:429-38.
13. Delogne C, Lawford PV, Habesch SM, Carolan VA. Characterization of the calcification of cardiac valve bioprostheses by environmental scanning electron microscopy and vibrational spectroscopy. J Microsc. 2007;228:62-77.
14. Sacks MS, Schoen FJ. Collagen fiber disruption occurs independent of calcification in clinically explanted bioprosthetic heart valves. J Biomed Mater Res. 2002;62:359-71.
15. Vyavahare N, Ogle M, Schoen FJ, Zand R, Gloeckner DC, Sacks M, et al. Mechanisms of bioprosthetic heart valve failure: fatigue causes collagen denaturation and glycosaminoglycan loss. J Biomed Mater Res. 1999;46:44-50.
16. Raghavan D, Starcher BC, Vyavahare NR. Neomycin binding preserves extracellular matrix in bioprosthetic heart valves during in vitro cyclic fatigue and storage. Acta Biomater. 2009;5:983-92.
17. Butany J, Feng T, Luk A, Law K, Suri R, Nair V. Modes of failure in explanted mitroflow pericardial valves. Ann Thorac Surg. 2011;92:1621-7.
18. Butany J, Zhou T, Leong SW, Cunningham KS, Thangaroopan M, Jegatheeswaran A, et al. Inflammation and infection in nine surgically explanted Medtronic Freestyle stentless aortic valves. Cardiovasc Pathol. 2007;16:258-67.
19. Nair V, Law KB, Li AY, Phillips KR, David TE, Butany J. Characterizing the inflammatory reaction in explanted Medtronic Freestyle stentless porcine aortic bioprosthesis over a 6-year period. Cardiovasc Pathol. 2012;21:158-68.

20. Skowasch D, Schrempf S, Wernert N, Steinmetz M, Jabs A, Tuleta I, et al. Cells of primarily extra-valvular origin in degenerative aortic valves and bioprostheses. Eur Heart J. 2005;26:2576-80.
21. Shetty R, Pibarot P, Audet A, Janvier R, Dagenais F, Perron J, et al. Lipid-mediated inflammation and degeneration of bioprosthetic heart valves. Eur J Clin Invest. 2009;39:471-80.
22. Spray TL, Roberts WC. Structural-Changes in Porcine Xenografts Used as Substitute Cardiac Valves - Gross and Histologic Observations in 51 Glutaraldehyde-Preserved Hancock Valves in 41 Patients. Am J Cardiol. 1977;40:319-30.
23. Simionescu A, Simionescu DT, Deac R. Biochemical pathways of tissue degeneration in bioprosthetic cardiac valves. ASAIO J. 1996;42:M561-7.
24. Anderson JM, Rodriguez A, Chang DT. Foreign body reaction to biomaterials. Semin Immunol. 2008;20:86-100.
25. Christenson EM, Anderson JM, Hiltner A. Oxidative mechanisms of poly(carbonate urethane) and poly(ether urethane) biodegradation: in vivo and in vitro correlations. J Biomed Mater Res A. 2004;70:245-55.
26. McBane JE, Santerre JP, Labow RS. The interaction between hydrolytic and oxidative pathways in macrophage-mediated polyurethane degradation. J Biomed Mater Res A. 2007;82:984-94.
27. Stachelek SJ, Alferiev I, Choi H, Chan CW, Zubiate B, Sacks M, et al. Prevention of oxidative degradation of polyurethane by covalent attachment of di-tert-butylphenol residues. J Biomed Mater Res A. 2006;78:653-61.
28. Monboisse JC, Borel JP. Oxidative damage to collagen. EXS. 1992;62:323-7.
29. Curran SF, Amoruso MA, Goldstein BD, Berg RA. Degradation of soluble collagen by ozone or hydroxyl radicals. FEBS Lett. 1984;176:155-60.
30. Au V, Madison SA. Effects of singlet oxygen on the extracellular matrix protein collagen: oxidation of the collagen crosslink histidinohydroxylysinonorleucine and histidine. Arch Biochem Biophys. 2000;384:133-42.
31. Henrotin Y, Deberg M, Mathy-Hartert M, Deby-Dupont G. Biochemical biomarkers of oxidative collagen damage. Adv Clin Chem. 2009;49:31-55.
32. Hawkins CL, Davies MJ. Oxidative damage to collagen and related substrates by metal ion/hydrogen peroxide systems: random attack or site-specific damage? Biochim Biophys Acta. 1997;1360:84-96.
33. Schubert MA, Wiggins MJ, Anderson JM, Hiltner A. Comparison of two antioxidants for poly(etherurethane urea) in an accelerated in vitro biodegradation system. J Biomed Mater Res. 1997;34:493-505.
34. Christenson EM, Anderson JM, Hiltner A. Antioxidant inhibition of poly(carbonate urethane) in vivo biodegradation. J Biomed Mater Res A. 2006;76:480-90.
35. Schubert MA, Wiggins MJ, DeFife KM, Hiltner A, Anderson JM. Vitamin E as an antioxidant for poly(etherurethane urea): In vivo studies. J Biomed Mater Res. 1996;32:493-504.
36. Stachelek SJ, Alferiev I, Ueda M, Eckels EC, Gleason KT, Levy RJ. Prevention of polyurethane oxidative degradation with phenolic antioxidants covalently attached to the hard segments: structure-function relationships. J Biomed Mater Res A. 2010;94:751-9.
37. Webb CL, Schoen FJ, Levy RJ. Covalent binding of aminopropanehydroxydiphosphonate to glutaraldehyde residues in pericardial bioprosthetic tissue: stability and calcification inhibition studies. Exp Mol Pathol. 1989;50:291-302.
38. Webb CL, Benedict JJ, Schoen FJ, Linden JA, Levy RJ. Inhibition of bioprosthetic heart valve calcification with aminodiphosphonate covalently bound to residual aldehyde gorups. Ann Thorac Surg. 1988;46:309-16.
39. Everaerts F, Torrianni M, van Luyn M, van Wachem P, Feijen J, Hendriks M. Reduced calcification of bioprostheses, cross-linked via an improved carbodiimide based method. Biomaterials. 2004;25:5523-30.
40. Cheung DT, Perelman N, Ko EC, Nimni ME. Mechanisms of crosslinking proteins by glutaraldehyde III. Rreaction with collagen in tissues. Connect Tissue Res. 1985;13:109-15.

41. Migneault I, Dartiguenave C, Bertrand MJ, Waldron KC. Glutaraldehyde: behavior in aqueous solution, reaction with proteins, and application to enzyme crosslinking. Biotechniques. 2004;37:790-6, 8-802.
42. Munnelly AE, Cochrane L, Leong J, Vyavahare NR. Porcine vena cava as an alternative to bovine pericardium in bioprosthetic percutaneous heart valves. Biomaterials. 2012;33:1-8.
43. Schoen FJ, Tsao JW, Levy RJ. Calcification of bovine pericardium used in cardiac valve bioprostheses. Am J Pathol. 1986;123:134-45.
44. Hermanson G. Bioconjugate Techniques: Academic Press; 2008.
45. Leong J, Munnelly AE, Liberio B, Cochrane L, Vyavahare N. Neomycin and carbodiimide crosslinking as an alternative to glutaraldehyde for enhanced durability of bioprosthetic heart valves. J Biomat Appl. 2011;0:1-13.
46. Kos I, Reboucas JS, DeFreitas-Silva G, Salvemini D, Vujaskovic Z, Dewhirst MW, et al. Lipophilicity of potent porphyrin-based antioxidants: comparison of ortho and meta isomers of Mn(III) N-alkylpyridylporphyrins. Free Radic Biol Med. 2009;47:72-8.
47. Shoulders MD, Raines RT. Collagen structure and stability. Annu Rev Biochem. 2009;78:929-58.
48. Fujisawa S, Kadoma Y, Yokoe I. Radical-scavenging activity of butylated hydroxytoluene (BHT) and its metabolites. Chem Phys Lipids. 2004;130:189-95.
49. Lambert CR, Black HS, Truscott TG. Reactivity of butylated hydroxytoluene. Free Radic Biol Med. 1996;21:395-400.
50. Jovanovic SV, Steenken S, Tosic M, Marjanovic B, Simic MG. Flavonoids as Antioxidants. J Am Chem Soc. 1994;116:4846-51.
51. Stachelek SJ, Alferiev I, Fulmer J, Ischiropoulos H, Levy RJ. Biological stability of polyurethane modified with covalent attachment of di-tert-butyl-phenol. J Biomed Mater Res A. 2007;82:1004-11.
52. Everaerts F, Torrianni M, Hendriks M, Feijen J. Quantification of carboxyl groups in carbodiimide cross-linked collagen sponges. J Biomed Mater Res A. 2007;83:1176-83.
53. Everaerts F, Torrianni M, Hendriks M, Feijen J. Biomechanical properties of carbodiimide crosslinked collagen: influence of the formation of ester crosslinks. J Biomed Mater Res A. 2008;85:547-55.
54. Salvemini D, Riley DP, Cuzzocrea S. SOD mimetics are coming of age. Nat Rev Drug Discov. 2002;1:367-74.
55. Petersen SV, Oury TD, Ostergaard L, Valnickova Z, Wegrzyn J, Thogersen IB, et al. Extracellular superoxide dismutase (EC-SOD) binds to type i collagen and protects against oxidative fragmentation. J Biol Chem. 2004;279:13705-10.
56. Monboisse J, Braquet P, Randoux A, Borel J. Non-enyzmatic degradation of acid-soluble calf skin collagen by superoxide ion: protective effect of flavonoids. Biochem Pharmacol. 1983;32:53-8.
57. Goldstein S, Merenyi G. The chemistry of peroxynitrite: implications for biological activity. Methods Enzymol. 2008;436:49-61.
58. Ischiropoulos H, Zhu L, Beckman JS. Peroxynitrite formation from macrophage-derived nitric oxide. Arch Biochem Biophys. 1992;298:446-51.
59. Batinic-Haberle I, Spasojevic I, Hambright P, Benov L, Crumbliss AL, Fridovich I. Relationship among redox potentials, proton dissociation constants of pyrrolic nitrogens, and in vivo and in vitro superoxide dismutating activities of manganese(III) and iron(III) water-soluble porphyrins. Inorg Chem. 1999;38:4011-22.
60. Batinic-Haberle I. Manganese porphyrins and related compounds as mimics of superoxide dismutase. Methods Enzymol. 2002;349.
61. Tovmasyan A, Sheng H, Weitner T, Arulpragasam A, Lu M, Warner DS, et al. Design, mechanism of action, bioavailability and therapeutic effects of Mn porphryin-based redox modulators. Med Prin Pract. 2013.
62. Batinic-Haberle I, Reboucas JS, Spasojevic I. Superoxide dismutase mimics: chemistry, pharmacology, and therapeutic potential. Antioxid Redox Signal. 2010;13:877-918.

63. Batinic-Haberle I, Tovmasyan A, Roberts ER, Vujaskovic Z, Leong KW, Spasojevic I. SOD Therapeutics: Latest Insights into Their Structure-Activity Relationships and Impact on the Cellular Redox-Based Signaling Pathways. Antioxid Redox Signal. 2014;20:2372-415.
64. Miriyala S, Spasojevic I, Tovmasyan A, Salvemini D, Vujaskovic Z, St Clair D, et al. Manganese superoxide dismutase, MnSOD and its mimics. Biochim Biophys Acta. 2012;1822:794-814.
65. Zhao QH, McNally AK, Rubin RK, Renier M, Wu Y, Rose-Caprara V, et al. Human plasma a2-macroglobulin promotes in vitro oxidative stress cracking of Pellethane 2363-80A: in vivo and in vitro correlations. J Biomed Mater Res. 1993;27:379-89.
66. Zhao QH, Casas-Bejar J, Urbanski P, Stokes K. Glass wool-H2O2/CoCl2 test system for in vitro evaluation of biodegradative stress cracking in polyurethane elastomers. J Biomed Mater Res. 1995;29:467-75.
67. Schubert MA, Wiggins MJ, Schaefer MP, Hiltner A, Anderson JM. Oxidative biodegradation mechanisms of biaxially strained poly(etherurethane urea) elastomers. J Biomed Mater Res. 1995;29:337-47.
68. Levy RJ, Schoen FJ, Levy JT, Nelson AC, Howard SL, Oshry LJ. Biologic determinants of dystrophic calcification and osteocalcin deposition in glutaraldehyde-preserved porcine aortic valve leaflets implanted subcutaneously in rats. Am J Pathol. 1983;113:143-55.
69. Schoen FJ, Levy RJ, Hilbert SL, Bianco RW. Antimineralization treatments for bioprosthetic heart valves. Assessment of efficacy and safety. J Thorac Cardiovasc Surg. 1992;104:1285-8.
70. Gallegos RP, Nockel PJ, Rivard AL, Bianco RW. The current state of in-vivo pre-clinical animal models for heart valve evaluation. J Heart Valve Dis. 2005;14:423-32.
71. Westaby S, Bianco RW, Katsumata T, Termin P. The Carbomedics "Oxford" Photofix stentless valve (PSV). Semin Thorac Cardiovasc Surg. 1999;11:206-9.
72. Ferrans VJ, Spray TL, Billingham ME, Roberts WC. Structural-Changes in Glutaraldehyde-Treated Porcine Heterografts Used as Substitute Cardiac Valves - Transmission and Scanning Electron-Microscopic Observations in 12 Patients. Am J Cardiol. 1978;41:1159-84.
73. Kato Y, Uchida K, Kawakishi S. Oxidative-Degradation of Collagen and Its Model Peptide by Ultraviolet-Irradiation. J Agric Food Chem. 1992;40:373-9.
74. Kato Y, Uchida K, Kawakishi S. Oxidative fragmenation of collagen and prolyl peptide by Cu(II)/H2O2. J Biol Chem. 1992;267:23646-51.
75. Rahman I, van Schadewijk AA, Crowther AJ, Hiemstra PS, Stolk J, MacNee W, et al. 4-Hydroxy-2-nonenal, a specific lipid peroxidation product, is elevated in lungs of patients with chronic obstructive pulmonary disease. Am J Respir Crit Care Med. 2002;166:490-5.
76. Chiou C-C, Chang P-Y, Chan E-C, Wu T-L, Tsao K-C, Wu JT. Urinary 8-hydroxydeoxyguanosine and its analogs as DNA marker of oxidative stress: development of an ELISA and measurement in both bladder and prostate cancers. Clin Chim Acta. 2003;334:87-94.
77. Kettle AJ. Detection of 3-chlorotyrosine in proteins exposed to neutrophil oxidants. Methods Enzymol. 1999;300:111-20.
78. Feeney MB, Schoneich C. Tyrosine modifications in aging. Antioxid Redox Signal. 2012;17:1571-9.
79. Vyavahare N, Hirsch D, Lerner E, Baskin JZ, Schoen FJ, Bianco R, et al. Prevention of bioprosthetic heart valve calcification by ethanol preincubation. Efficacy and mechanisms. Circulation. 1997;95:479-88.
80. Giulivi C, Traaseth NJ, Davies KJ. Tyrosine oxidation products: analysis and biological relevance. Amino Acids. 2003;25:227-32.
81. Ischiropoulos H. Protein tyrosine nitration--an update. Arch Biochem Biophys. 2009;484:117-21.
82. Mohiuddin I, Chai H, Lin PH, Lumsden AB, Yao Q, Chen C. Nitrotyrosine and chlorotyrosine: clinical significance and biological functions in the vascular system. J Surg Res. 2006;133:143-9.
83. Souza JM, Giasson BI, Chen Q, Lee VM, Ischiropoulos H. Dityrosine cross-linking promotes formation of stable alpha -synuclein polymers. Implication of nitrative and oxidative stress in the pathogenesis of neurodegenerative synucleinopathies. J Biol Chem. 2000;275:18344-9.

84. Leeuwenburgh C, Rasmussen JE, Hsu FF, Mueller DM, Pennathur S, Heinecke JW. Mass spectrometric quantification of markers for protein oxidation by tyrosyl radical, copper, and hydroxyl radical in low density lipoprotein isolated from human atherosclerotic plaques. J Biol Chem. 1997;272:3520-6.
85. Citardi MJ, Song W, Batra PS, Lanza DC, Hazen SL. Characterization of oxidative pathways in chronic rhinosinusitis and sinonasal polyposis. Am J Rhinol. 2006;20:353-9.
86. Helderman F, Segers D, de Crom R, Hierck BP, Poelmann RE, Evans PC, et al. Effect of shear stress on vascular inflammation and plaque development. Curr Opin Lipidol. 2007;18:527-33.
87. World CJ, Garin G, Berk B. Vascular shear stress and activation of inflammatory genes. Curr Atheroscler Rep. 2006;8:240-4.
88. Vyavahare NR, Jones PL, Hirsch D, Schoen FJ, Levy RJ. Prevention of glutaraldehyde-fixed bioprosthetic heart valve calcification by alcohol pretreatment: further mechanistic studies. J Heart Valve Dis. 2000;9:561-6.
89. McGee-Russell S. Histochemical methods for calcium. J Histochem Cytochem. 1958;6:22-42.
90. Junqueira LC, Bignolas G, Brentani RR. Picrosirius staining plus polarization microscopy, a specific method for collagen detection in tissue sections. Histochem J. 1979;11:447-55.
91. Connolly JM, Bakay MA, Alferiev IS, Gorman RC, Gorman JH, 3rd, Kruth HS, et al. Triglycidyl amine crosslinking combined with ethanol inhibits bioprosthetic heart valve calcification. Ann Thorac Surg. 2011;92:858-65.
92. Robb JD, Harris MA, Minakawa M, Rodriguez E, Koomalsingh KJ, Shuto T, et al. Melody valve implantation into the branch pulmonary arteries for treatment of pulmonary insufficiency in an ovine model of right ventricular outflow tract dysfunction following tetralogy of Fallot repair. Circ Cardiovasc Interv. 2011;4:80-7.
93. Schoen FJ, Kujovich JL, Webb CL, Levy RJ. Chemically determined mineral content of explanted porcine aortic valve bioprostheses: correlation with radiographic assessment of calcification and clinical data. Circulation. 1987;76:1061-6.
94. Jones ML. Mastering the Trichrome Stain. Connection [Internet]. 2010 April 2, 2014:[79-84 pp.].
95. Woessner JF. The determination of hydroxyproline in tissue and protein samples containing small proportions of this imino acid. Arch Biochem Biophys. 1961;93:440-7.
96. Ischiropoulos H. Biological tyrosine nitration: a pathophysiological function of nitric oxide and reactive oxygen species. Arch Biochem Biophys. 1998;356:1-11.
97. Balasubramanian D, Kanwar R. Molecular pathology of dityrosine cross-links in proteins: structural and functional analysis of four proteins. Mol Cell Biochem. 2002;234-235:27-38.
98. Webb CL, Benedict JJ, Schoen FJ, Linden JA, Levy RJ. Inhibition of bioprosthetic heart valve calcification with aminodiphosphonate covalently bound to residual aldehyde groups. Ann Thorac Surg. 1988;46:309-16.
99. Golomb G, Schoen FJ, Smith MS, Linden J, Dixon M, Levy RJ. The Role of Glutaraldehyde-Induced Cross-Links in Calcification of Bovine Pericardium Used in Cardiac-Valve Bioprostheses. Am J Pathol. 1987;127:122-30.
100. Levy RJ, Schoen FJ, Howard SL. Mechanism of calcification of porcine bioprosthetic aortic valve cusps: role of T-lymphocytes. Am J Cardiol. 1983;52:629-31.
101. Vashi AV, Werkmeister JA, Vuocolo T, Elvin CM, Ramshaw JA. Stabilization of collagen tissues by photocrosslinking. J Biomed Mater Res A. 2012;100:2239-43.
102. Christian AJ, Lin H, Alferiev IS, Connolly JM, Ferrari G, Hazen SL, et al. The susceptibility of bioprosthetic heart valve leaflets to oxidation. Biomaterials. 2014;35:2097-102.
103. Maestro MM, Turnay J, Olmo N, Fernandez P, Suarez D, Garcia Paez JM, et al. Biochemical and mechanical behavior of ostrich pericardium as a new biomaterial. Acta Biomater. 2006;2:213-9.
104. Stadtman ER, Levine RL. Free radical-mediated oxidation of free amino acids and amino acid residues in proteins. Amino Acids. 2003;25:207-18.
105. Soby L, Johnson P. Determination of asparagine and glutamine in polypeptides using bis(l,l-trifluoroacetoxy)iodobenzene. Anal Biochem. 1981;113:149-53.

106. Boyum A, Skrede KK, Myhre O, Tennfjord VA, Neurauter CG, Tolleshaug H, et al. Calprotectin (S100A8/S100A9) and myeloperoxidase: co-regulators of formation of reactive oxygen species. Toxins (Basel). 2010;2:95-115.
107. Collins SJ, Ruscetti FW, Gallagher RE, Gallo RC. Normal functional characteristics of cultured human promyelocytic leukemia cells (HL-60) after induction of differentiation by dimethylsulfoxide. J Exp Med. 1979;149:969-74.
108. Collins SJ, Ruscetti FW, Gallagher RE, Gallo RC. Terminal differentiation of human promyelocytic leukemia cells induced by dimethyl sulfoxide and other polar compounds. P Natl Acad Sci USA. 1978;75:2458-62.
109. Levy R, Rotrosen D, Nagauker O, Leto TL, Malech HL. Induction of the respiratory burst in HL-60 cells. Correlation of function and protein expression. J Immunol. 1990;145:2595-601.
110. Antai AB, Eyong EU, Eteng MU, Itam EH, Eko ME, Ita SO. Serum protein and enzyme levels in rats following administration of ethanolic leaf extract of Ageratum conyzoides (goat weed). Niger J Physiol Sci. 2009;24:117-20.
111. Sugatani J, Wada T, Osabe M, Yamakawa K, Yoshinari K, Miwa M. Dietary inulin alleviates hepatic steatosis and xenobiotics-induced liver injury in rats fed a high-fat and high-sucrose diet: association with the suppression of hepatic cytochrome P450 and hepatocyte nuclear factor 4alpha expression. Drug Metab Dispos. 2006;34:1677-87.
112. Kidane AG, Burriesci G, Cornejo P, Dooley A, Sarkar S, Bonhoeffer P, et al. Current developments and future prospects for heart valve replacement therapy. J Biomed Mater Res B Appl Biomater. 2009;88:290-303.
113. Yoganathan AP, Chandran KB, Sotiropoulos F. Flow in prosthetic heart valves: state-of-the-art and future directions. Ann Biomed Eng. 2005;33:1689-94.
114. Schoen FJ, Levy RJ. Founder's Award, 25th Annual Meeting of the Society for Biomaterials, perspectives. Providence, RI, April 28-May 2, 1999. Tissue heart valves: current challenges and future research perspectives. J Biomed Mater Res. 1999;47:439-65.
115. Bebbington D, Monck NJ, Gaur S, Palmer AM, Benwell K, Harvey V, et al. 3,5-Disubstituted-4-hydroxyphenyls linked to 3-hydroxy-2-methyl-4(1H)-pyridinone: potent inhibitors of lipid peroxidation and cell toxicity. J Med Chem. 2000;43:2779-82.
116. Poli G, Leonarduzzi G, Biasi F, Chiarpotto E. Oxidative stress and cell signalling. Curr Med Chem. 2004;11:1163-82.
117. Blackwell TS, Blackwell TR, Holden EP, Christman BW, Christman JW. In vivo antioxidant treatment suppresses nuclear factor-kB activation and lung inflammation. J Immunol. 1996;157:1630-7.
118. Golden TR, Patel M. Catalytic antioxidants and neurodegeneration. Antioxid Redox Signal. 2009;11:555-70.
119. Kos I, Benov L, Spasojevic I, Reboucas JS, Batinic-Haberle I. High lipophilicity of meta Mn(III) N-alkylpyridylporphyrin-based superoxide dismutase mimics compensates for their lower antioxidant potency and makes them as effective as ortho analogues in protecting superoxide dismutase-deficient Escherichia coli. J Med Chem. 2009;52:7868-72.
120. Winterbourn CC. Toxicity of iron and hydrogen peroxide: the Fenton reaction. Toxicol Lett. 1995;82-83:969-74.
121. Batinic-Haberle I, Benov L, Spasojevic I, Fridovich I. The ortho effect makes manganese(III) meso-tetrakis(N-methylpyridinium-2-yl)porphyrin a powerful and potentially useful superoxide dismutase mimic. J Biol Chem. 1998;273:24521-8.
122. Day BJ, Fridovich I, Crapo JD. Manganic porphyrins possess catalase activity and protect endothelial cells against hydrogen peroxide-mediated injury. Arch Biochem Biophys. 1997;347:256-62.
123. Doctrow SR, Huffman K, Marcus CB, Tocco G, Malfroy E, Adinolfi CA, et al. Salen-manganese complexes as catalytic scavengers of hydrogen peroxide and cytoprotective agents: structure-activity relationship studies. J Med Chem. 2002;45:4549-58.
124. Jaramillo MC, Briehl MM, Crapo JD, Batinic-Haberle I, Tome ME. Manganese porphyrin, MnTE-2-PyP5+, Acts as a pro-oxidant to potentiate glucocorticoid-induced apoptosis in lymphoma cells. Free Radic Biol Med. 2012;52:1272-84.

125. Eastoe JE. The amino acid composition of mammalian collagen and gelatin. Biochem J. 1955;61:589-600.
126. Postigo F, Mora M, De Madariaga MA, Nonell S, Sagrista ML. Incorporation of hydrophobic porphyrins into liposomes: characterization and structural requirements. Int J Pharm. 2004;278:239-54.
127. Hood E, Simone E, Wattamwar P, Dziubla T, Muzykantov V. Nanocarriers for vascular delivery of antioxidants. Nanomedicine-UK. 2011;6:1257-72.
128. Stone WL, Mukherjee S, Smith M, Das SK. Therapeutic uses of antioxidant liposomes. Methods Mol Biol. 2002;199:145-61.
129. Howard MD, Greineder CF, Hood ED, Muzykantov VR. Endothelial targeting of liposomes encapsulating SOD/catalase mimetic EUK-134 alleviates acute pulmonary inflammation. J Control Release. 2014;177:34-41.
130. Hood ED, Greineder CF, Dodia C, Han J, Mesaros C, Shuvaev VV, et al. Antioxidant protection by PECAM-targeted delivery of a novel NADPH-oxidase inhibitor to the endothelium in vitro and in vivo. J Control Release. 2012;163:161-9.
131. Muzykantov VR. Targeting of superoxide dismutase and catalase to vascular endothelium. J Control Release. 2001;71:1-21.
132. Tovmasyan A, Weitner T, Sheng H, Lu M, Rajic Z, Warner DS, et al. Differential coordination demands in Fe versus Mn water-soluble cationic metalloporphyrins translate into remarkably different aqueous redox chemistry and biology. Inorg Chem. 2013;52:5677-91.
133. Reboucas JS, Spasojevic I, Batinic-Haberle I. Quality of potent Mn porphyrin-based SOD mimics and peroxynitrite scavengers for pre-clinical mechanistic/therapeutic purposes. J Pharm Biomed Anal. 2008;48:1046-9.
134. Ewing JF, Janero DR. Microplate superoxide dismutase assay employing a nonenzymatic superoxide generator. Anal Biochem. 1995;232:243-8.
135. Sacks MS, Hamamoto H, Connolly JM, Gorman RC, Gorman JH, 3rd, Levy RJ. In vivo biomechanical assessment of triglycidylamine crosslinked pericardium. Biomaterials. 2007;28:5390-8.
136. McCord JM, Fridovich I. The reduction of cytochrome c by milk xanthine oxidase. J Biol Chem. 1968;243:5753-60.
137. Shuvaev VV, Tliba S, Nakada M, Albelda SM, Muzykantov VR. Platelet-endothelial cell adhesion molecule-1-directed endothelial targeting of superoxide dismutase alleviates oxidative stress caused by either extracellular or intracellular superoxide. J Pharmacol Exp Ther. 2007;323:450-7.
138. Nancollas GH, LoRe M, Perez L, Richardson C, Zawacki SJ. Mineral phases of calcium phosphate. Anat Rec. 1989;224:234-41.
139. Miller JD, Weiss RM, Heistad DD. Calcific aortic valve stenosis: methods, models, and mechanisms. Circ Res. 2011;108:1392-412.
140. Branchetti E, Poggio P, Sainger R, Shang E, Grau JB, Jackson BM, et al. Oxidative stress modulates vascular smooth muscle cell phenotype via CTGF in thoracic aortic aneurysm. Cardiovasc Res. 2013;100:316-24.
141. Branchetti E, Sainger R, Poggio P, Grau JB, Patterson-Fortin J, Bavaria JE, et al. Antioxidant enzymes reduce DNA damage and early activation of valvular interstitial cells in aortic valve sclerosis. Arterioscler Thromb Vasc Biol. 2013;33:e66-74.
142. Aitken JB, Shearer EL, Giles NM, Lai B, Vogt S, Reboucas JS, et al. Intracellular targeting and pharmacological activity of the superoxide dismutase mimics MnTE-2-PyP5+ and MnTnHex-2-PyP5+ regulated by their porphyrin ring substituents. Inorg Chem. 2013;52:4121-3.
143. Tal E, Guggenheim K. Effect of Manganese on Calcification of Bone. Biochem J. 1965;95:94-7.
144. Iyengar AKS, Sugimoto H, Smith DB, Sacks MS. Dynamic In Vitro Quantification of Bioprosthetic Heart Valve Leaflet Motion Using Structured Light Projection. Annals of Biomedical Engineering. 2001;29:963-73.
145. Jaramillo MC, Frye JB, Crapo JD, Briehl MM, Tome ME. Increased manganese superoxide dismutase expression or treatment with manganese porphyrin potentiates dexamethasone-induced apoptosis in lymphoma cells. Cancer Res. 2009;69:5450-7.

146. Jaafar-Maalej C, Diab R, Andrieu V, Elaissari A, Fessi H. Ethanol injection method for hydrophilic and lipophilic drug-loaded liposome preparation. J Liposome Res. 2010;20:228-43.
147. Otto C, Bonow R. Valvular Heart Disease. Braunwald's Heart Disease: A Textbook of Cardiovascular Medicine. Philadelphia, PA: Elseiver; 2012. p. 1468-539.
148. Gujral JS, Hinson JA, Jaeschke H. Chlorotyrosine protein adducts are reliable biomarkers of neutrophil-induced cytotoxicity in vivo. Comp Hepatol. 2002;3.
149. Waykole P, Heidemann E. Dityrosine in collagen. Connect Tissue Res. 1976;4:219-22.
150. van Oeveren W, Tielliu IF, de Hart J. Comparison of modified chandler, roller pump, and ball valve circulation models for in vitro testing in high blood flow conditions: application in thrombogenicity testing of different materials for vascular applications. Int J Biomater. 2012;2012:673163.
151. Dahm M, Husmann M, Eckhard M, Prufer D, Groh E, Oelert H. Relevance of immunologic reactions for tissue failure of bioprosthetic heart valves. Ann Thorac Surg. 1995;60:S348-52.
152. Human P, Zilla P. The possible role of immune responses in bioprosthetic heart valve failure. J Heart Valve Dis. 2001;10:460-6.
153. Jones JA, McNally AK, Chang DT, Qin LA, Meyerson H, Colton E, et al. Matrix metalloproteinases and their inhibitors in the foreign body reaction on biomaterials. J Biomed Mater Res A. 2008;84:158-66.
154. Babior BM, Lambeth JD, Nauseef W. The neutrophil NADPH oxidase. Arch Biochem Biophys. 2002;397:342-4.
155. Bentham J, Qureshi S, Eicken A, Gibbs J, Ballard G, Thomson J. Early percutaneous valve failure within bioprosthetic tricuspid tissue valve replacements. Catheter Cardiovasc Interv. 2013;82:428-35.
156. Juni RP, Duckers HJ, Vanhoutte PM, Virmani R, Moens AL. Oxidative stress and pathological changes after coronary artery interventions. J Am Coll Cardiol. 2013;61:1471-81.
157. Fattori R, Piva T. Drug-eluting stents in vascular intervention. Lancet. 2003;361:247-9.
158. Miller JD, Chu Y, Brooks RM, Richenbacher WE, Pena-Silva R, Heistad DD. Dysregulation of antioxidant mechanisms contributes to increased oxidative stress in calcific aortic valvular stenosis in humans. J Am Coll Cardiol. 2008;52:843-50.
159. Yang X, Meng X, Su X, Mauchley DC, Ao L, Cleveland JC, Jr., et al. Bone morphogenic protein 2 induces Runx2 and osteopontin expression in human aortic valve interstitial cells: role of Smad1 and extracellular signal-regulated kinase 1/2. J Thorac Cardiovasc Surg. 2009;138:1008-15.
160. Yang X, Fullerton DA, Su X, Ao L, Cleveland JC, Jr., Meng X. Pro-osteogenic phenotype of human aortic valve interstitial cells is associated with higher levels of Toll-like receptors 2 and 4 and enhanced expression of bone morphogenetic protein 2. J Am Coll Cardiol. 2009;53:491-500.
161. Briand M, Pibarot P, Despres JP, Voisine P, Dumesnil JG, Dagenais F, et al. Metabolic syndrome is associated with faster degeneration of bioprosthetic valves. Circulation. 2006;114:I512-7.